BUILDING SEISMIC FRAGILITIES USING RESPONSE SURFACE METAMODELS

A Thesis
Presented to
The Academic Faculty

By

Peeranan Towashiraporn

In Partial Fulfillment
of the Requirements for the Degree
Doctor of Philosophy in
Civil and Environmental Engineering

Georgia Institute of Technology
August 2004

BUILDING SEISMIC FRAGILITIES USING RESPONSE SURFACE METAMODELS

Approved by:

Barry J. Goodno, CEE, Chairman

James I. Craig, AE

Reginald DesRoches, CEE

Bruce R. Ellingwood, CEE

Donald W. White, CEE

Date Approved 08/19/04

ACKNOWLEDGMENT

I am deeply indebted to my advisors, Dr. Barry Goodno and Dr. James Craig, for their constant support. Without their help, this work would not be possible. I would also like to thank the members of my committee: Dr. Reginald DesRoches, Dr. Bruce Ellingwood, and Dr. Donald White. Their advice and patience is truly appreciated.

I would like to thank my colleagues at Georgia Tech for their valuable suggestions and their friendship; especially to Choi, Thitikorn, Joonam, Leonardo, Gary, Gaurav, Susendar, Tumay, Bassem, Bryant, and Tianyi. Those days in Mason 522 will not be forgotten.

Lastly, I would like to thank my family and my girlfriend for their unconditional support and encouragement throughout my quest for a Ph.D. at Georgia Tech.

TABLE OF CONTENTS

LIST OF TABLES

LIST OF FIGURES

SUMMARY

Building fragility describes the likelihood of damage to a building due to random ground motions. Conventional methods for computing building fragilities are either based on statistical extrapolation of detailed analyses on one or two specific buildings or make use of Monte Carlo simulation with these models. However, the Monte Carlo technique usually requires a relatively large number of simulations in order to obtain a sufficiently reliable estimate of the fragilities, and it quickly becomes impractical to simulate the required thousands of dynamic time-history structural analyses for physics-based analytical models.

An alternative approach for carrying out the structural simulation is explored in this work. The use of Response Surface Methodology in connection with the Monte Carlo simulations simplifies the process of fragility computation. More specifically, a response surface is sought to predict the structural response calculated from complex dynamic analyses. Computational cost required in a Monte Carlo simulation will be significantly reduced since the simulation is performed on a polynomial response surface function, rather than a complex dynamic model. The methodology is applied to the fragility computation of an unreinforced masonry (URM) building located in the New Madrid Seismic Zone. Different rehabilitation schemes for this structure are proposed and evaluated through fragility curves. Response surface equations for predicting peak drift are generated and used in the Monte Carlo simulation. Resulting fragility curves

show that the URM building is less likely to be damaged from future earthquakes when rehabilitation is properly incorporated.

The thesis concludes with a discussion of an extension of the methodology to the problem of computing fragilities for a collection of buildings of interest. Previous approaches have considered uncertainties in material properties, but this research incorporates building parameters such as geometry, stiffness, and strength variabilities as well as nonstructural parameters (age, design code) over an aggregation of buildings in the response surface models. Simulation on the response surface yields the likelihood of damage to a group of buildings under various earthquake intensity levels. This aspect is of interest to governmental agencies or building owners who are responsible for planning proper mitigation measures for collections of buildings.

CHAPTER 1

INTRODUCTION

1.1 STATEMENT OF THE PROBLEM

In general, building responses are influenced by (a) the loads acting on the building, (b) the geometry of the building, and (c) the strength of materials used in construction. Deterministic responses are calculated from the designed or expected values of loading and building parameters. However, sources of uncertainty exist in all aspects mentioned above and actual values may deviate from their mean values. For building responses due to seismic events, it is well known that the most uncertain aspect is the loading itself [Galambos et al., 1982]. Characteristics of future earthquakes cannot be predicted with certainty. Moreover, building geometry can differ from initial design due to construction practice, which can vary from one building to another and, more importantly, is very difficult to quantify. Properties of the construction materials also possess uncertainties due to manufacturing processes or inherent unpredictability within materials themselves. Another source of uncertainty, and probably the most overlooked, comes from modeling error or prediction accuracy of the building models. Computational models cannot precisely replicate physical buildings in real situations. However, this type of uncertainty is epistemic and can be reduced with better knowledge

of real buildings, more refined analysis models, and calibration based on experimental studies.

Deterministic seismic response analysis only provides values of building response from specific seismic events and may be misleading in some cases. On the other hand, probabilistic seismic response computation takes into account uncertainties arising from both seismic loading and structural aspects.

Building seismic fragility is a common measure of damage likelihood due to random ground motions. Fragility relationships are usually expressed in terms of a damage probability matrix [ATC, 1985] or in terms of fragility curves.

Seismic fragility, by definition, is the probability of damage exceeding certain limit state conditions at a given seismic intensity level. Probabilistic description of response or damage is required for computing exceedance probabilities. Conventional methods use the Monte Carlo technique to simulate probability distribution of outcomes when analytical solutions are not readily available. The Monte Carlo technique is conceptually straightforward, as it generates artificial random samples from the distribution of inputs. However, the Monte Carlo technique usually requires a relatively large number of simulations in order to obtain a sufficiently reliable estimate of the probability distribution. It quickly becomes impractical to simulate the required thousands of dynamic time-history structural analyses to formulate probabilistic characteristics of seismic responses. This thesis proposes an efficient means for predicting building seismic responses in a simplified manner and hence significantly reduces the computational cost required in the Monte Carlo simulation.

1.2 RESEARCH OBJECTIVES AND SCOPE

The primary goal of this thesis is to present a new approach utilizing metamodels to calculate seismic fragility. The metamodels associate a dependent variable or output to the independent input parameters in a function-like manner. The approach incorporates uncertainties in seismic loadings as well as structural parameters. The metamodel, in particular a response surface function, is adopted in the process for prediction of seismic responses or damage. Conventional Monte Carlo simulation is carried out on the response surface models to obtain damage probability distributions and, consequently, fragility of buildings. Computational cost required in a Monte Carlo simulation is significantly reduced since the simulation is performed on a polynomial response surface function, rather than a complex dynamic model.

The proposed approach is implemented in two cases: (1) through fragility calculations of a specific building and (2) as a preliminary step in rapid fragility assessment of building portfolios. In the first case, a single unreinforced masonry building typical of firehouse construction in Mid-America is considered. Uncertainties that exist in material properties are included in the model. Uncertainties from seismic loadings are captured by applying ground motions with a wide variety of hazard characteristics to the building. An ideal solution is to use a sufficiently large set of records of actual earthquakes. However, in Mid-America, historical records of major seismic activities are scarce. As a result, Wen and Wu [2001] developed a suite of synthetic ground motions appropriate for three cities in Mid-America. Rix [2003] refined the methodology and used detailed local soil data to develop another set of synthetic ground motions. However, due to its availability, Wen and Wu's suite of ground motions

is used exclusively in this research. Even though response due to an earthquake is dependent on direction of ground motion input, only two-dimensional weak axis response of the building is considered in this thesis. The use of metamodels in computing seismic fragilities is presented in both cases of the existing and rehabilitated firehouses. Performance of the rehabilitation schemes are evaluated through the resulting fragility curves.

In the second case, benefits from using the metamodels become more appealing in performing rapid fragility assessment of building portfolio. Conventional loss estimation packages use generic fragility curves typical of different building classifications to quantify probable damage. However, buildings in the same classification may have different fragility relations due to variability in geometries or other building aspects. This could lead to an inaccurate estimation of building portfolio losses. The methodology proposed in this thesis provides an efficient means for rapidly deriving fragility relations specific to each building in the portfolio. This aspect is of interest to governmental agencies or building owners who are responsible in planning for proper mitigation measures for their building portfolios.

1.3 THESIS ORGANIZATION

This thesis is organized into seven chapters. The first chapter begins with introduction to the thesis, problem statement, scope and outline of the thesis.

The second chapter of the thesis introduces the concept of fragility curves for displaying the likelihood of building damage due to random seismic events. This chapter also explains conventional ways of generating fragility curves, including fragility curves

using expert opinion, empirical fragility curves, and analytical fragility curves. Examples from past developments are given in details in this chapter. Focus is placed on the analytical fragility curves, which will be used as part of the proposed methodology presented in this thesis.

Chapter 3 begins with introduction to the concept of a metamodel, its definition, and history. Examples of different metamodels are mentioned. The Response Surface Methodology (RSM) is one of the most widely-used and well-proven metamodels [Simpson et al., 2001] in many engineering applications. Metamodels based on response surfaces statistically approximate desired responses in the form of polynomial functions of random predictor variables. The Design of Experiments (DOE) technique provides the locations of these data points. History and past applications of RSM are also presented in this chapter. RSM has been implemented in the preliminary design process for aircraft in the field of aerospace engineering systems design. Response surfaces relate aircraft performance measures to their configuration parameters. Appropriate design configurations can then be obtained from optimization analysis of the response surfaces. Another application of RSM is in the area of structural reliability, which is more closely related to civil engineering problems. Response surfaces are commonly used to approximate limit state functions which cannot always be explicitly represented in closed-form solutions.

The main thrust of the thesis is described in Chapter 3. Response Surface metamodels are implemented as an alternative and more efficient means for calculating seismic fragility of buildings. The use of Response Surface Methodology in connection with the use of Monte Carlo simulations simplifies the process of fragility computation.

More specifically, a response surface is sought to predict the structural response calculated from complex dynamic analyses. Three approaches for computing building seismic fragilities are proposed in the thesis. All three approaches are similar in the sense that building seismic responses are characterized by response surface functions of the building input parameters, and consequently, incorporate uncertainties in structural systems directly in the functions. The main difference among the three approaches is the way the seismic uncertainties are treated. Approach 1 simply generates a response surface for each ground motion in a suite and they are randomly selected in the simulation process. On the other hand, approaches 2 and 3 make use of the dual response surface concept [Lin and Tu, 1995] by generating response surfaces of the mean and standard deviation of building responses due to a suite of ground motions. The proposed approaches are verified with a fragility analysis of a single degree of freedom (SDOF) system. Comparison is made between the proposed approaches and conventional methods.

Chapter 4 presents a proof-of-concept application in a fragility investigation of a typical firehouse in Mid-America. Firehouses are essential for emergency response and must be operational during and after an earthquake event. Most firehouses in the region are constructed of unreinforced masonry (URM). A 2-story URM model building (Yi et al. [2002] and Yi [2004]) is chosen as representative of firehouses in the region. Unreinforced masonry walls undergo complex inelastic behavior under cyclic loading through cracking of materials. Various behaviors (i.e., rocking, bed-joint sliding, etc.) can be observed depending on material properties and, more importantly, geometry of each wall component. Composite spring models [Park et al., 2002] are used for capturing

inelastic behaviors of each component in the URM walls and computing overall seismic responses. Nonlinear time-history analysis is used as a basis for computing building responses. A suite of synthetic ground acceleration records [Wen and Wu, 2001] for Mid-America cities is applied. Deterministic responses are comparable with those of finite element models [Kim and White, 2001]. However, unreinforced masonry is a non-homogeneous material and generally exhibits uncertain properties. In addition, earthquake events in Mid-America are so scarce that few historical data exist. As a result, probabilistic aspects of the problem must be considered. The proposed approach of using response surface metamodels to assess building seismic fragility is applied for a URM firehouse. Peak drift in walls is chosen as a damage or response measure according to FEMA guidelines [FEMA, 2000a]. Four independent parameters characterize structural uncertainties and are used as basic input variables in response surface generation. Seismic uncertainties are captured by a suite of ground motions synthesized from spatially distributed sources, paths, and magnitudes. Monte Carlo simulations performed over response surface metamodels reveal seismic fragility of the URM firehouse in the form of fragility curves.

Rehabilitation plans for the vulnerable URM firehouse using passive metallic damping devices are investigated in Chapter 5. While application of metallic damping devices is quite common in the framed-type structures, much less attention has been paid to implementation in URM buildings. This thesis demonstrates innovative rehabilitation schemes utilizing differential flexibility between URM walls and timber floor diaphragms. Deterministic and probabilistic analyses show promising results for the Mid-America firehouse when rehabilitation is properly incorporated.

Chapter 6 discusses an extension of the methodology in a preliminary step toward loss assessment of building portfolios. The methodology is implemented in rapid fragility calculation of buildings in the target portfolio. Response surface metamodels, in this case, include not only material property parameters, but also building characteristics (i.e., configuration and age). Response surface metamodels are generated using building parameters from building inventory data for a region where the building portfolio of interest is located. Building parameters become deterministic when response of a specific building is calculated. Randomness exists in material property parameters and seismic loadings. Monte Carlo simulation is performed on the metamodel to generate building specific fragility curves.

Seismic fragility of a hypothesized building portfolio consisting of a collection of low-rise steel moment resisting frame buildings (or S1-L according to HAZUS classification [NIBS, 1999]) in Shelby County, Tennessee is investigated as an example application. A three-story moment frame building based on the SAC study [FEMA, 2000b] is modeled to represent a typical S1-L building in the region. Structural parameters describing building configuration and material properties are introduced as potential input variables for the response surface models. However, the growing number of input variables significantly increases analysis cases required to generate response surfaces. A screening process is performed to select the most influential input parameters in response calculations. Responses (peak inter-story drifts) are computed at predetermined data points or combinations of input parameters. A Response Surface polynomial function for approximating peak inter-story drift can then be formulated from

a least-square regression analysis. Fragility relations for each building in the hypothetical portfolio are obtained through Monte Carlo simulations.

Chapter 7 presents a summary of this thesis and discusses its potential impact. Recommendations for the future research are also presented in this chapter.

CHAPTER 2

TRADITIONAL FRAGILITY CURVE GENERATION

Conventional building response analyses use deterministic approaches in which loadings and structural characteristics are based on the best estimates or expected values from field data and experimental results. However, seismic loadings are clearly nondeterministic. Moreover, resistance of building structures also exhibits stochastic characteristics arising from uncertainties in construction processes, physical properties and modeling abstraction. As a result, a purely deterministic description of structural responses to earthquakes can be misleading in some cases. Probabilistic seismic response analysis takes into account uncertainties in both seismic loading and structural characteristics. Building seismic fragility is commonly used in this matter as a measure of potential damage in a building.

2.1 DEFINITION OF FRAGILITY

Building seismic fragility describes the likelihood of damage due to random ground motions. The seismic fragility of a structure is mathematically defined as the probability of failure of the structure conditional on specific ground motion intensity. Let I_j be a specific value of the hazard intensity at the j^{th} level. Let D be the load effect due to this random event on the global response of the structure. Let C_i be the random structural

capacity to withstand this load effect corresponding to the i^{th} limit state. Accordingly, the building seismic fragility is calculated as:

$$PF_{ij} = \text{Prob}\left[D \geq C_i \middle| I_j \right] \tag{2.1}$$

where PF_{ij} denotes the probability of failure with respect to the i^{th} limit state at the j^{th} hazard intensity level. The fragility curve for a limit state i can be constructed by evaluating PF_{ij} at different levels of hazard intensity (j). Graphical representation of example fragility curve for limit state i is shown in Figure 2.1.

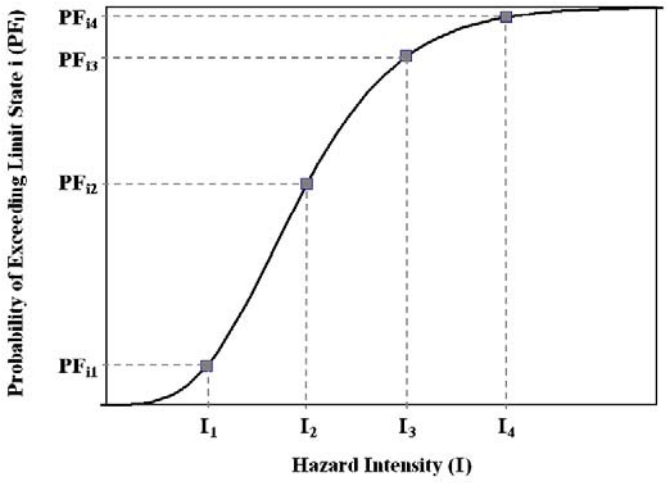

Figure 2.1: Example Fragility Curve of Limit State i

Generally, fragility curves can be generated using (1) actual earthquake damage data, (2) engineering judgment, and (3) analytical methods. These approaches will be summarized in the following sections.

2.2 FRAGILITY CURVES USING ACTUAL DAMAGE DATA

This approach is based primarily on actual damage data obtained from field investigations after an earthquake or from experiments to generate fragility curves. This kind of fragility curve is essentially close to exact results because it is derived directly from real structures and real earthquakes. However, the quality is still limited by the limited numbers of sampled structures that can be examined.

This type of fragility curve is useful in characterizing the seismic performance of a collection of similar structures in an earthquake-prone area. Earthquake intensity data at each structure site and corresponding damage on the structure are collected following an earthquake. The raw data is then statistically processed to generate fragility curves. This process usually requires a large number of data in order for reliable estimates of fragility. This empirical fragility curves are often used to calibrate the fragility curves developed analytically. Past development of empirical fragility curves are listed as follows.

Yamazaki et al. [1999] constructed a series of fragility curves for expressway bridges in Japan based on actual damage data from the 1995 Hyogoken-Nanbu (Kobe) earthquake. Damage data from 216 expressway bridges throughout Japan were collected after an earthquake. Five damage ranks from collapse to no damage were assigned to all bridges. Earthquake intensities values, which are peak ground acceleration (PGA) values, at some bridge locations were measured by the accelerometers during the earthquake. Earthquake intensities at other unequipped brides are estimated based on available records. Based on these damage-intensity data, fragility curves for the expressway bridges were constructed assuming a lognormal distribution for the cumulative

probability of damage. Results from this study were used in planning for appropriate traffic control immediately after earthquakes.

A similar approach was proposed by Shinozuka et al. [2000b] for developing empirical fragility curves for the Hanshin Expressway Public Corporation's (HEPC's) bridge columns in Japan. Records of the damage resulting from the 1995 Kobe earthquake were used as a basis for generating fragility curves. The states of damage and PGA values from a sample of 770 singly supported reinforced concrete columns were considered. It was also assumed that the fragility curve could be represented by a two-parameter lognormal distribution. Contrary to the work done by Yamazaki et al [1999], which used the method of least squares, the maximum likelihood method was employed to estimate the lognormal distribution parameters.

O'Rourke and So [1999, 2000] presented a method for developing empirical fragility curves for on-grade steel liquid storage tanks. The fragility curves are based on the seismic damage records of over 400 tanks in 9 earthquake events. One of the 5 damage states and corresponding peak ground acceleration (PGA) were given to each tank. The seismic fragility relations were built using logistic regression analysis. The fragility relations developed in this study were then compared with the corresponding relations available in HAZUS and ATC studies. It was found that actual tanks performed better than that calculated in the existing approaches.

From a comprehensive database of bridge damage for the Northridge and Loma Prieta earthquakes, Basöz and Kiremidjian [1999] generated fragility curves to quantify bridge seismic fragilities. The bridge damage descriptions were obtained from bridge damage reports compiled by the California Department of Transportation (CalTrans). A

four-level damage measures (minor, moderate, major, and collapse) was used to describe bridge damage. Earthquake intensity levels at the bridge sites were either recorded by USGS or simulated though a scenario event. Similar to the O'Rourke and So [1999, 2000] approach, a logistic regression analysis was utilized to describe a relationship between the conditional probability and the earthquake intensity, which was taken as the PGA in this study.

Fragility curves derived from actual damage data provides valuable perception of potential impact from future earthquakes. However, damage data obtained from the field needs to constitute a statistically large sample size. Scarcity of data may lead to unreliable prediction of seismic fragilities.

2.3 FRAGILITY CURVES USING ENGINEERING JUDGMENT

When the required actual earthquake damage and building inventory data are not available, one can develop such data from experiences and judgments of earthquake engineering experts. These data are then processed statistically for earthquake damage estimates of the region. One of the best-known methodologies for generating fragility curves based on engineering judgment is from ATC-13 [ATC, 1985]. This project summarized damage probability matrices (DPM) for families of structures with similar structural types. Damage probability matrices describe the discrete probabilities of damage in different damage states at various levels of ground shaking. It is comparable and can easily be converted to fragility curves. Based on ATC-13, the structures in California were classified into 78 classes based on size, structural system, and type. Modified Mercalli Intensity (MMI) was selected as an earthquake intensity level in this study. The three-round questionnaire process was carried out involving 71 senior-level

specialists in earthquake engineering to obtain damage information for each structure. Damage was expressed in terms of damage factors. The damage data obtained from the questionnaires were tested using Beta, Normal, and Lognormal probability distribution functions. It was found from the results that the Beta distribution fitted the data uniformly and better than the other distributions. Beta distribution was then used to describe probabilistic damage and to create damage probability matrices (DPM) for all 78 classes of structures. Damage probability matrix is equivalent to the fragility curve in the sense that both represent a probability of exceeding a specific damage state conditioning on a ground motion intensity level, which is MMI in this study.

Several improvements to the ATC-13 approach have been made by Anagnos et al. [1995]. Two major changes related to a new building classification and fragility formulations for those classes based on the damage probability matrices in ATC-13. ATC-13 categorized building structures into 40 different classes. Anagnos et al. [1995] reduced the number of building classes to 17, considering only framing types and structural materials used. Fragility curves, which could be transformed from ATC-13 damage probability matrices, were then created for each building class. Analogous to ATC-13, the damage factor was used to describe the damage states in this study. For each building class and MMI level, integrations were performed on the Beta probability distributions from ATC-13 to calculate probabilities of exceeding a particular damage state or fragilities. Repetition of the process over different MMI levels yielded a set of fragility data points. Lognormal curves were assumed and fitted through the resulting points using least-square error techniques. Comparison of these curves suggested a possible consolidation of building classes when the curves are sufficiently close.

2.4 FRAGILITY CURVES USING ANALYTICAL APPROACHES

An analytical approach for generating fragility curves is implemented when the actual earthquake damage data are limited and cannot provide sufficient statistical information. Analytical fragility curves are developed from seismic response analysis of structures. This methodology is often applicable in regions with infrequent seismic activities, such as in central and eastern United States. Analytical approach is a basis for developing fragility curves in this research as its applications are focused in the Mid-America region.

In general, analytical fragility curves can be constructed following these procedures.

(1) The first step is to identify an appropriate seismic intensity parameter. Seismic hazard intensity is commonly measured by the peak values from the ground motion time history, including peak ground acceleration (PGA), peak ground velocity (PGV), or peak ground displacement (PGD). The use of spectral values as a seismic intensity measure is also common in fragility calculations. Spectral acceleration (S_a) and spectral displacement (S_d) are the two measures regularly used for fragility curves. There are advantages and disadvantages of using the two types of intensity measures. The use of peak values is simple since they can readily be obtained from the records. However, peak ground motion parameters may provide poor correlation with structural responses. On the other hand, spectral parameter is a direct measure of the demand of the excitation on structural responses. The drawback of the use of spectral values is that it is structure-dependent.

(2) Uncertainties from the earthquakes are implicitly incorporated in the analysis by the use of an ensemble of ground acceleration records with a wide variety of seismic hazards. Both actual and synthesized records can be used in this matter. Ground motion records in an ensemble are scaled such that they have the same level of seismic intensity.

(3) Uncertainties that are inherited in a structural aspect must be considered. The source of this aleatory uncertainty comes from randomness in construction material properties. Probabilistic density functions of each random parameter can be obtained from existing experimental results or field surveys.

(4) A response measure that best describes damage from seismic loadings is selected. Damage limit states corresponding to the selected damage measure must also be identified. Parameters such as base shear, maximum roof displacement, peak inter-story drift, damage indices, ductility ratio, and energy dissipation capacity can be used to identify the damage states depending on the types of structure being investigated.

(5) Appropriate computational structural models are established for determining seismic responses. Structural uncertainties (i.e., material properties) must be included in these models as well.

(6) A statistical approach is employed to formulate a large number of seismic response analyses on the models with stochastic properties subjected to an ensemble of ground motions scaled to a specific intensity level.

(7) Damage probabilities are calculated from the computed seismic responses. These probability values are conditioned on a specific intensity level. Repetition of the process over all intensity levels results in a series of probabilities of exceeding limit states at various intensity levels or fragility curves.

The most direct means of statistical analysis to obtain probabilistic description of response is through Monte Carlo simulation [Kleijnen, 1974]. The Monte Carlo technique is a brute-force simulation technique which randomly generates values for uncertain input variables to simulate scenarios of a problem. These values are taken from within a fixed range and selected to fit a probability distribution (e.g., uniform distribution, normal distribution, lognormal distribution, etc.) In Monte Carlo simulation, the random selection process is repeated many times to create multiple scenarios. Each time a value is randomly selected, it forms one possible scenario and outcome to the problem is evaluated. Together, these scenarios give a range or probability distribution of possible outcomes. In the case of seismic response analysis, structural uncertainty parameters (e.g., material properties) and seismic inputs are randomly selected, based on their probability distributions, to form many structure-earthquake combinations. Seismic analysis performed on each combination yields a seismic response of interest (e.g., peak drift, damage indices, etc.) When the selection process is repeatedly carried out for hundreds or thousands of times, probabilistic descriptions of seismic response can be formulated. Probabilities of response exceeding certain values can be obtained.

Mosalam et al. [1997] made use of the Monte Carlo simulation technique on the seismic fragility analysis of the unreinforced masonry infilled frames. Five random

parameters from the pushover curve were assumed to follow lognormal distribution. A total of 600 synthetic ground motions were considered in this study. For each earthquake record, 200 building samples were generated from the Monte Carlo simulation. Seismic analyses were performed on those building samples to calculate inter-story drift responses. The probabilities of exceeding specific inter-story drift limit states were computed based on the results of 200 runs. The process recurred for all ground acceleration records yielding 600 probability values for each limit state. The fragility curves were plotted by fitting these exceedance probability data points to appropriate regression models.

The advantage of the Monte Carlo technique is that it calculates probabilities from the outcomes of the simulated scenarios regardless of a specific probability distribution of the outcomes. However, it requires a relatively large number of simulations in order to obtain a sufficiently reliable estimate for probability of damage. Mann et al. [1974] suggested that the number of simulations might need to be of the order of 10,000 to 20,000 for approximately 95% confidence limit, depending on the function being evaluated. It will be computationally impractical, if not impossible, to simulate thousands or even hundreds of nonlinear time-history analyses.

Sampling techniques have been proposed, as an alternative to Monte Carlo simulation, in selecting random input variables. The Latin Hypercube sampling technique [McKay et al., 1979] is a one of a number of efficient sampling techniques which ensures that the entire range of input variables is sampled. For small samples, the method provides unbiased point estimates (e.g. mean values or probabilities of exceeding certain values) with relatively small sampling error in comparison to many other Monte

Carlo methods. Latin hypercube sampling selects *n* different values from each input variables in the following manner. The probability distribution of each input variable is divided into *n* intervals of equal probability (shown in Figure 2.2). The *n* values obtained for each input variable are combined in a random manner with the values of other variables to form *n* random combinations of input variables. Evaluation of output or response from each combination of variables yields *n* values of response. The *n* responses are fitted to the appropriate probability density function. The probability of exceeding certain values of response can then be calculated based on the fitted distribution.

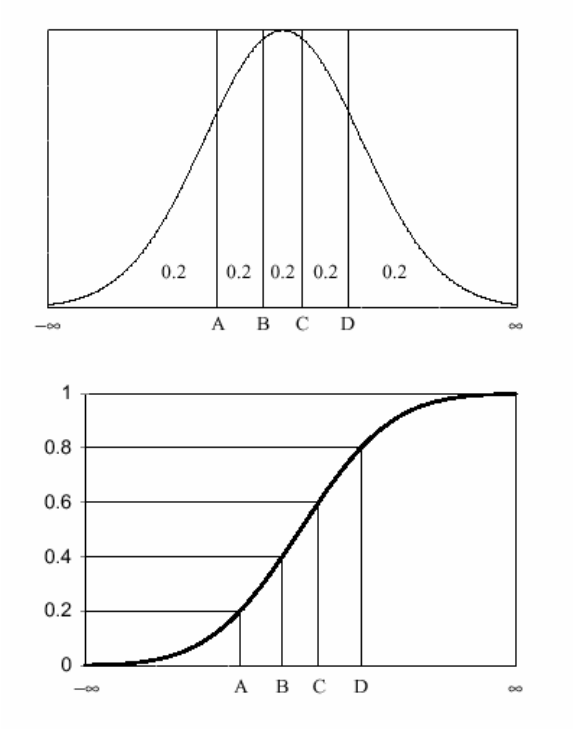

Figure 2.2: Latin Hypercube Sampling of Size n = 5 for a Normal Probability Distribution [Wyss and Jorgensen, 1998]

A number of researchers have suggested several analytical approaches using the Latin Hypercube technique for assessing fragilities of the structures as shown in the subsequent paragraphs.

Hwang and Huo [1994a, 1994b] proposed an analytical method for establishing fragility curves and a damage probability matrix of a five-story reinforced concrete frame building. Synthetic ground motions were generated from probability-based scenario earthquakes. Peak ground acceleration (PGA) ranging from 0.05g to 0.5g was used as a ground shaking parameter. For each PGA level, fifty earthquake acceleration time histories were generated. Five damage states of the building, which varied from nonstructural damage to collapse, were categorized using the building damage index. Structural uncertainties taken into account in this study were the viscous damping ratio, strength, and elastic modulus of construction materials. For each random structural parameter, 50 samples were randomly generated within two standard deviations around the means. These samples were then combined using the Latin Hypercube sampling technique to assemble 50 structural models. These structural models obtained from the sampling process were then paired with 50 samples of ground acceleration records to create 50 samples of earthquake-site-structure systems in each PGA level. A nonlinear time-history analysis was carried out on each sample to determine the building damage index. At the end, 50 values of damage index were obtained in each PGA level. A probability distribution of the building damage index was assumed to follow a lognormal probability function. Regression analysis was performed to determine the lognormal distribution parameters. Conditioning on this particular PGA level, the probability of

damage or the fragility was then calculated for each damage state. This process was repeated over other PGA levels to complete the fragility curves.

Analogous methodology with minor difference in details (e.g., structural types, damage states, etc.) has been presented by several researchers. Seya et al. [1993] applied this methodology in a probabilistic seismic analysis of a five-story steel frame building. Uncertainties in structural and seismic parameters were taken into account. In this study, the damage state was defined in terms of the system ductility ratio obtained from a nonlinear time-history analysis. Peak ground acceleration (PGA) is used as an earthquake intensity measure. For a given PGA level, a lognormal probability distribution function was fitted to the computed response data. Probabilities of damage could be calculated from these fitted lognormal relations. The fragility curves were then constructed by evaluating the probability of damage at different levels of PGA. Song and Ellingwood [1999] investigated the role of inherent uncertainty on the seismic reliability of special moment steel frames with welded connections. Simple damage states based on overall or interstory drifts were implemented. Four parameters from the hysteresis model of degraded connection behavior were treated as structural uncertainties. Factorial analysis was performed to study the effect and significance of each parameter. It was concluded that only two parameters had a statistically significant effect on the response. Additional structural parameters included the material properties and the damping ratio. An ensemble of 9 simulated ground accelerations was considered an equally likely representation of ground motion at the site. The Latin Hypercube sampling was chosen to represent combinations of structural and seismic uncertainties in calculating the dynamic response. The responses were rank-ordered and plotted on lognormal

probability paper for each spectral acceleration level. The lognormal distribution parameters were determined from regression analysis and the maximum likelihood estimates (MLE). The seismic fragilities were then calculated from these probability functions.

Dumova-Jovanoska [2000] proposed the use of Modified Mercalli Intensity (MMI) scale as an earthquake intensity indicator in the development of fragility curves and damage probability matrices for reinforced concrete structures in Macedonia. A normal probability distribution was assumed for the damage measures and the validity of the fitted values was checked by the Chi-square test. Since the MMI could be regarded as a discrete intensity level, the fragility curves were depicted as a piece-wise combination of lines connecting between two MMI levels.

Hwang et al. [2000] further simplified the statistical process by forgoing a process of calculating exceeding probability for each PGA level. Instead, an overall relationship between the damage measures and ground-shaking parameters (PGA or S_a) was set up through a regression analysis. Using the Latin Hypercube technique, 100 unscaled earthquake samples and 10 structure samples were combined and a total of 100 earthquake-structure samples were established. Dynamic analyses of these sample resulted in 100 pairs of PGA (or S_a) and damage measures and the functional relationship is established through a regression analysis. Both demand and capacity of the structure is assumed to follow a lognormal probability density function. Probabilities of demand exceeding capacity or fragility can be calculated as a function of seismic intensity.

More recently, similar approach was proposed by Cornell et al. [2002]. It was assumed in this study that structural uncertainties remained deterministic following the

notion that uncertainties in the loadings were much more pronounced in the case of earthquakes. A single structure was subjected to a collection of unscaled ground motions. A relationship between the median of the drift demands (responses) and corresponding spectral accelerations (seismic intensity) of the earthquakes were approximated by a power function. Parameters of this power function were estimated from a regression analysis of nonlinear dynamic results. Dispersions of the drift demands given S_a were measured assuming a lognormal distribution of the drift demands. As a result, the fragilities or the probability of exceeding certain values of drift demands given S_a were easily obtained based on the lognormality assumption.

It can be observed that there is dissimilarity among the past research in the selection of the probability density functions for fitting the sampled seismic responses. The probability distributions considered by the researchers include the lognormal distribution (by Hwang and Huo [1994a, 1994b], Seya et al. [1993], Shinozuka et al. [2000a, 2000b], Song and Ellingwood [1999], and Cornell et al. [2002]), the normal distribution (by Dumova-Jovanoska [2000]), and the Extreme Type I distribution (by Jaw and Hwang [1988]). Questions arise on the issue of which type of distributions provides the best estimates and whether the best estimate is a close representation of the real probabilistic description of the response. Unlike the past research, this thesis presents an alternative means for deriving the exceedance probabilities of the seismic response from a straightforward Monte Carlo simulation in which an assumption for a specific density function is of no use.

In summary, for analytical fragility curves, there are two ways of computing probabilities of damage. The most direct and accurate means uses Monte Carlo technique

to simulate a large number of random samples and calculate probability essentially by counting the actual outcomes. This is a brute-force method that provides accurate values of probability of damage, but is very computational expensive. Another means uses a sampling technique such as a Latin Hypercube to simplify the random simulation process. It significantly reduces the number of samples to a manageable level and approximates the probability values by curve-fitting a small number of responses to an assumed probability distribution. However, probabilities of exceeding a certain limit state are based on limited data and may not represent the actual outcomes. Graphical representations of the two processes (Figure 2.3) are equivalent to that used by Fox [1994] to describe the methods in probabilistic design system. According to Figure 2.3, method (a) applies a more accurate Monte Carlo to an accurate but complex representation of seismic response analysis. Method (b) applies an inaccurate Latin Hypercube sampling technique to an accurate seismic analysis model.

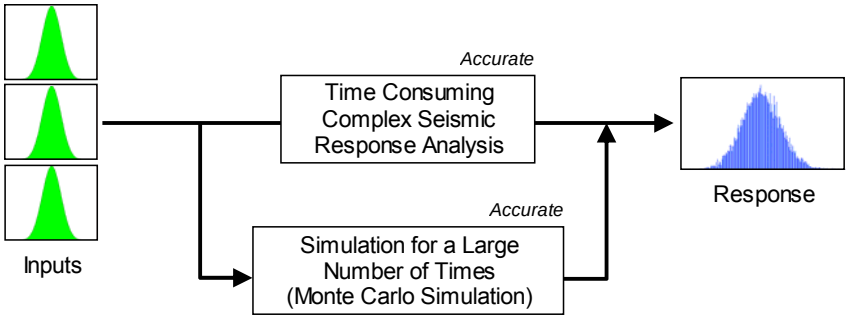

(a)

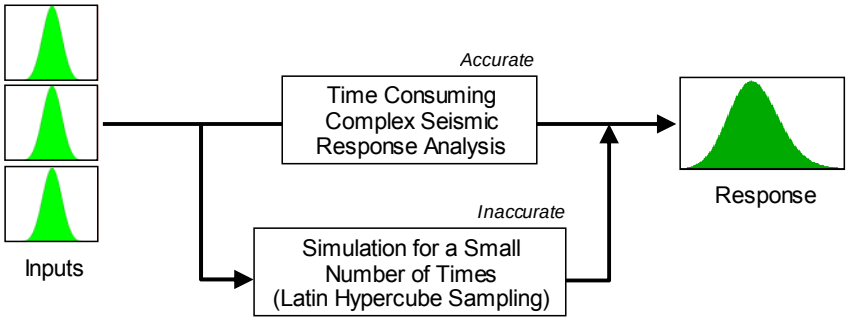

(b)

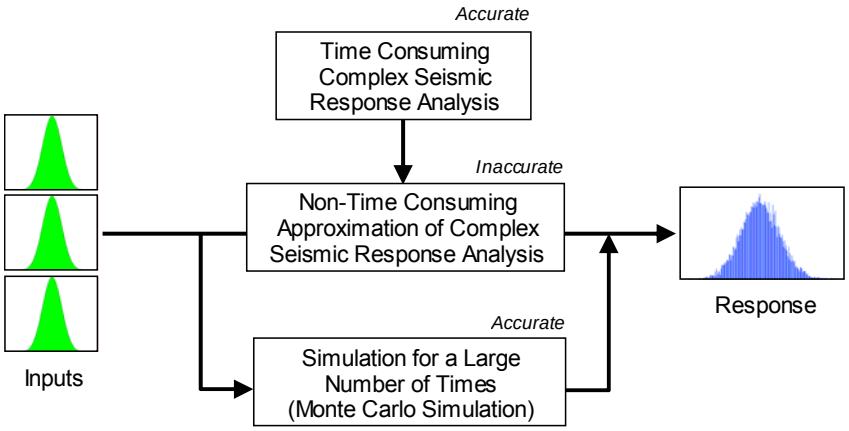

(c)

Figure 2.3: Methods for Computing Probability Density of Responses

This thesis explores an alternative means of simplifying the fragility calculation process. The existing method uses a sampling technique to simplify the process of simulating complex seismic analyses and, hence, approximates the probabilistic characteristics of the seismic responses by fitting limited data to a particular probability distribution. On the other hand, this thesis proposes an effective means to approximate the seismic response analysis using metamodels (Figure 2.3c). Since the models become more computational tractable, the direct Monte Carlo simulation can be applied to the approximated model (metamodel) and the probability of exceeding certain levels can be calculated independent of any specific density function. Detailed development of the metamodels and approaches for computing building seismic fragilities are presented in Chapter 3.

CHAPTER 3

RESPONSE SURFACE METAMODELS IN FRAGILITY CALCULATION

The previous chapter presents the conventional means of generating analytical fragility curves. Sampling techniques have been used for approximating a brute-force simulation of complex seismic response analyses (Figure 2.3b). A problem arises when the probability distribution derived by fitting a small number of data points may not be representative of the actual population of the responses. Instead of trying to approximate the density function of the responses, this thesis proposes an approach for approximating building seismic responses in a closed-form fashion (Figure 2.3c). The probability distribution of the response can be analytically derived from the functional relationship of the random input variables. However, such derivation is generally difficult especially when the function is nonlinear. As an alternative, a Monte Carlo simulation can be naively performed on an approximated model with little computational cost to obtain the probability distribution of the response. The use of a metamodel (or model of a model) technique in conjunction with Monte Carlo technique for approximating seismic fragilities is presented in detail.

3.1 DEFINITION OF METAMODELS

In most cases, the exact relationship between a response and a set of input variables that influence the response is implicit and the response has to be computed by running a "black box" complex computer code. In many circumstances, however, computational expense of running computer analysis codes may become prohibitive when a large number of models are involved.

A metamodel is a statistical approximation of the complex and implicit phenomena. Response is estimated in a closed-form function of input variables which is computationally simpler to run. If the true but unknown relationship between response (y) and a vector of input variables (ξ) in nature is represented as

$$y = f(\xi) \tag{3.1}$$

Then a metamodel g (ξ) is sought to approximate the true relationship f (ξ). The relationship between y and ξ becomes

$$y = g(\xi) + \varepsilon \tag{3.2}$$

where ε represents a total error term. This error term is the sum of a lack-of-fit or bias error (ε_{bias}) resulting from approximation of f (ξ) with g (ξ) or an approximation of the reality and a random error (ε_{random}) due solely to experimental and observational error (i.e., repeating experiments at a specific set of ξ produces different values of y). The error term is assumed to be a zero-mean random variable. However, the random error term (ε_{random}) does not exist in the case of computer analysis where repeated analytical evaluations of ξ always yield the same value of y. Expectation of the response function is in the form

$$E[y] = g(\xi) \tag{3.3}$$

which can be derived by running computer analysis codes at predefined levels of ξ (i.e., experimental designs), observing responses, and fitting data to an appropriate model.

Construction of metamodels generally involves 3 main steps: (1) choosing an experimental design for selecting a set of ξ for observing or running analysis for y, (2) choosing a functional form of g (ξ) for metamodel representation, and (3) fitting the model to the observed data. Several options in each step result in various approximation techniques that can be used as metamodels, as shown in Figure 3.1. Typical metamodels include polynomial regression models of complex analyses based on experimental designs (e.g., the response surface methodology), artificial neural networks, kriging or inductive learning metamodels.

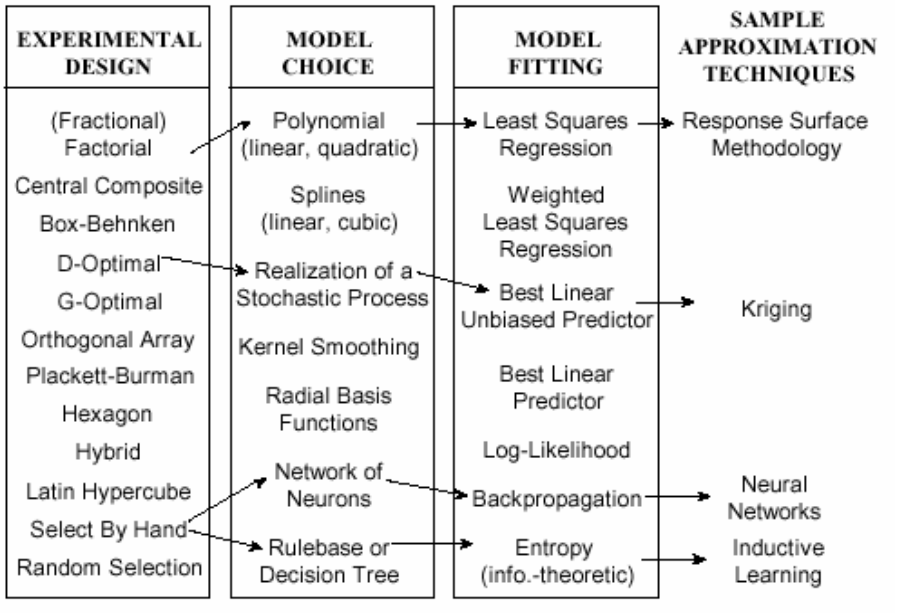

Figure 3.1: Steps for Constructing Metamodels [Simpson et al., 2001]

3.2 THE RESPONSE SURFACE METHODOLOGY

One of the most widely-used metamodels is the Response Surface Methodology (RSM). The origin of the RSM can be traced back to the works done by several researchers in the early 1930's or even earlier. However, it was not until Box and Wilson [1951] formally developed the methodology to determine the optimal condition in the chemical investigations. Since then, the RSM has been successfully applied in many different fields of study such as chemical engineering, industrial engineering, manufacturing, aerospace engineering, structural reliability, and computer simulation.

Response Surface Methodology refers not simply to the use of a response surface as a multivariate function but also to the process for determining the polynomial coefficients themselves. A response surface equation is simply a polynomial regression to a data set. The process is straightforward if a sufficiently large data set is available, that is if the number of members in the data set is at least as large as the number of coefficients in the polynomial. On the other hand, if the data set must be determined and if the process is time-consuming and computationally expensive, then the overall usefulness of the method will depend on the use of an efficient method for selecting the fewest possible members. Design of Experiments (DOE) techniques provide the needed basis for this critical step in the methodology.

3.2.1 Design of Experiments

As per the general 3 steps of constructing metamodels, the first step is to generate an appropriate experimental design. The experimental design systematically defines an

efficient set experimental sampling points at which the responses must be computed or observed. There are many types of experimental design that can be used for this purpose [Montgomery, 1997], but the most common ones are a Full Factorial design (FFD) and a Central Composite design (CCD).

The DOE takes levels of input variables to systematically formulate different combinations at which the outputs are observed or computed. In the DOE domain, it is more convenient to use the "coded" or "standardized" input variables (x_i) instead of their actual values (ξ_i). For example, let's assume that the actual input variables ξ_i has a region of interest defined by the lower and upper bounds $\xi_{i,low}$ and $\xi_{i,high}$, respectively. The coded variable x_i can be calculated as

$$x_i = \frac{\xi_i - \frac{\xi_{i,high} + \xi_{i,low}}{2}}{\frac{\xi_{i,high} - \xi_{i,low}}{2}} \tag{3.4}$$

This coded variable x_i has a value of -1 for the lower level, a value of 0 for the mid-level, and a value of +1 for the high level. In some cases, the experimental design may include variable levels that locate outside the original range. It results in coded values below -1 or above +1. An example of this type of experimental design is the CCD, which will be explained in the subsequent paragraphs.

Choosing meaningful ranges for the input variables must be done with great care. On the one hand, the ranges should be large enough to include all possible parameter spaces. On the other hand, the ranges cannot be so large that they reduce the prospect of a good regression fit of the response surfaces to the actual response.

The simplest experimental design for collecting observations is the Full Factorial Design (FFD) or the 3^k Factorial Design. In this arrangement, each input variable is assumed to take on 3 different values, which when equally spaced, produces the coded values –1, 0, and +1. It is required, in the FFD, that the responses are observed at all possible combinations of the levels of k input variables which have three levels each. The total number of variable level combinations (design points) becomes $N = 3^k$ points which can be impractically large, especially when a large number of input variables are under study or when the experiments are costly.

An unmanageable number of experiments required in the FFD leads to an introduction of the designs that require fewer design points, while maintaining acceptable accuracy in the prediction. Perhaps the most popular class of designs used in a second-degree model is the Central Composite Design (CCD). This consists of

(1). a complete 2^k factorial design, where the variable levels are coded to the usual -1 and +1 values. This is called the factorial portion or "cube" points of the design.

(2). Two axial points on the axis of each design variable at a distance of α from the design center. This portion is called the axial portion or "star" points of the design.

(3). n_0 center points ($n_0 \geq 1$).

Selection of the location of the axial or star points prompts further discussion since it affects the rotatability property of the CCD. Rotatability in the designs ensures that the variance of the estimated response is constant at a fixed distance from the center point. The CCD is considered rotatable if

$$\alpha = (2^k)^{1/4} \tag{3.5}$$

It is obvious that α is always greater than unity, which makes the star points located outside the original range. As a result, each input variable has to be evaluated at 5 levels ($-\alpha$, -1, 0, +1, and $+\alpha$). This may not be practical in some instances where it is physically difficult or impossible to extend the experiment beyond the region defined by the upper and lower limits of each input variable. In addition, this research seeks an efficient method with less computational effort as possible. The rotatability requirement can be dropped in such cases and the distance α is set at 1. Results from such a design prove that the response surface model provides good prediction even without the rotatability property.

The replications of the center points provide a means for estimating pure experimental error. However, this type of error does not exist in the computer analysis. Hence, only one replicate of the center point is required. As a result, the total number of distinct design points is $N = 2^k + 2k + 1$. Comparison in the number of experiments required by the FFD and the CCD is shown in Table 3.1. Graphical layouts of the FFD and the CCD (with $\alpha = 1.0$) considering 3 input parameters are displayed in Figure 3.2.

Table 3.1: Number of Experimental Samples for Different DOEs

DOE	Equation	3 Variables	5 Variables	7 Variables
Full Factorial Design	3^k	27	243	2187
Central Composite Design	$2^k + 2k + 1$	15	43	143

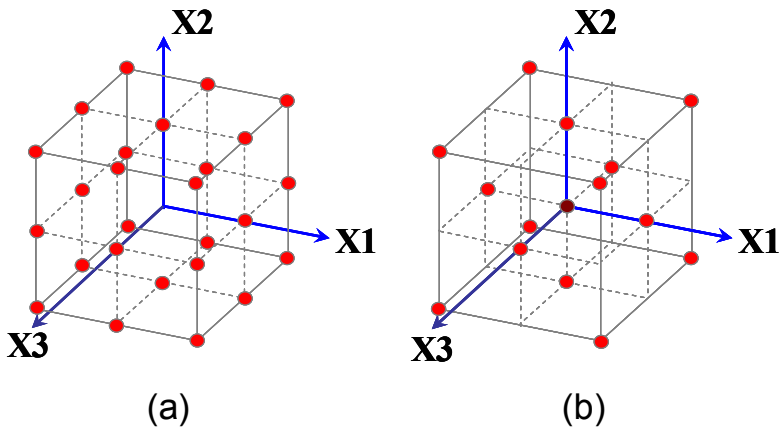

Figure 3.2: Graphical Layout of (a) Full Factorial Design, and (b) Central Composite Design, for Three Variables

There are other experimental designs that can be used for response surface application such as the Box-Behnken design, the Space Filling design, Taguchi's orthogonal arrays [Simpson et al., 2001], etc. However, they are not as widely used as the FFD and the CCD.

3.2.2 Response Surface Model Fitting

After performing a set of experiments or computer runs to obtain outputs according to the experimental designs, the next step is to take the vectors of inputs (**x**) and corresponding outputs (y) for fitting an appropriate model.

The most widely used response surface function is a mathematical polynomial function. Typical response surface model limits the order of polynomial to one or two since low-degree models contain fewer terms than higher-degree models and thus require fewer experiments to be performed. In the case of seismic analysis, the responses usually exhibit nonlinear behaviors; hence, the second-order polynomial is considered as a

response surface model in this research. The response function considering second-order polynomial model is as follows:

$$y = \beta_0 + \sum_{i=1}^{k} \beta_i x_i + \sum_{i=1}^{k} \beta_{ii} x_i^2 + \sum_{i=1}^{k-1} \sum_{j>i}^{k} \beta_{ij} x_i x_j + \varepsilon \tag{3.6}$$

where

y	=	Response or dependent variable
x_i , x_j	=	The coded input or independent variables
β_0 , β_i , β_{ii} , β_{ij}	=	Unknown coefficients to be estimated
ε	=	Bias or lack of fit error term
k	=	Number of input variables

Even though the response surface function in (3.6) contains higher-order terms, it is still considered as a linear regression model. Alternatively, the model can be written in the form of general linear model as follows:

$$y = \beta_0 + \sum_{i=1}^{p-1} \beta_i z_i + \varepsilon \tag{3.7}$$

where p is the number of parameters to be estimated. A vector of dummy first-order variables **z** replaces the original input variable **x** that contain quadratic terms. For example, a response function with 2 input variables (x_1 and x_2) which has the quadratic form of

$$y = \beta_0 + \beta_1 x_1 + \beta_2 x_2 + \beta_{11} x_1^2 + \beta_{22} x_2^2 + \beta_{12} x_1 x_2 + \varepsilon \tag{3.8}$$

can be converted into a general linear regression model as

$$y = \beta_0 + \beta_1 z_1 + \beta_2 z_2 + \beta_3 z_3 + \beta_4 z_4 + \beta_5 z_5 + \varepsilon \tag{3.9}$$

It can be seen that the dummy variables z_1, z_2, z_3, z_4, and z_5 are equivalent to the original variables x_1, x_2, x_1^2, x_2^2, and x_1x_2, respectively. The regression model becomes linear both in terms of parameters and independent variables.

A general matrix form of the linear model can be written as

$$\mathbf{Y} = \mathbf{Z\beta} + \boldsymbol{\varepsilon} \tag{3.10}$$

where

$$\mathbf{Y} = \begin{bmatrix} y_1 \\ y_2 \\ \vdots \\ y_N \end{bmatrix}_{N\times 1} \quad \text{is a vector of actual responses,}$$

$$\mathbf{Z} = \begin{bmatrix} 1 & z_{11} & z_{12} & \cdots & z_{1,p-1} \\ 1 & z_{21} & z_{22} & \cdots & z_{2,p-1} \\ \vdots & \vdots & \vdots & & \vdots \\ 1 & z_{N1} & z_{N1} & \cdots & z_{N,p-1} \end{bmatrix}_{N\times p} \quad \text{is a matrix of constant,}$$

$$\boldsymbol{\beta} = \begin{bmatrix} \beta_0 \\ \beta_1 \\ \vdots \\ \beta_{p-1} \end{bmatrix}_{p\times 1} \quad \text{is a vector of unknown parameters, and}$$

$$\boldsymbol{\varepsilon} = \begin{bmatrix} \varepsilon_1 \\ \varepsilon_2 \\ \vdots \\ \varepsilon_N \end{bmatrix}_{N\times 1} \quad \text{is a vector of error terms with expectation } E[\varepsilon] = 0.$$

Consequently, a random vector **Y** has expectation of

$$\mathbf{E}[\mathbf{Y}] = \mathbf{Z}\boldsymbol{\beta} \tag{3.11}$$

The parameters of the polynomials are usually determined by a least squares regression analysis by fitting to existing experimental data points. The method of least squares selects the values (b_0, b_1,…, b_{p-1}) for unknown parameters (β_0, β_1,…, β_{p-1}) such that they minimize the sum of squares of the differences between the actual output (y) and the approximated or fitted outputs ($\hat{y}$). Mathematically, the least squares method minimizes

$$S(\mathbf{b}) = \sum_{u=1}^{N} \left(y_u - \hat{y}_u(\mathbf{b})\right)^2 \tag{3.12}$$

where S is defined as the sum of squares function, N is the number of experimental points (N > p), and **b** is a vector of least squares estimates of parameters $\boldsymbol{\beta}$.

The estimates of the polynomial parameters can be obtained by solving the following matrix equation

$$\mathbf{b} = \left(\mathbf{Z}'\mathbf{Z}\right)^{-1}\left(\mathbf{Z}'\mathbf{Y}\right) \tag{3.13}$$

in which its derivation can be found in Chapter 3 of Box and Draper [1986]. The fitted response surface function becomes

$$\hat{y} = b_0 + \sum_{i=1}^{k} b_i x_i + \sum_{i=1}^{k} b_{ii} x_i^2 + \sum_{i=1}^{k-1} \sum_{j>i}^{k} b_{ij} x_i x_j \tag{3.14}$$

The use response surface methodology in connection with Monte Carlo simulation simplifies the process of generating fragility curves. Since the simulations are not performed on complex structural analyses, but rather on a polynomial equation, a lot

of computational time can be saved. The probability of damage conditional on seismic intensity can be calculated from the simulation results and fragility curves can be constructed.

3.2.3 Statistical Validation of Response Surface

Least-square regression analysis gives the parameter estimates for the response surface function. The next step is to evaluate an adequacy of fit of the model. There are a number of statistical measures that can be used to verify linear regression models. However, statistical testing is inappropriate in the cases where outputs are computed by deterministic computer runs and random error (ε_{random}) does not exist [Welch et al. 1990, Simpson et al. 2001]. The simplest measure for verifying model adequacy in deterministic computer experiments is the coefficient of determination (R^2).

$$R^2 = \frac{SSR}{SST} \tag{3.15}$$

where

$SSR = \mathbf{b}'\mathbf{X}'\mathbf{Y} - \frac{(\mathbf{1}'\mathbf{Y})^2}{N}$ is the Error Sum of Squares,

$SST = \mathbf{Y}'\mathbf{Y} - \frac{(\mathbf{1}'\mathbf{Y})^2}{N}$ is the Total Sum of Squares, and

$\mathbf{1}'$ is a 1 x N vector of ones.

The value of R^2 characterizes the fraction of total variation of the data points that is explained by the fitted model. It has a value between 0 and 1 (with 1 being a perfect

fit). However, the R^2 can be misleading in some cases since it always increases as more input variables are added. An adjusted-R^2 (R_A^2), which takes into account the number of parameters in the model, is introduced for evaluating the goodness-of-fit of the model. It can be computed as follow.

$$R_A^2 = 1 - \left(1 - R^2\right) \cdot \left(\frac{N-1}{N-p}\right) \tag{3.16}$$

The value of R_A^2 close to unity indicates a good fit of the response surface model to the experimental data points. Papila and Haftka [2000] suggested the value of R^2 (or R_A^2) of at least 0.9 to ensure adequate approximation of the model.

Even though the R_A^2 value explains how well the model fits to the experimental points, the value does not, however, reflect the prediction potential of the model to other points not used to generate model. In order to verify the overall accuracy of the response surface models, statistical tests at additional random data points in the design space must be performed. Those tests include the Average Absolute Error (%AvgErr), the Maximum Absolute Error (%MaxErr), and the Root Mean Square Error (%RMSE) [Venter et al., 1997]. These measures are defined as follow.

$$\%\text{AvgErr} = 100 \cdot \frac{\frac{1}{N} \cdot \sum_{i=1}^{N} \left| y_i - \hat{y}_i \right|}{\frac{1}{N} \cdot \sum_{i=1}^{N} y_i} \tag{3.17}$$

$$\%\text{MaxErr} = \underset{i}{\text{Max}} \left[100 \cdot \frac{\left| y_i - \hat{y}_i \right|}{\frac{1}{N} \cdot \sum_{j=1}^{N} y_j} \right] \tag{3.18}$$

$$\%\text{RMSE} = 100 \cdot \frac{\sqrt{\frac{1}{N} \cdot \text{PRESS}}}{\frac{1}{N} \cdot \sum_{i=1}^{N} y_i} \tag{3.19}$$

where

$$\text{PRESS} = \sum_{i=1}^{N} \left(y_i - \hat{y}_i \right)^2$$

Finally, in addition to the use of these measures, visual assessment of the residual and the correlation plots may be helpful in determining model accuracy.

3.3 PAST APPLICATIONS

While the application of a response surface methodology to determine fragility curves is novel, it is not uncommon in other applications. Response surface metamodel applications have been extensively employed over the past decade in the area of aerospace system design and structural reliability.

3.3.1 Applications in Aerospace System Design

The pioneering uses of the response surface are to approximate higher fidelity analyses at an early point in the design of an aerospace system when there is not enough detail to support such analyses. The goal of the preliminary design of aerospace systems is to determine a set of design parameters that optimizes the performance of a system. The optimization process usually involves iterative analyses of complex structural systems that quickly becomes computationally prohibitive. A response surface concept is utilized in this context to approximate complex system analyses and convey what a particular design will deliver.

Engelund et al. [1993] conducted an investigation to determine a set of optimal aerodynamic configuration design parameters for a space transportation system. The design of such a vehicle is a complex process even at the conceptual level. The response surface methodology was used to optimize a set of configuration parameters in order to achieve minimum vehicle dry weight, while maintaining other constraints. Mavris and Bandte [1995] and Mavris et al. [1996] carried out an economic uncertainty assessment of a High Speed Civil Transport (HSCT) using a combined response surface methodology and Monte Carlo simulation approach. Response surface for the average yield per Revenue Passenger Mile is constructed as a function of seven input variables. An uncertainty assessment using the Monte Carlo simulation is performed on the response surface model. DeLaurentis et al. [1996] incorporated a response surface equation in place of a complex aerodynamic analysis in a preliminary aircraft design in order to more efficiently search the design space for optimum aircraft configurations.

3.3.2 Applications in Structural Reliability

A general structural reliability problem considers a probability of failure of a structural system. Failure occurs when a limit state function reaches a certain predefined values. However, the limit state functions generally cannot be explicitly represented by closed form solutions. Response surface methodology has been used in this field for approximating these implicit limit state functions. Examples of application are shown as follow.

Bucher and Bourgund [1990] were among the first researchers to introduce an application of the response surface methodology in the field of structural reliability. The method is used to approximate limit state conditions of a nonlinear single-degree-of-

freedom oscillator and a frame structure. Good quality of the response surface prediction was observed. Rajashekhar and Ellingwood [1993] then evaluated an existing response surface approach in structural reliability analysis and proposed a way for selecting experimental points at the distribution extremes instead of the entire range of the distributions. Numerical examples were given to confirm an efficiency of the approach. Rajashekhar et al. [1996] compared the reliabilities, for various limit states, of reinforced concrete slabs by response surface approach with reliabilities obtained using traditional approaches. Yao and Wen [1996] extended the study into a time-variant problem. The research described a reliability calculation of structures under earthquake loads. A response surface methodology is utilized in approximating the maximum system response and providing an explicit limit state function. A method for measuring the accuracy of the response surface approximation was also presented.

Response surface methodology was found to provide good approximation of the complex analysis code both in the case of aerospace system design and structural reliability calculation. These successful applications have led to an idea that the method could be useful in other fields where complex and implicit analysis code can be replaced by a simple response surface function. Seismic fragility analysis of buildings typically requires repetitive runs of dynamic analysis code in order to obtain reliable damage statistics and it easily becomes computationally prohibitive. This research implements the response surface concept for predicting building damage (responses) due to earthquake loadings. The approaches are described as follows.

3.4 APPROACHES FOR CALCULATING BUILDING FRAGILITY

Building seismic fragility describes the likelihood of damage to a building due to various levels of earthquakes. It takes into account randomness in earthquake loadings and uncertainties in the structural characteristics (e.g., strength, modulus) for deriving probabilistic descriptions of the damage. Seismic fragility assessment requires repeated damage simulations of a building with random properties subjected to random earthquake inputs. Each realization of seismic damage is carried out either through a time-history or a pushover analysis. It usually becomes impractical because of the large number of time-consuming analyses needed to obtain reliable statistics of the outcomes. A response surface metamodel is sought to approximate an implicit building seismic damage computation using an explicit polynomial function. Monte Carlo simulation is then performed over the simpler metamodel instead of the complex dynamic analyses. The process for calculating seismic fragility based on the use of response surface metamodels is described in the subsequent paragraphs.

Figure 3.3 depicts a general process for generating fragility curves utilizing response surface metamodel concept. The first step is to define the input and output (or response) variables for the response surface. An appropriate building response or damage measure, such as a peak inter-story drift, is defined as an output variable. Random building parameters characterizing response calculation are used as input variables, and the applicable range of each input variable is defined. When a large (generally more than 5) number of input variables are identified, a screening process is generally used to determine the subset of variables that have the largest influence on the output (response). A DOE technique is utilized for selecting an efficient set of input

variable combinations (experimental sampling). Finally, a seismic intensity measure is defined, and the ground motion records in an ensemble are scaled such that they have the same level of intensity.

Next, detailed computational analysis is performed on a building model constructed to represent one combination of input variables defined by the DOE step. Each of the scaled acceleration records is used as loading input for this analysis, and the chosen seismic response (e.g., interstory drift, peak drift, peak acceleration, etc) is extracted from each analysis run. The process is repeated for each combination of input variables defined in the DOE step. Least-square regression analysis is then performed over the sampled input data points and corresponding outputs to form a polynomial response surface function. This response surface model is computationally inexpensive. Monte Carlo techniques with a large number of simulations can be carried out using probability density functions for the input variables. Consequently, the probability of the chosen response exceeding certain damage limit states can be extracted from the simulation outcomes. This probability value is conditioned on a specific earthquake intensity level and represents one point in a fragility curve. Repetition of the process over different levels of earthquake intensity provides exceedance probability values at other intensity levels, and the fragility curves can be constructed.

The main advantage of the response surface metamodel is that while it provides an admittedly simple functional relation between the most significant input variables and the output (response), the model is computationally very efficient.

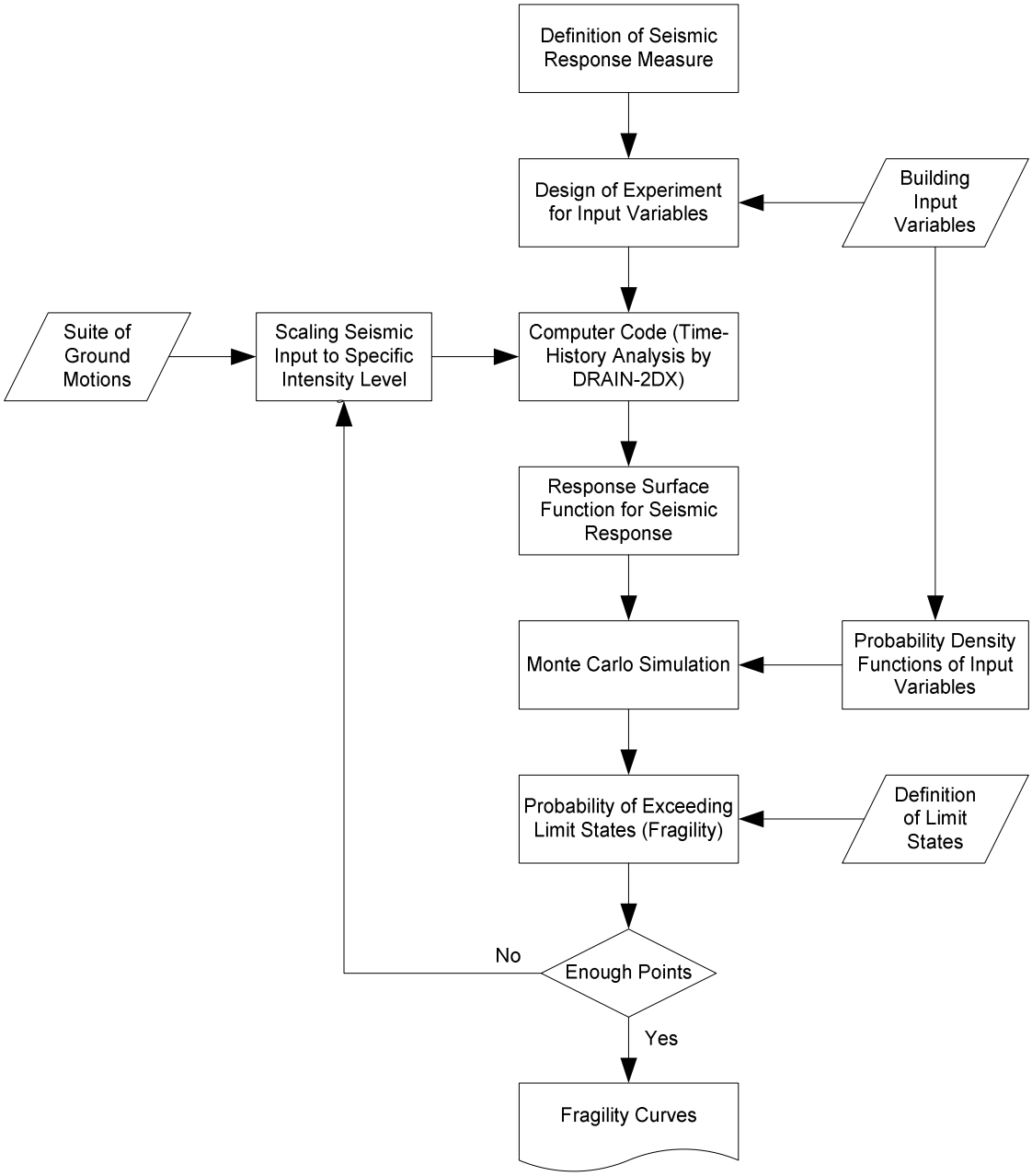

Figure.3.3: Process of Computing Seismic Fragility Using Metamodels

This research proposes 3 approaches for computing building seismic fragilities. Approach 1 and Approach 2 follow the general process shown in Figure 3.3. The main difference between the two approaches is on the way seismic uncertainties are treated. Approach 1 simply generates a response surface for each ground motion in a suite and they are randomly selected in the simulation process. On the other hand, Approach 2 makes use of the dual response surface concept [Lin and Tu, 1995] by generating response surfaces of the mean and standard deviation of building responses due to a suite of ground motions. Approach 3 further simplifies the process by adding a predictor variable describing the intensity of the earthquakes in the response surface metamodel. Details of the three approaches are given in the following paragraphs.

Approach 1 is the least efficient use of response surface in fragility computation. However, it follows closely the conventional notion in selection of earthquake loadings at random. The process starts by a general process of defining a suite of ground motions and its intensity measure. Each ground motion in the pool is then scaled to a specific level of intensity. In this approach, response surface models are generated for predicting building seismic response due to each individual ground motion in the suite as shown below.

$$\hat{y}_i = g_i(\mathbf{x}),\ i = 1..n,$$

where n is the number of ground motions. As a result, the number of response surface models is same as number of ground motions in the suite.

Monte Carlo technique is then applied not only for sampling to the probability density functions of the input parameters, but also in the random selection of response

surface metamodels to use. Response surface metamodels are chosen with equal probability based on an assumption that each earthquake is equally likely to occur. The process of random selection of the response surface functions implicitly takes into account randomness in earthquake inputs. Damage probabilities or fragilities can be extracted from a large number of trials.

Approach 2 is proposed to overcome an unwieldy process of generating response surface models for individual earthquakes in Approach 1. Approach 2 takes a concept of dual response surface [Lin and Tu, 1995] and implements in the fragility computation. In this approach, seismic responses due to all ground motions in the suite are computed at each experimental design point. These seismic responses are assumed to follow a specific probability distribution for each design point. Mean and standard deviation values of the response distribution are calculated. Dual response surface models for the mean and standard deviation of the building responses are generated, as shown in (3.20) and (3.21), respectively.

$$\hat{y}_{\mu} = g(\mathbf{x}) \tag{3.20}$$

$$\hat{y}_{\sigma} = h(\mathbf{x}) \tag{3.21}$$

The overall response surface model for predicting seismic demand becomes

$$\hat{y} = \hat{y}_{\mu} + Z(\mathbf{x}) \tag{3.22}$$

where $Z(\mathbf{x})$ represents a random departure from the predicted mean response due to randomness in earthquakes. This random term is assumed to have a Normal distribution with zero mean and the standard deviation of $\hat{y}_{\sigma}$. Theoretically, samples from Normal distributions can fall in the negative range of the response, which is not meaningful in the

case of seismic demands. However, the probability of this event was found to be very small and had little impact on the response statistics computed from (3.20) and (3.21). The normality assumption is validated in the subsequent sections.

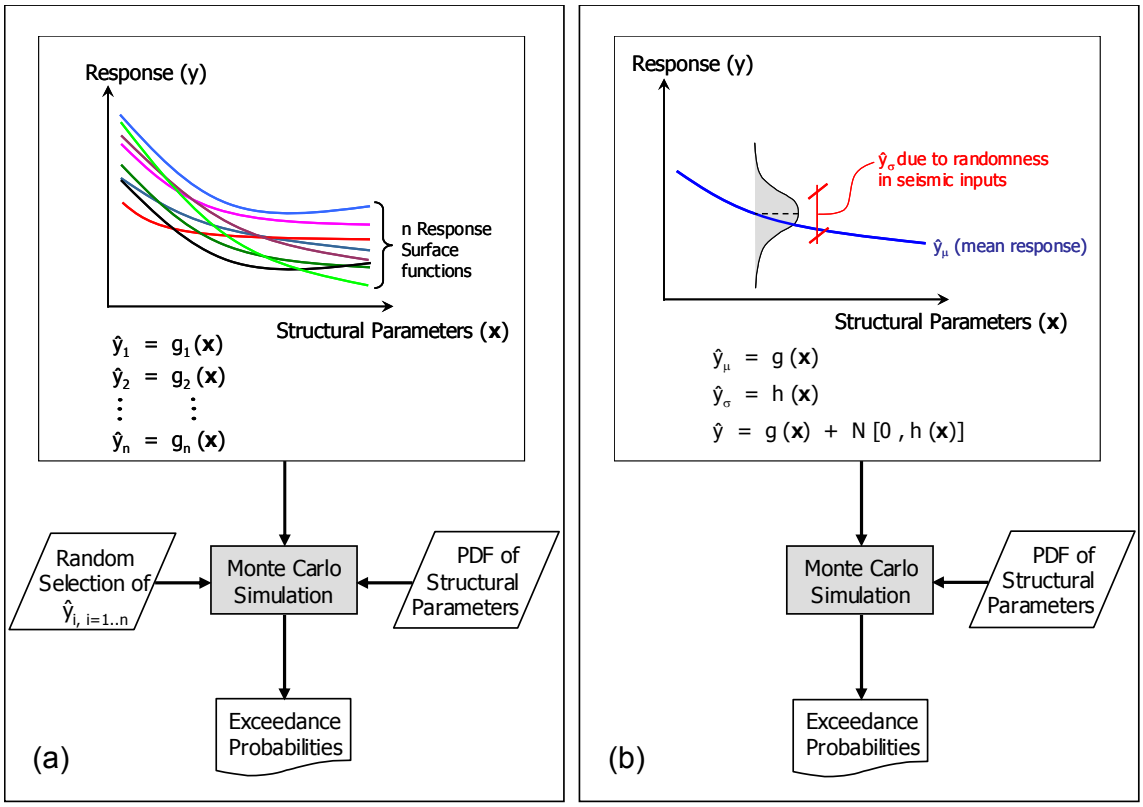

Figure 3.4: Graphical Layouts of the Implementation of (a) Approach 1, and (b) Approach 2

Graphical layouts of Approach 1 and Approach 2 are shown in Figure 3.4. For simple representation, each response surface model is shown as a 2-dimensional plot of the response (y) in a vertical axis and a vector of structural parameters (**x**) in a consolidated horizontal axis. The two approaches differ in the process of building the

metamodels, yet the use of the models are generally the same except that Approach 1 requires a random selection of the response surface models.

The downside of the proposed process (Figure 3.3) is the fact that the response surface is conditioned on a specific level of earthquake intensity. Hence, the entire process of generating the response surface models has to be repeated for different levels of earthquake intensity. Approach 3 is proposed as a modification of Approach 2 to overcome this weak point. In this approach, an earthquake intensity parameter (s) is included in the response surface model in addition to the structural uncertainty parameters (**x**). Figure 3.5 shows a schematic view of a response surface model in Approach 3. The seismic intensity parameter (s) is displayed as an added dimension to the plots between the response (y) and a vector of input parameters (**x**). Similar concept to Approach 2 with the dual response surfaces of the mean (3.23) and standard deviation (3.24) of responses is implemented in Approach 3.

$$\hat{y}_{\mu} = g(\mathbf{x}, s) \tag{3.23}$$

$$\hat{y}_{\sigma} = h(\mathbf{x}, s) \tag{3.24}$$

Hence, the overall response surface model can be shown as

$$\hat{y} = g(\mathbf{x}, s) + N[0, h(\mathbf{x}, s)] \tag{3.25}$$

where g(**x**,s) and h(**x**,s) are the response surface metamodels for predicting the mean and standard deviation of the building responses due to a suite of ground motions, respectively.

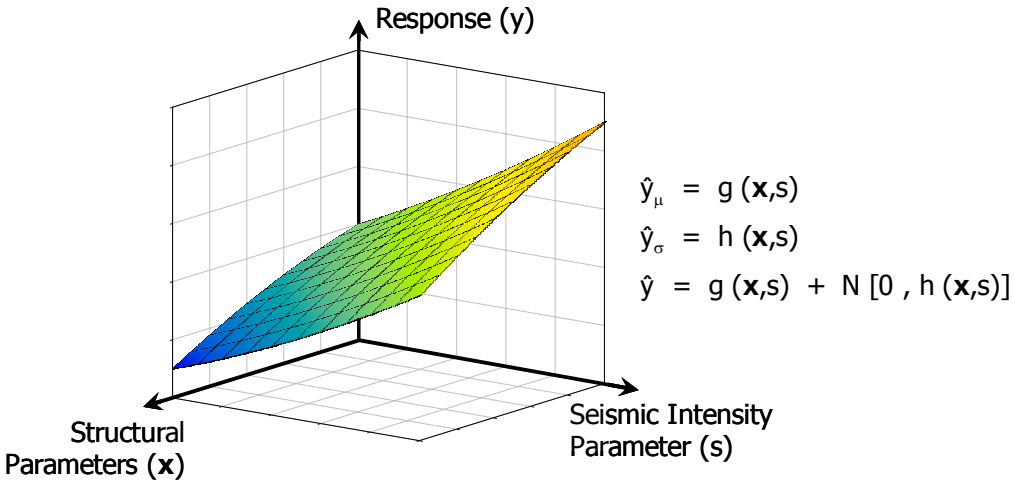

Figure 3.5: Graphical Layout of a Response Surface Model in Approach 3

The response surface developed in Approach 3 is not specific to a certain level of earthquake intensity. The computation of the response depends not only on the structural properties, but also on the level of seismic intensity. The required computational cost may increase in the initial metamodel building process due to the added parameter. However, the overall process is much more efficient since the needs for repetitive generation of response surface models are eliminated. Metamodels for different levels of seismic intensity can be obtained directly by evaluating the response surface at specific values of intensity measures.

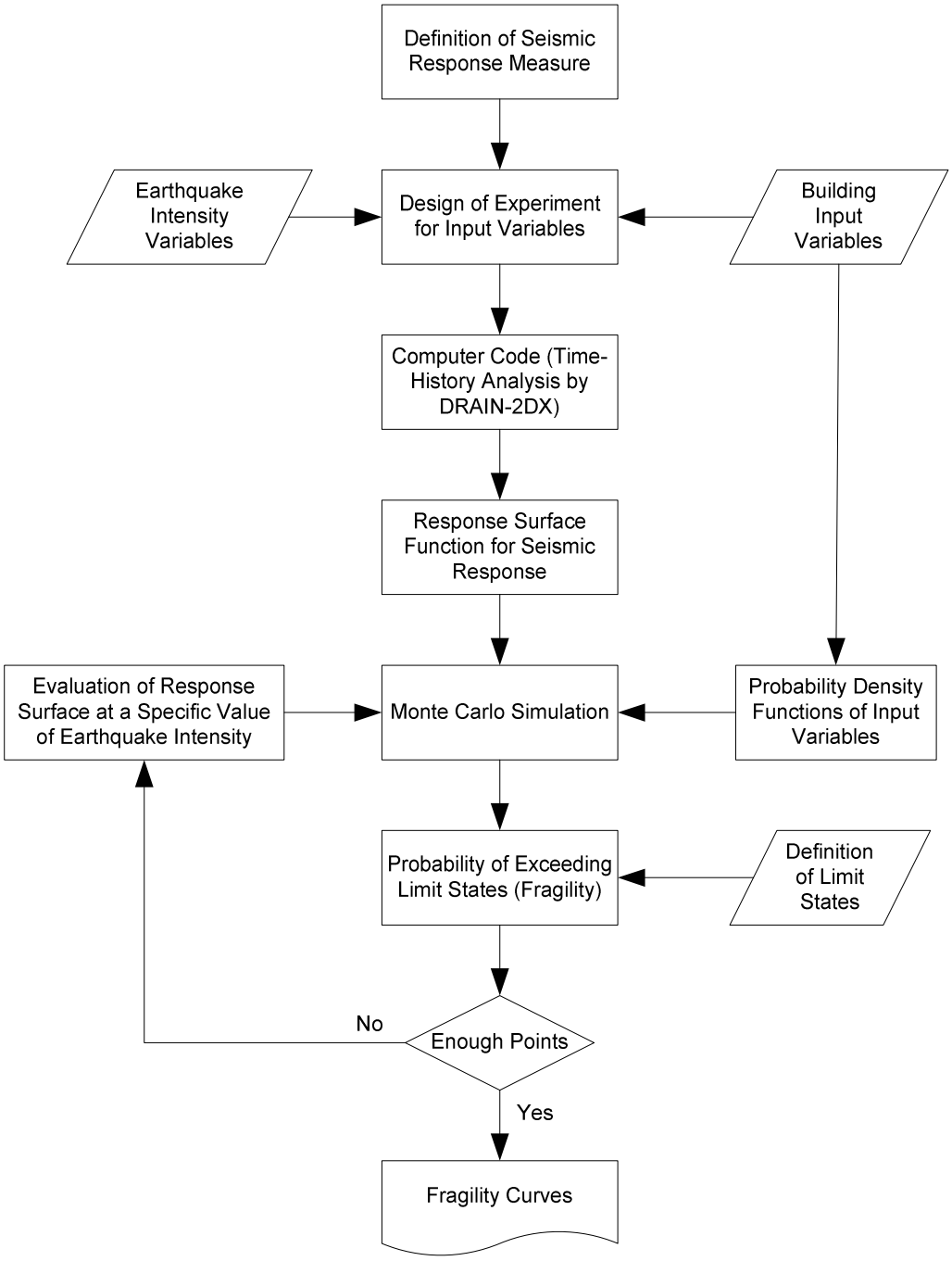

Figure.3.6: Modified Fragility Computation Process for Approach 3

The general process of constructing fragility curves is modified for Approach 3, as shown in Figure 3.6. Processes for building a response surface begin in a similar fashion as previous approaches, except that a Design of Experiments table is constructed based on both structural uncertainty parameters and seismic intensity parameter. One can view a seismic intensity parameter as a control variable and structural parameters as random variables in a response surface function. A control variable is fixed at a certain level of earthquake intensity while the random variables are varied according to their probability distribution in a Monte Carlo simulation. Damage probabilities obtained from the simulation are, in turn, conditioned on that particular level of intensity. In order to draw a fragility curve, the process is repeated at a simulation level by adjusting the control variable or seismic intensity parameter to other intensity values. It becomes computationally much cheaper than repetitively building many response surfaces as in Approach 1 and Approach 2.

Implementations of Approach 1, 2, and 3 for computing probabilistic descriptions of seismic response of a simple system are shown in the next section.

3.5 IMPLEMENTATION OF THE APPROACHES: SDOF SYSTEM

For the purposes of demonstrating and comparing the three proposed approaches, a simple structure is chosen as an example. Derivations of probabilistic response of a linear-elastic single-degree-of-freedom (SDOF) system are presented in detail. Even though the structure in this case is so simple that the benefit of using the metamodels will not be fully appreciated, its simplicity, however, makes it possible that the approach validation can be done through the conventional and time-consuming method.

3.5.1 Description of the Structure

A rather simple structural model that can be used in a seismic response analyses is the nonlinear spring-mass SDOF system. The system is composed of a spring with an elastic stiffness (k) and yield force or strength (F_y) connecting a lumped mass (m) to the ground as shown in Figure 3.7. Damping characteristic of the system is represented by a Rayleigh-type damping, which is proportional to mass and stiffness of a structure. For a SDOF system, a damping ratio can be computed as

$$\zeta = \frac{a_0}{2} \cdot \frac{1}{\omega_n} + \frac{a_1}{2} \cdot \omega_n \tag{3.26}$$

where $\omega_n = \sqrt{\frac{k}{m}}$ is the natural circular frequency of vibration of the SDOF system, and a_0 and a_1 are the mass and stiffness proportional damping coefficients, respectively.

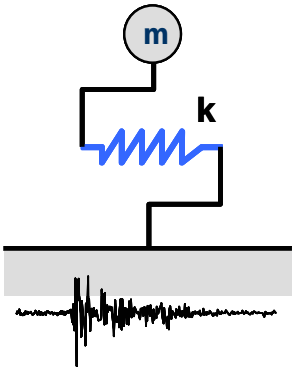

Figure 3.7: SDOF System and Hysteretic Behavior

A time-history dynamic analysis is implemented in this study for deriving structural responses. Time-dependent acceleration inputs are applied at the base of the

structure and the structural responses are obtained at each time step by numerical integration.

Maximum displacement of the SDOF system is chosen as a response measure for damage assessment. Fragility analysis requires that the computed responses are described probabilistically. This can be accomplished by simulating cases with random structural properties and earthquake inputs. Randomness in structural characteristics is described by the probability density function of each parameter. These random parameters are, in turn, used as input variables of the response surface model. In this study, the random parameters include mass, stiffness, damping, and strength of the SDOF system. However, since the damping ratio is dependent on mass and stiffness of the system (3.26), it is not used in the response surface models.

Table 3.2 summarizes the input variables and their assumed probabilistic density characteristics. Combinations of these structural properties represent SDOF structures with fundamental periods ranging from 1.2 to 3.1 seconds. A baseline structure is constructed using mean values of the structural properties. It has the mass of 8 kip-sec^2/in and the elastic stiffness of 80 kips/in resulting in a fundamental period of 2 seconds and a damping ratio of 0.03.

Table 3.2: Structural Properties and Probabilistic Characteristics

Random Parameters	Distribution	Min	Mean	Max
Mass, m (kip-sec^2/in)	Uniform	4	8	12
Strength, F_y (kips)	Uniform	400	500	600
Stiffness, k (kip/in)	Uniform	50	80	110

3.5.2 Selection of Earthquake Ground Motion Records

Uncertainty in seismic inputs is taken into account by the use of a suite of earthquake records. Ground motions in a suite should be obtained from historical seismic events in a region of interest. However, in the region with fewer seismic activities (e.g., Mid-America region), recorded events may be too scarce that available data are statistically insufficient. In this case, earthquake accelerograms are analytically synthesized considering local seismic source and soil properties of the region. A large number of simulations must be carried out to obtain sufficiently large samples. Ground motion records in the suite consequently possess randomness in epicentral distance, focal depth, magnitude, attenuation, and slip distribution. Wen and Wu [2001] developed a set of synthetic ground motion records for 3 Mid-America cities (i.e., Carbondale, Memphis, and St. Louis). Two groups of 10 acceleration records are generated for each city, with equal probabilities of occurrence in each group. In the end, there are a total of 60 synthesized acceleration records and they are used collectively in this research. Each record is systematically named based on its location and probability of occurrence. For example, the record "m02_10s" is the 6^{th} record generated for Memphis with 10% probability of occurrence. Examples of the time-history plots for these synthetic ground motions can be found in Wen and Wu [2001].

Typical earthquake intensity measures include the peak ground acceleration (PGA) and the spectral acceleration at a fundamental period of the structure (S_a). Selection of an appropriate intensity measure is based primarily on its correlation with the damage potential or, in this case, peak displacement. Correlation plots between peak displacement from the SDOF system and both intensity measures are shown in Figure 3.8

and Figure 3.9. It is apparent from these plots that spectral acceleration or S_a provides much higher correlation with structural response than that of the peak ground acceleration. As a result, S_a is chosen as a seismic intensity measure in this study.

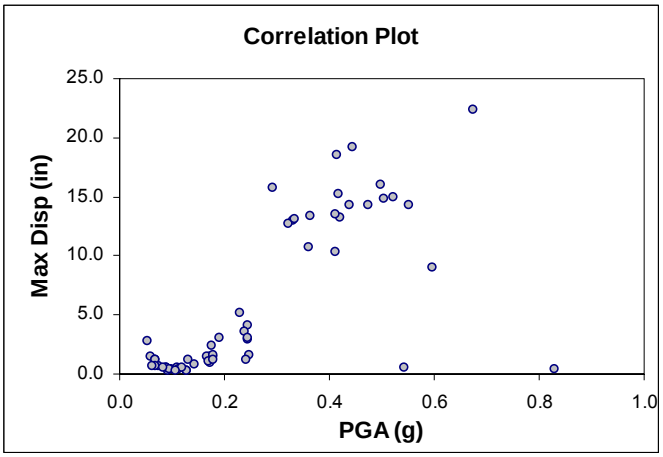

Figure 3.8: Correlation Plot between Maximum Displacements from the SDOF System and Peak Ground Acceleration (PGA) of the Ground Motion Records

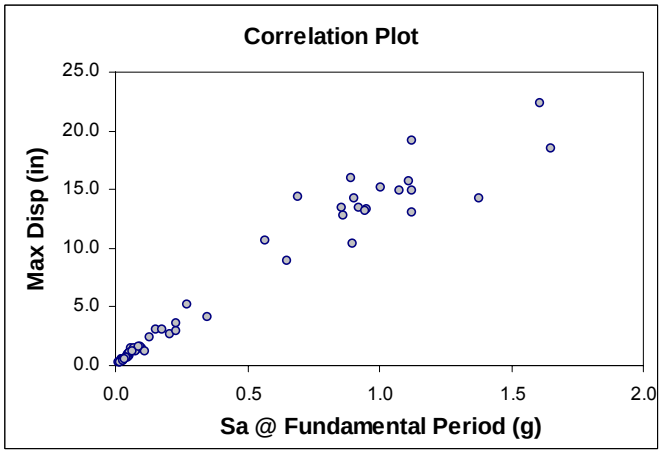

Figure 3.9: Correlation Plot between Maximum Displacements from the SDOF System and Spectral Acceleration (S_a) of the Ground Motion Records

The ground motion records in a suite are scaled such that they have the same level of earthquake intensity, that is a spectral acceleration (S_a) at a fundamental period of the baseline structure (2 seconds). For example, the i^{th} earthquake record has a spectral acceleration of $S_{a,i}$ is scaled such that its spectral acceleration becomes $S_{a,target}$. The scale factor for the i^{th} record is

$$F_i = \frac{S_{a,target}}{S_{a,i}} \tag{3.27}$$

The scaling of the ground motion records ensures that the damage probabilities calculated based on a suite of ground motions is conditioned on a specific seismic intensity level.

Based on the definition of a response or damage measure and an earthquake intensity measure, the fragility of this SDOF system for a given hazard level (0.4g) can be expressed following (2.1) as

$$PF_i = Prob\left[Max.Displ. \geq d_i \middle| \; S_a = 0.4g\right]$$

where PF_i is a fragility of performance or damage level i and d_i is a performance or damage threshold described in term of a maximum displacement.

Subsequent sections present detailed implementation of the 3 approaches in deriving probability distributions of the maximum displacement of a SDOF system.

3.5.3 Approach 1

Approach 1 generates response surface metamodels for approximating maximum displacement of the SDOF system under a specific earthquake motion. The number of response surface models is the same as the number of earthquake records in a suite.

Design of Experiments

Input variables for a response surface model generation are initially those that define randomness in structural properties (Table 3.2). Variable or design space is formed by defining an operating range of each input variable in a way that the range covers most of the area under the probability density of the structural parameter. For this particular example, since each random parameter is uniformly distributed over a finite region, design space is defined according to each parameter's probability distribution. Selection of the location of the center point for each variable space is less relevant in the case of seismic response analysis since much higher variability exists in earthquake than that in structural properties. Mean values of the structural parameters are used as center points. Finally, each parameter is normalized using (3.4) to have its range between -1 and +1. These normalized variables are used for formulating a Design of Experiments (DOE) cases.

Table 3.3 shows the input variables for response surface model, both in the actual and normalized forms.

Table 3.3: Input Variables for Response Surface Metamodels

Random Structural Parameters	Input Variables	Lower Bound	Center Point	Upper Bound
Mass, m	ξ_1	4	8	12
	x_1	-1	0	+1
Strength, F_y	ξ_2	400	500	600
	x_2	-1	0	+1
Stiffness, k	ξ_3	50	80	110
	x_3	-1	0	+1

In order to make the response surface metamodel more efficient, the initial set of input parameters is screened such that only the most influential input variables are used to construct the model. Even though the screening process is not overly essential in this particular example as the initial set of inputs contains only 3 variables, it is still an important part of the response surface methodology and should not be overlooked. The screening process, however, will be more crucial in the case when the number of input variables becomes unmanageable (5 or higher).

The contributions of each input variable to the response computation can be shown graphically by a Pareto plot [Montgomery, 1997]. Figure 3.10 shows such a plot for the 3 input variables in this example. The horizontal bars represent degrees of significance from the input variables. It is obvious from this figure that x_2 is the least influential parameter and can be screened out without making significant effect to the response prediction.

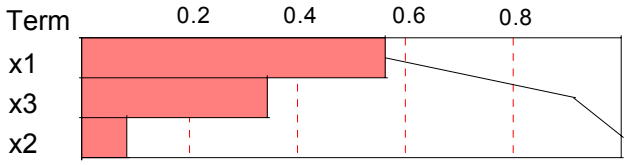

Figure 3.10: Pareto Plot of Input Variables for the SDOF System

Past research identified the full factorial design (FFD) and the central composite design (CCD) as appropriate DOE for the response surface metamodel generation. Initial study has shown that both of the designs produce comparable results. However, the

number of cases (or nonlinear time-history analyses) required to complete the FFD is significantly higher than the CCD. As a result, this research only considers the use of the CCD for a response surface formulation due to its efficiency.

An example of a DOE table for structural responses due to a specific scaled ground motion input (m02_10s scaled to 0.4g S_a) is displayed in Table 3.4. The value of a maximum displacement listed for each case of DOE is obtained from the nonlinear time-history analysis of a SDOF system. There are a total of 9 different SDOF systems to be analyzed following the CCD for 2 input variables (x_1 and x_3). Each SDOF system has structural properties according to the corresponding DOE case and is subjected to single ground acceleration record. Take DOE case 9 as an example, the SDOF system in this case is composed of a spring with a stiffness of 110 kips/in and a lumped mass of 12 kip-sec^2/in. A scaled ground acceleration record is applied to this system and the displacement at the mass level is computed at every time step. The maximum displacement (5.68 in) is extracted and recorded in the DOE table (Table 3.4) as a response quantity of this DOE case.

Table 3.4: DOE Table for SDOF Systems subjected to m02_10s Accelerogram

Case	x_1	x_3	Actual Max Disp (y), in.	Predicted Max Disp ($\hat{y}$), in.
1	-1	-1	4.38	5.10
2	-1	0	3.25	2.22
3	-1	+1	2.22	2.53
4	0	-1	11.00	10.04
5	0	0	4.60	5.71
6	0	+1	4.74	4.59
7	+1	-1	13.60	13.84
8	+1	0	8.16	8.08
9	+1	+1	5.68	5.52

Response Surface Model Fitting

In approach 1, a response surface model predicts maximum displacement in a SDOF system due to a particular earthquake given levels of input variables (mass, damping coefficients, and stiffness). A second-degree polynomial function is chosen for a response surface model in this study. A typical response surface function for 3 input variables is in the form of

$$\hat{y} = b_0 + b_1 x_1 + b_3 x_3 + b_{11} x_1^2 + b_{31} x_3 x_1 + b_{33} x_3^2$$

where $\hat{y}$ is the predicted maximum drift and x_1, x_2, and x_4 are the input variables representing randomness in structural properties as shown in Table 3.3. Coefficients of a polynomial function are determined by the least-square regression analysis of the inputs (x's) and responses (y) listed in the DOE table. The matrix of all coefficients (**b**) can be obtained following (3.13) as

$$b = \begin{bmatrix} b_0 \\ b_1 \\ b_3 \\ b_{11} \\ b_{31} \\ b_{33} \end{bmatrix} = \begin{bmatrix} 5.713 \\ 2.932 \\ -2.723 \\ -0.565 \\ -1.440 \\ 1.600 \end{bmatrix}$$

and the fitted response surface function can be rewritten as follows:

$$\hat{y} = 5.713 + 2.932x_1 - 2.723x_3 - 0.565x_1^2 - 1.44x_3x_1 + 1.6x_3^2 \qquad (3.28)$$

It is found in this study that, unlike the early study of the response surface models [Bucher and Bourgund, 1990] which the cross terms were neglected, the cross term in this model is significant to the computation of the response and must be included for accuracy of the approximation. A comparison between the actual maximum drifts computed by the dynamic analyses (actual responses) and the maximum drifts predicted by the response surface model (predicted responses) is also shown in Table 3.4 for each case of the Design of Experiments. It is obvious from this table that the response surface is able to predict the maximum displacement due to an earthquake (m02_10s) reasonably well at the design points.

The coefficient of determination (R^2) and an adjusted-R^2 (R_A^2) for this model are 0.965 and 0.907, respectively. The high values of R^2 and R_A^2 obtained from this model indicates high association between the computed and the approximated maximum displacements at the design points.

The response surface is shown in Figure 3.11. For the purpose of illustration, the response (y) or maximum displacement is plotted against the two input parameters (x_1 and x_3) over their ranges. The two-dimensional illustrations of this response surface function can also be shown in Figure 3.12. In this plot, the response (y) is plotted against each of the input variables (x's) while other input variables are held constant. The plot shows how the response computation changes with the input variables over its range.

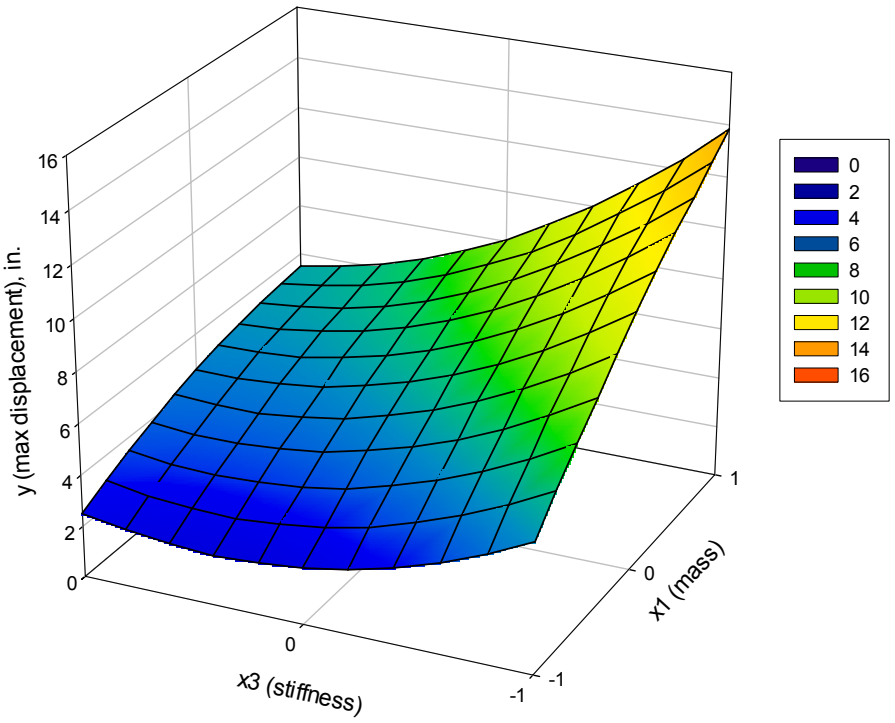

Figure 3.11: Response Surface of y as a function of x_1 and x_3

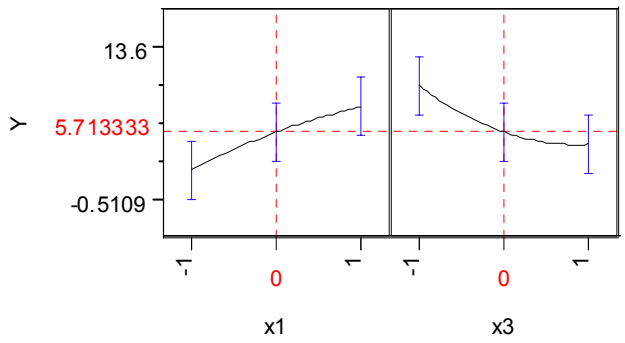

Figure 3.12: Prediction Profiler of a Response Surface Model

The response surface shown previously is contingent on a particular ground motion (m02_10s). The process of generating response surface models must be repeated for all other ground acceleration records, which have the same intensity level, in the suite. This results in 60 different response surface functions ($\hat{y}_1$ to $\hat{y}_{60}$) for all of the 60 earthquake records in the suite.

The main purpose of this section is only to demonstrate the process of using the response surface metamodels in damage probability calculation. Model checking and validation are not performed for this example. Chapters 4, 5 and 6 of the thesis, which implement the approaches to real structures, provide model validation in great detail.

Response Simulation

A response surface metamodel in Approach 1 approximates the maximum displacements of a SDOF system due to a given ground acceleration record from a set of known structural properties. However, the earthquake loading cannot be predicted with certainty. As a result, structural response or maximum displacement cannot be calculated with exactness without taking uncertainties in seismic loading into account. These

uncertainties are taken care of by a random selection of a response surface model from a pool of all earthquake-specific models ($\hat{y}_1$ to $\hat{y}_{60}$). Random samplings are performed over a large number (10,000) of trials resulting in 10,000 values of maximum displacement. Frequency and cumulative frequency plots of the maximum displacement are shown in Figure 3.13.

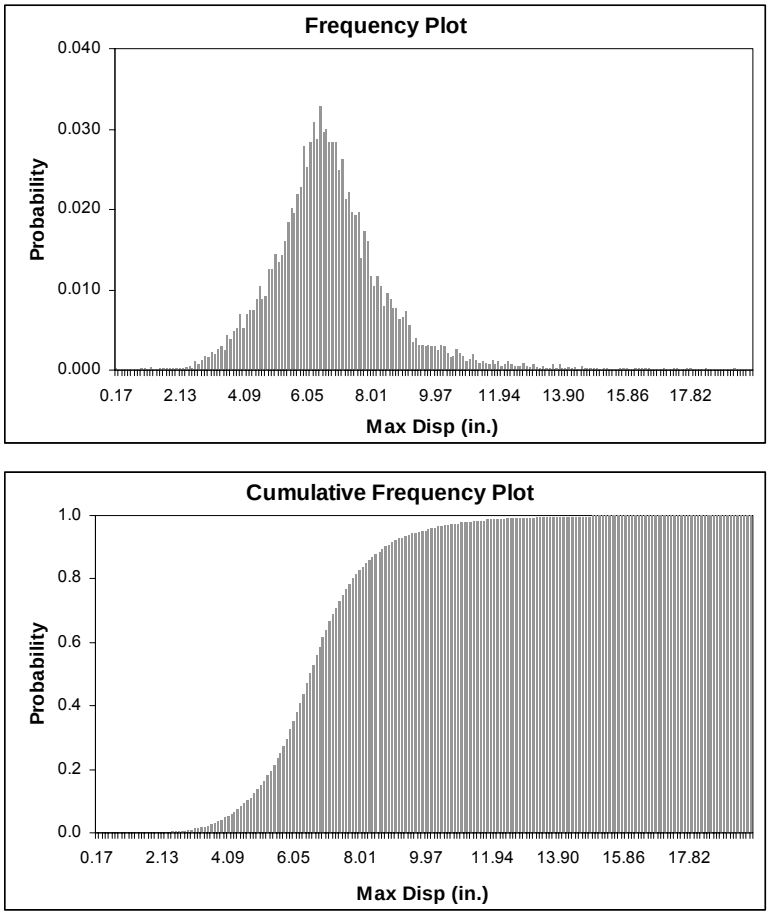

Figure 3.13: Frequency and Cumulative Frequency Plots for Maximum Displacement of a SDOF System

The probability of exceeding limit states for this particular level of seismic intensity (S_a = 0.4g) or fragility can be calculated by the ratio between the number of times the computed maximum displacements exceed the limit state thresholds and the total number of simulation trials (10,000 trials). For example, assuming that a damage threshold is defined by a maximum displacement of 8 in., the fragility of this SDOF system for a hazard level of 0.4g S_a is computed by

$$PF = \frac{1}{10{,}000} \cdot \sum_{i=1}^{10{,}000} I(D_i \geq 8\,\text{in.}) = \frac{1724}{10000} = 0.1724$$

I is an indicator function giving a value of 1 if the condition ($D_i \geq$ 8 in.) is met, and 0 otherwise. D_i is the maximum displacement value computed by the response surface function of input variables from the i^{th} simulation.

3.5.4 Approach 2

Approach 2 overcomes an inefficient process of generating response surface models for individual ground motion records in Approach 1. Instead, the response surface models in this approach independently predict the mean and standard deviation of the maximum displacements due to all acceleration records in a suite. The overall metamodel includes a term representing an expected response and a term taking into account a record-to-record dispersion, and consequently incorporates uncertainties in seismic loadings.

Design of Experiments

Similar to Approach 1, the input variables for the response surface model in Approach2 are those structural properties (Table 3.3) that are most influential to the response computation (i.e., x_1 and x_3). However, the output variables in this approach are

the mean and the standard deviation of the maximum displacements calculated from 60 ground motions.

A combination of parameter levels in each DOE case symbolizes a SDOF system with a specific set of structural properties. In approach 2, each SDOF structure (or DOE case) is subjected to all 60 ground motions in the suite. The maximum displacement due to each ground acceleration input is recorded. It is assumed that the seismic responses given a specific S_a are normally distributed. This assumption is validated by fitting a set of maximum displacements computed from a suite of records to a Normal distribution [Ang and Tang, 1975]. Figure 3.14 shows that the normality assumption is valid for the set of maximum displacements. The mean value and standard deviation obtained from the fitted distribution are used as the output variables for the response surface models (y_μ and y_σ, respectively). Computation of mean and standard deviation of the responses is repeated for all other DOE cases and the DOE table is formed, as shown in Table 3.5.

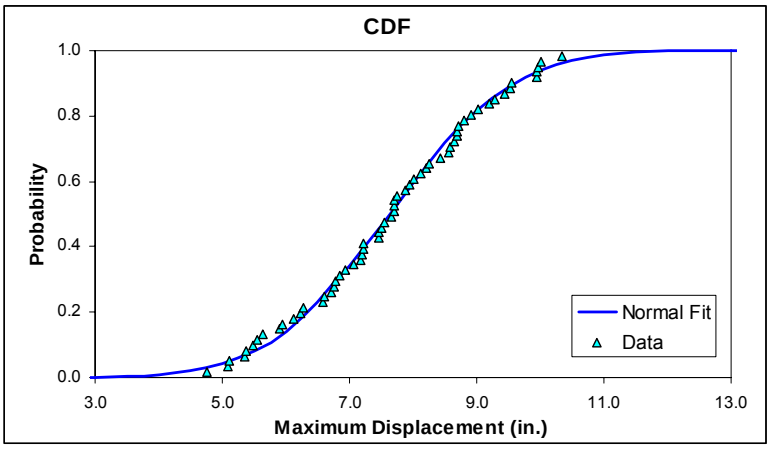

Figure 3.14: Normal Probability Distribution Fit of Maximum Displacements due to a Suite of Earthquakes at a Given Level of S_a

Table 3.5: DOE Table for SDOF Systems subjected to a Suite of Accelerograms

Case	x_1	x_3	y_1 (in.)	y_2 (in.)	…	y_{60} (in.)	Mean (y_μ)	Std Dev (y_σ)
1	-1	-1	4.34	2.39	…	7.53	6.28	3.04
2	-1	0	4.92	2.32	…	3.70	4.39	2.72
3	-1	+1	4.11	2.81	…	4.79	3.56	2.17
4	0	-1	5.29	9.42	…	6.31	6.05	2.02
5	0	0	6.35	4.62	…	6.00	4.42	2.15
6	0	+1	3.34	2.73	…	5.35	4.01	1.64
7	+1	-1	7.24	5.39	…	8.34	6.01	2.01
8	+1	0	5.44	8.34	…	6.02	4.33	1.88
9	+1	+1	5.22	6.01	…	5.96	4.82	0.96

Response Surface Model Fitting

Response surface polynomial functions of the mean and standard deviation of the maximum displacements for a given level of S_a (S_a = 0.4g) are generated in the same fashion as in Approach 1. Again, the model for 4 input variables can be expressed in the form of

$$\hat{y} = b_0 + b_1 x_1 + b_3 x_3 + b_{11} x_1^2 + b_{31} x_3 x_1 + b_{33} x_3^2$$

The polynomial coefficients are estimated using (3.13) where the matrix **Z** is similar to that presented in Approach 1. The dual responses y_μ and y_σ, in a matrix form, can be written as

$$\mathbf{Y_\mu} = \begin{bmatrix} 6.28 \\ 4.39 \\ 3.56 \\ \vdots \\ 4.82 \end{bmatrix} \begin{matrix} \text{Case 1} \\ \text{Case 2} \\ \text{Case 3} \\ \vdots \\ \text{Case 9} \end{matrix}$$

and

$$\mathbf{Y_\sigma} = \begin{bmatrix} 3.04 \\ 2.72 \\ 2.17 \\ \vdots \\ 0.96 \end{bmatrix} \begin{matrix} \text{Case 1} \\ \text{Case 2} \\ \text{Case 3} \\ \vdots \\ \text{Case 9} \end{matrix},$$

respectively.

Least-square regression analyses of the matrix of generalized input variables (**Z**) against both matrices for the output variables ($\mathbf{Y_\mu}$ and $\mathbf{Y_\sigma}$) result in response surface polynomial functions for $\hat{y}_\mu$ and $\hat{y}_\sigma$ as follows:

$$\hat{y}_{\mu} = 4.332 + 0.155x_1 - 0.992x_3 + 0.072x_1^2 - 0.383x_3x_1 + 0.742x_3^2 \quad (3.29)$$

and

$$\hat{y}_{\sigma} = 2.121 - 0.513x_1 - 0.383x_3 + 0.193x_1^2 - 0.045x_3x_1 - 0.277x_3^2 \quad (3.30)$$

The model for the mean response has R^2 and R_A^2 of 0.984 and 0.958, while the model for the standard deviation has R^2 and R_A^2 of 0.951 and 0.868, respectively. Both models exhibit high correlation between the actual maximum displacements and those that are approximated by the metamodels.

Response Simulation

In Approach 2, separate response surface models for the mean and standard deviation of maximum displacements of the SDOF system due to all 60 ground motions are generated. The overall metamodel is composed of the two response surface models, $\hat{y}_{\mu}$ and $\hat{y}_{\sigma}$. Following the normality assumption, the metamodel can be mathematically expressed as

$$\hat{y} = \hat{y}_{\mu} + N[0, \hat{y}_{\sigma}] \quad (3.31)$$

In this model, the first term predicts an expected or a mean value of the maximum displacements due to a suite of ground motions, while the second term represents the earthquake-to-earthquake dispersion in response computation and consequently incorporates randomness in earthquake excitations. In order to simulate the probability density of the maximum displacements, distributions of the input variables are defined

(Table 3.2). Monte Carlo sampling technique selects values of input variable corresponding to their probability distributions. A combination of the input variables in each simulation step reflects a SDOF system with properties corresponding to the selected input values. The maximum displacement is approximated by evaluating both response surface models ($\hat{y}_\mu$ and $\hat{y}_\sigma$) and combining them according to (3.31). A schematic view of the each simulation step is shown in Figure 3.15. The response surface is shown here, for simplicity, as a 2-dimensional plot between y and x_3. As an example, let *a* be a value that is randomly selected from the uniform distribution of x_3. The responses $\hat{y}_\mu$ and $\hat{y}_\sigma$ are evaluated for $x_3 = a$ and the maximum displacement for this simulation step can be computed as

$$\hat{y}(x_3 = a) \quad = \quad \hat{y}_\mu(x_3 = a) \quad + \quad N[0, \hat{y}_\sigma(x_3 = a)]$$

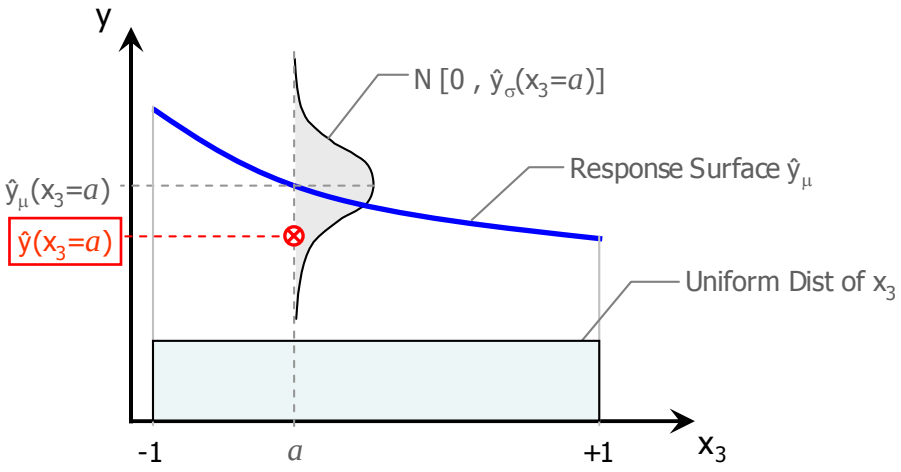

Figure 3.15: Illustration of Simulation Process in Approach 2

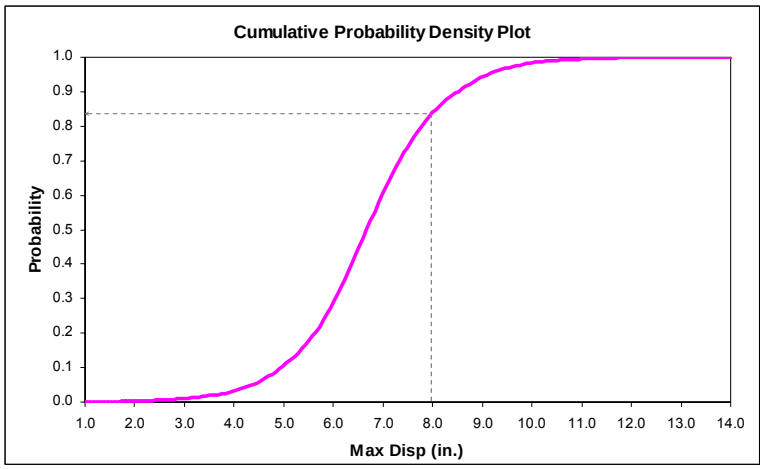

Figure 3.16: Cumulative Probability Density of Maximum Displacements by Approach 2

In this example, repeating random combinations are performed 10,000 times to produce response statistics of the maximum displacement ($\hat{y}$). A cumulative frequency (or cumulative density) plot is shown in Figure 3.16.

Damage probability for an 8-inch displacement threshold conditioning on the spectral acceleration value of 0.4g is calculated to be 0.1706.

3.5.5 Approach 3

A major drawback in Approach 1 and Approach 2 is that the response surface models are generated for specific levels of earthquake intensity. A need for repetitive analyses with increasing S_a levels for a complete fragility curve requires extensive computational cost. Approach 3 is proposed to forego this process by including the seismic intensity parameter as one of the predictors in the response surface models. The metamodel in this case can be used for computing damage probabilities at any levels of S_a within the predefined range.

Design of Experiments

In Approach 3, the input variables in the response surface model are composed of 2 components, random variables and a control variable. Random variables are those that define uncertainties in structural properties including mass (x_1) and stiffness (x_3) of the SDOF system. On the other hand, the control variable is deterministic with its fixed values characterizing different response prediction models. The control variable in this case is the spectral acceleration (S_a) that defines earthquake intensity level (referred to as x_{EQ}). Evaluation of response surface at different values of S_a yield models for predicting maximum displacement due to specific levels of S_a.

For constructing a response surface model, the control variable is treated in a similar way as other random variables. The lower bound, center point, and upper bound of the control variable S_a must be defined. In this example, the values of 0.1g and 0.7g characterize the boundary of variable range for S_a while the value of 0.4g defines the center point (Table 3.6). Three batches of 60 scaled ground motions are generated. The first batch contains accelerograms with spectral acceleration values scaled to 0.1g representing a lower bound case. The second and third batches are scaled to the center point and upper bound, correspondingly.

A Central Composite Design (CCD) is utilized to formulate 15 combinations of 3 input variables as shown in Table 3.7. The variables x_1, x_2, and $x_4$describe structural properties for a SDOF system, while x_{EQ} indicates the level of S_a and, in turn, the batch of acceleration records to use for the analysis. For example, in case 1, the SDOF system has a mass of 4 kip-sec^2/in and a spring stiffness of 50 kip/in. This particular system is subjected to a suite of ground motions that are scaled to have a spectral acceleration of

0.1g (or the first batch). A maximum displacement resulting from nonlinear time-history analysis is recorded for each ground motion. Normality assumption is again made for the distribution of the maximum displacements. The mean and the standard deviation values for this particular case are extracted from the fitted distribution.

Table 3.6: Input Variables for a Response Surface in Approach 3

Random Structural Parameters	Input Variables	Lower Bounds	Center Points	Upper Bounds	Units
Mass, m	ξ_1	4	8	12	kip-sec^2/in
	x_1	-1	0	+1	-
Stiffness, k	ξ_3	50	80	110	kip/inch
	x_3	-1	0	+1	-
Spectral Acceleration, S_a	ξ_{EQ}	0.1	0.4	0.7	g
	x_{EQ}	-1	0	+1	-

Table 3.7: Design of Experiments Table for Approach 3

Case	x_1	x_3	x_{EQ}	y_1 (in.)	y_2 (in.)	…	y_{60} (in.)	Mean (y_μ)	Std Dev (y_σ)
1	-1	-1	-1	2.25	2.80	…	1.79	2.07	0.76
2	-1	-1	+1	14.70	17.89	…	11.78	12.73	4.32
3	-1	0	0	6.57	4.57	…	6.19	5.56	2.17
4	-1	+1	-1	1.06	0.90	…	0.96	1.31	0.61
5	-1	+1	+1	8.79	6.08	…	7.54	10.22	3.76
⋮	⋮	⋮	⋮	⋮	⋮	⋱	⋮	⋮	⋮
14	+1	+1	-1	1.38	1.67	…	1.28	1.46	0.11
15	+1	+1	+1	9.65	11.83	…	8.97	10.26	1.05

Response Surface Model Fitting

Similar to the previous approaches, the mean and standard deviation of the maximum displacements are approximated by second-degree polynomial functions. Five input variables are used in the models to describe the response computation. The coefficients of the polynomial are derived by (3.13) and the response surface models for the mean ($\hat{y}_\mu$) and standard deviation ($\hat{y}_\sigma$) of response are expressed as follows:

$$\hat{y}_\mu = 6.68 + 0.513x_1 - 0.901x_3 + 4.871x_{EQ} - 0.426x_1^2 + 0.43x_3x_1 + 0.473x_3^2 + 0.324x_{EQ}x_1 - 0.75x_{EQ}x_3 - 0.163x_{EQ}^2 \quad (3.32)$$

and

$$\hat{y}_\sigma = 1.622 - 0.038x_1 - 0.713x_3 + 1.314x_{EQ} + 0.441x_1^2 - 0.442x_3x_1 + 0.913x_3^2 - 0.058x_{EQ}x_1 - 0.563x_{EQ}x_3 - 0.438x_{EQ}^2 \quad (3.33)$$

Response Simulation

Response surface models constructed in Approach 3 are unconditional of specific levels of earthquake intensity. Evaluation of the polynomial functions for different values of control variable x_{EQ} (normalized form of S_a) produces models for response prediction at specific intensity levels. Monte Carlo simulation is then carried out over the metamodels of random variables for response statistics derivation.

Damage probability conditioning to a particular S_a value of 0.4g is computed here for consistent comparison with results from Approach 1 and Approach 2. A normalized form of S_a that is employed in the response surface models can be calculated according to (3.4) as follows:

$$x_{EQ} = \frac{0.4g - \frac{0.7g + 0.1g}{2}}{\frac{0.7g - 0.1g}{2}} = 0$$

Consequently, the response surface models of a mean and standard deviation of maximum displacements for a spectral acceleration of 0.4g are obtained by substituting $x_{EQ} = 0$ in (3.32) and (3.33) and, hence, they become

$$\hat{y}_{\mu|S_a=0.4g} = 6.68 + 0.513x_1 - 0.901x_3 - 0.426x_1^2 + 0.43x_3x_1 + 0.473x_3^2 \qquad (3.34)$$

and

$$\hat{y}_{\sigma|S_a=0.4g} = 1.622 - 0.038x_1 - 0.713x_3 + 0.441x_1^2 - 0.442x_3x_1 + 0.913x_3^2 \qquad (3.35)$$

The overall metamodel takes the form of (3.31) in which a normality assumption on the distribution of maximum displacement is exercised. Simulation is performed by randomly selecting values for input variables under their probability density assumptions and calculating responses from the models. Ten thousands of simulated cases result in a cumulative frequency or probability density plot, as shown in Figure 3.17.

Assuming that the damage threshold of the maximum displacement is 8 inches, damage probability of this SDOF system, subjected to earthquake intensity of 0.4g, is 0.1823.

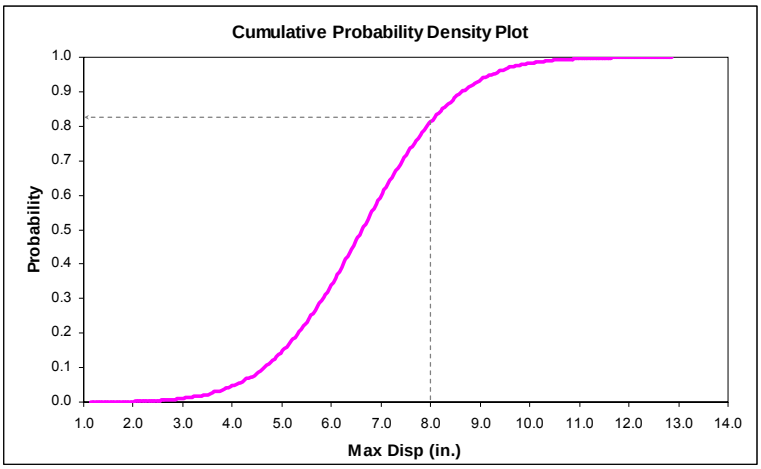

Figure 3.17: Cumulative Probability Density of Maximum Displacements by Approach 3

3.5.6 Benchmark Case: Direct Monte Carlo Simulation

The proposed approaches perform simulation of random variables through an approximated metamodel to generate statistics of the seismic response. Cumulative density plots of the maximum displacement produced by the 3 approaches are found to be very similar (Figure 3.18a). Further comparison with conventional method must also be performed to ensure reliability of the proposed approaches.

In order to verify the use of the metamodels in fragility analysis, a benchmark case using direct Monte Carlo simulation (MCS) is developed. The term "direct" refers to the process of carrying out a Monte Carlo simulation directly on a structural analysis model rather than a simplified metamodel. The structural property parameters that are selected corresponding to their probabilistic descriptions are combined at random to generate a large number of SDOF systems (10,000 systems in this example). Based on an assumption that earthquakes in a suite are equally likely to occur, ground motion records are randomly selected (with replacement) to pair with the 10,000 SDOF systems.

Nonlinear dynamic analysis is performed on each earthquake-structure combination and the maximum displacement is extracted. Cumulative frequency plot is constructed from 10,000 values of maximum displacement from the dynamic analyses.

It is assumed again that the damage threshold of the maximum displacement is 8 inches; the damage probability of this SDOF system, subjected to earthquake intensity of 0.4g, is 0.1603.

Cumulative probability distribution of the maximum displacement from the benchmark case is compared with those obtained from Approach 1, Approach 2, and Approach 3 (Figure 3.18b, Figure 3.18c, and Figure 3.18d, respectively). It is found that each of the proposed approaches is able to produce results similar to those from the benchmark case. This proves that the use of response surface metamodels is adequate for the fragility analysis of a structure.

Note that even for a very simple SDOF system, Monte Carlo simulation on the dynamic analyses of the structures is still computational expensive. The task of response simulation would be impossible to accomplish for much more complex structural systems.

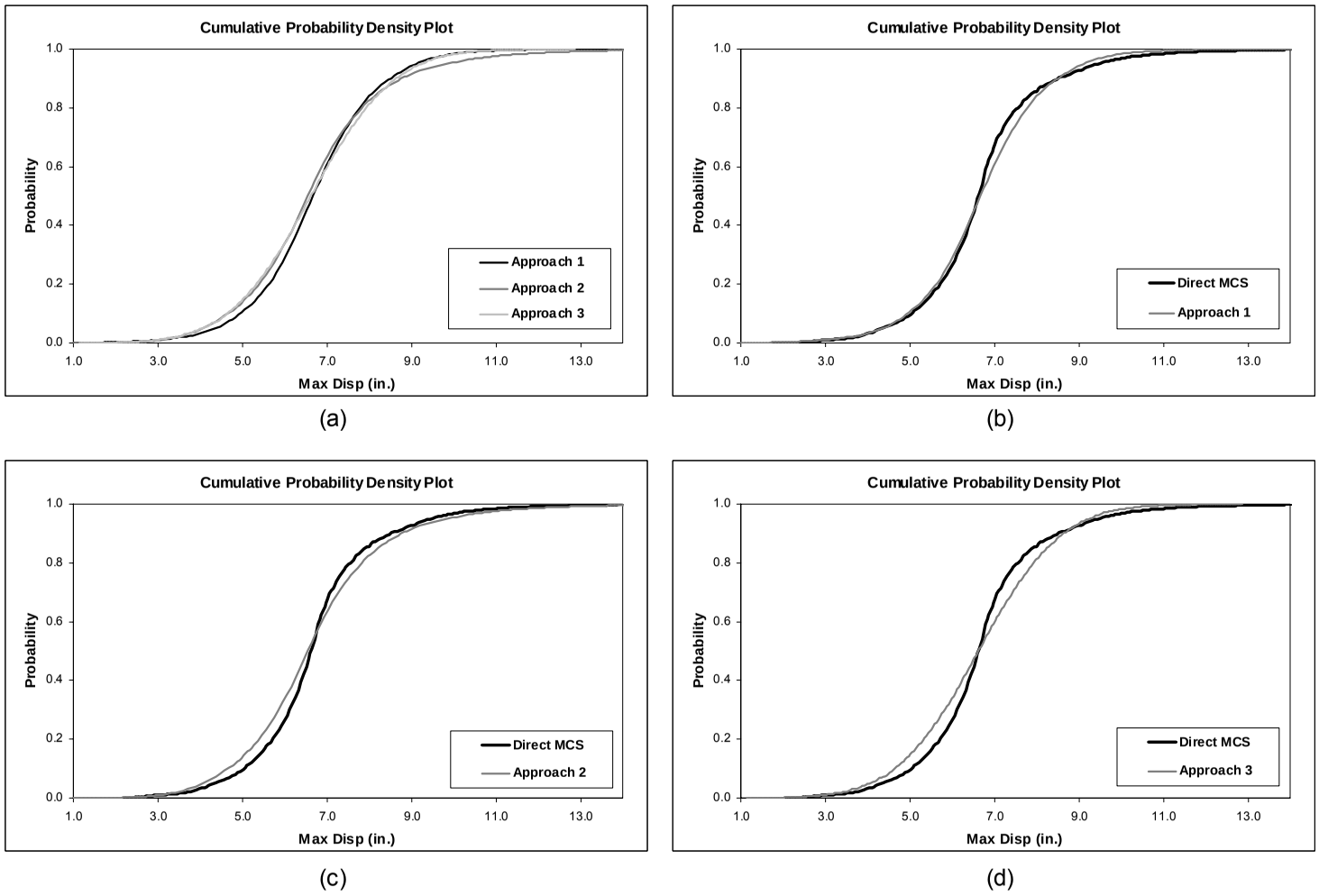

Figure 3.18: Comparison of Cumulative Probability Density Plots: (a) Between the 3 Approaches, (b) Approach 1 vs Direct MCS, (c) Approach 2 vs Direct MCS, and (d) Approach 3 vs Direct MCS

The added value of the use of metamodels is due to its efficiency. Significant reduction in computational efforts is achieved from using the proposed approaches. Table 3.8 presents a comparison on the number of dynamic analysis cases required by different approaches. A comparison is first made on the number of cases for calculating damage probabilities at a given intensity level. In the proposed approaches, central composite design generates 9 and 15 structural combinations for the 2 and 3 input variables, respectively. Sixty ground acceleration records are used to represent an uncertainty from seismic loadings. Dynamic analyses of structural combinations with all ground acceleration records construct metamodels which are used in the response simulation. Second, in order to complete a fragility curve, damage probabilities at other intensity levels are also needed. Further comparison on the total number of dynamic analysis for repetitive process over different levels of intensity is made. For this comparison, it is assumed that 10 intensity levels are desired for a fragility curve derivation. The total number of analysis cases is obtained by a multiplication of 10 to the number of cases required at each given intensity level. However, Approach 3 does not require any further analysis case since the metamodel in this approach is not specific to a particular intensity level and the damage probabilities can be computed by evaluating the existing metamodels at different values of intensity measure. It is apparent that while the proposed approaches using response surface metamodels produce outcomes similar to a conventional method, they are computationally much more efficient.

Table 3.8: Comparison of Number of Analysis Required by Different Approaches

Approaches	Number of Dynamic Analysis Required	
	For Damage Probability at a Specific Intensity Level	For Fragility Curve Generation
Direct MCS	10,000	100,000‡
Approach 1	9* × 60† = 540	5,400‡
Approach 2	9* × 60† = 540	5,400‡
Approach 3	15* × 60† = 900	900

* Number of cases from the Central Composite Design

† 60 ground acceleration records in a suite

‡ 10 levels of earthquake intensity used for generating fragility curves

3.5.7 Effects from the Number of Earthquakes

So far in this research, a suite of 60 accelerograms has been utilized for capturing an uncertainty arising from earthquake loadings to the structures. It has been suggested, however, that fewer number of records might be used (Song and Ellingwood [1999], Shinozuka et al. [2000a, 2000b]). A study is then performed on the effect of the number of accelerogram that can be used in a fragility analysis. In particular, only one-third (20 accelerograms) of the original suite is used in the process of establishing metamodels and the results are observed. Figure 3.19 shows a comparison of the cumulative probability distribution plots of the maximum displacements obtained from the process that utilize 60 and 20 ground acceleration records. It can be seen from these plots that the reduction in the number of records to 20 does not present significant discrepancy from the original case that uses 60 records. By using a smaller number of ground motions, the number of dynamic analysis required for completing a fragility curve can be reduced to one-third of

the original values shown in Table 3.8. Based on this finding, a suite of 20 accelerograms will be used as a basis for generating metamodels in subsequent chapters.

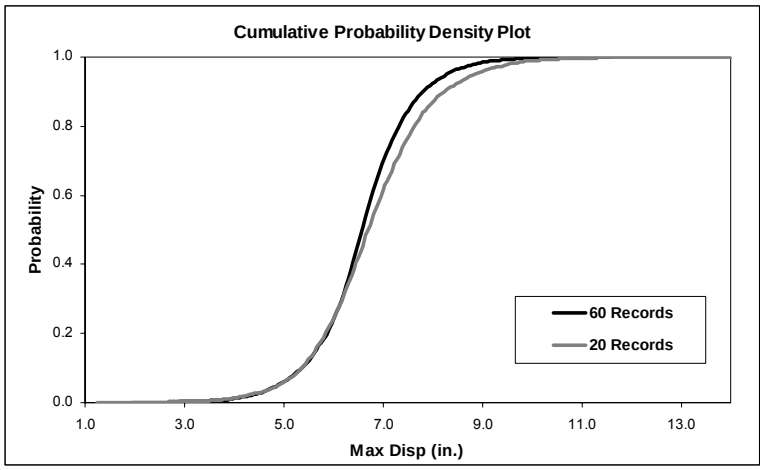

Figure 3.19: Effect of Number of Acceleration Records on Cumulative Distribution of Maximum Displacements

The method of using response surface metamodels in fragility calculation is proved to be efficient in a simple test case. Implementations of this approach in real structures are carried out in the following chapters.

CHAPTER 4

FRAGILITY ASSESSMENT OF AN UNREINFORCED MASONRY STRUCTURE

The use of response surface metamodels for computing seismic fragilities has been proven to be accurate and efficient for the simple SDOF case. Focus is now shifted to an implementation of the approaches for a real structure in this chapter. Fragility of a two-story unreinforced masonry building typical of firehouse construction in Mid-America is of interest.

4.1 SEISMIC RISK IN MID-AMERICA

The majority of earthquake engineering research focuses on problems arising in areas of the world with high seismic activity, and much less attention is directed at hazard mitigation in areas where the recurrence interval for large earthquakes is much longer but the inventory of at-risk structures may be far greater. The low-probability high-consequence problem exists in many regions of the U.S., where the infrequency of damaging earthquakes has been wrongly interpreted as low risk. The New Madrid seismic zone (NMSZ) is regarded as the most hazardous seismic zone in the central United States (referred to as Mid-America in this study). The series of earthquake events during 1811 and 1812 in New Madrid, Missouri are considered among the largest

earthquakes in the contiguous United States. However, due to the infrequent nature of major earthquakes in this region, most existing buildings in this region were designed only for gravity and wind loads. The consequences of earthquakes, especially major events that would affect a large part of Mid-America, have been largely neglected.

4.2 ESSENTIAL FACILITIES

Essential facilities are defined as buildings that support functions related to post-earthquake emergency response and disaster management such as hospitals, fire stations, police stations, emergency shelters, etc. As a consequence, the unimpeded availability and functionality of essential facilities during and immediately following an earthquake is a top priority. It is proposed that any new essential facilities in the region must be designed to the highest level of seismic performance (operational). For existing essential facilities, appropriate rehabilitation measures must be incorporated to achieve the same performance level or else replacement must be considered.

The lack of proper seismic design in conjunction with much needed availability of essential facilities after an earthquake led to the idea of investigating the seismic fragility of those at-risk buildings. An accurate understanding of the essential facility systems in the NMSZ is the first step in addressing this problem. A regional assessment of essential facilities was carried out by French and Olshansky [2000] to assemble a building inventory in the region. Over 5,000 such buildings were identified and more than 1,300 of these were inventoried visually and/or by telephone. It was found that nearly a third of these facilities (see Table 4.1) are constructed of unreinforced masonry (URM). In addition, past earthquake reconnaissance reports also suggested that unreinforced masonry construction is highly susceptible to damage from earthquakes. Seismic

fragility assessment of URM structures can provide an insight to a component of seismic risk to a large number of essential facilities in the region. As a result, this type of construction is chosen in this research for a seismic fragility assessment using the proposed approaches (see Chapter 3).

Table 4.1: Number of Facilities by Structure Types [French and Olshansky, 2000]

Structure Types	Number	Percent
C1 – Concrete	9	0.7
C2 – Concrete	78	6.0
C3 – Concrete Frame	83	6.4
MH – Mobile Home	17	1.3
PC1 – Precast Concrete	10	0.8
PC2 – Precast Concrete	5	0.4
RM1 – Reinforced Masonry	72	5.5
RM2 – Reinforced Masonry	30	2.3
S1 – Steel Frame	54	4.1
S2 – Steel Frame	21	1.6
S3 – Prefabricated Steel	91	7.0
S4 – Steel Frame	22	1.7
S5 – Steel Frame	163	12.5
URM – Unreinforced Masonry	428	32.8
W1 – Wood Frame	81	6.2
W2 – Wood Frame	43	3.3
Unknown	99	7.6
Total	1306	100

4.3 TYPICAL URM STRUCTURES IN MID-AMERICA

Typical URM essential facilities in Mid-America are relatively small and low-rise (one or two-story in height). The building is composed of 2 main components: the URM bearing walls and the floor and roof diaphragms. The walls are generally stiff and constructed with many openings for windows and doors. Walls with openings are referred to as perforated walls. The diaphragms are usually constructed of timber and, as a result, are much more flexible than the walls.

A benchmark building is selected as a representation of existing URM low-rise buildings in Mid-America. The building was designed and constructed for an experimental research (Yi et al. [2002] and Yi [2004]) conducted at Georgia Tech to determine the lateral load resistance of a URM building (Figure 4.1). The full-scale 2-story test building was designed to represent a typical construction of an existing URM firehouse in Mid-America. Four unreinforced masonry walls, referred to as wall A, wall B, wall 1, and wall 2, define the test structure. The detailed dimensions of each wall and a plan view are shown in Figure 4.2. The building is 24 feet by 24 feet in plan and has story heights of 12 feet and 10 feet for the first and second stories, respectively. Wall A and, on the opposite side, wall B are of the same configuration. Wall 1 only has a door on the first floor and two window openings on the second floor. On the other hand, wall 2 has a large door opening in the bottom floor designed to represent a fire apparatus entrance.

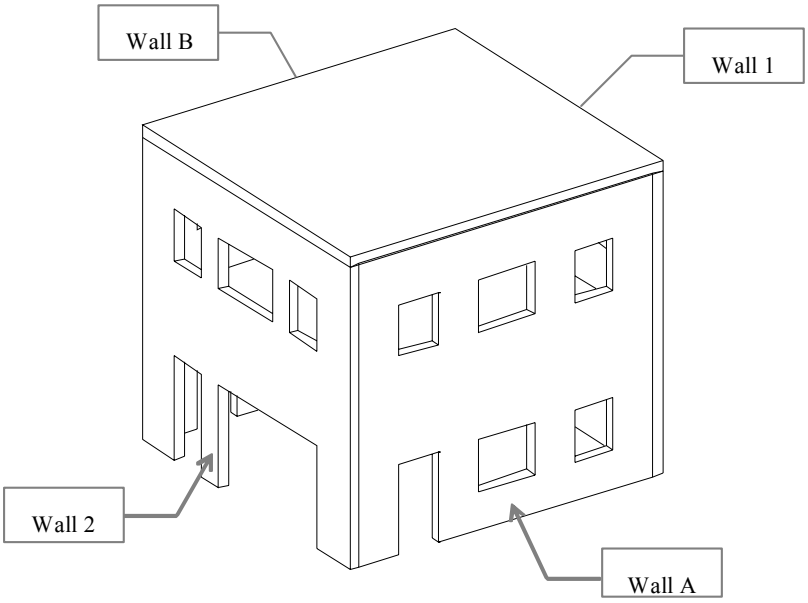

Figure 4.1: Typical Low-Rise URM Building in Mid-America

Material properties are obtained from the experimental studies (Yi et al. [2002] and Yi [2004]). In this experiment, masonry prism specimens and 4-brick specimens are constructed for material tests. Basic properties are listed in Figure 4.2.

Table 4.2: Basic Material Properties for the URM Test Structure

Properties	Mean Values
Masonry Density (lb/in^3)	0.06944
Masonry Compressive Strength (psi)	1458
Masonry Elastic Modulus (ksi)	600
Masonry Bed-Joint Shear Strength (psi)	60

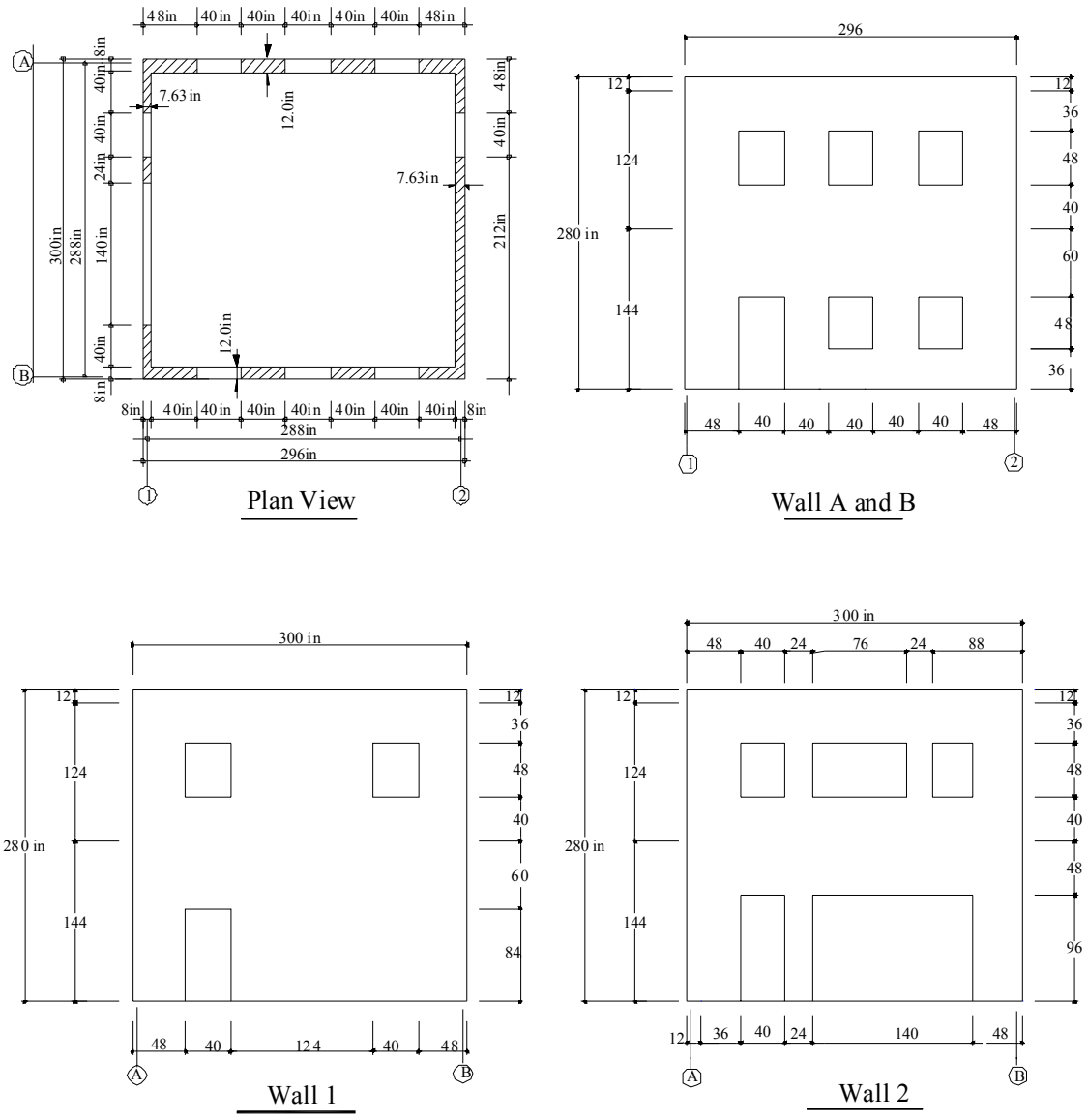

Figure 4.2: Detailed Dimensions of the Test Structure

4.4 MODELING URM BUILDINGS

Unreinforced masonry is a non-homogeneous material made up of 2 components: the masonry bricks and the mortar. URM properties are dependent upon the properties of its constituents. Structural behavior of the URM can be very complex even under static loadings. The most refined approach for analyzing a URM wall is the so-called brick-by-brick approach which models individual masonry brick as a solid element connecting to each other by the interface elements representing the mortar. However, for the purpose of seismic fragility analysis of the URM building, repeated dynamic analyses are required and this approach can quickly become impractical. As a result, a more tractable structural model is needed in this study.

4.4.1 2D Versus 3D Analyses

Under the earthquake excitation, the particular direction of seismic loading cannot be anticipated. It is unlikely that the actual earthquake loading will be in the direction orthogonal to the building axes. In addition, many real buildings have irregular layouts that can result in a building structure that behaves in complex three-dimensional ways under seismic loadings. Therefore, three-dimensional analysis should produce a more accurate description of the behavior of the structure, and this might include torsional responses due to asymmetry of the rigidity and mass distributions of each component with respect to the loading direction. However, in the interest of achieving a simpler model for dynamic analysis, the models developed in the present study are based on two-dimensional behavior only. The 2D model presented in this study is simple enough for repetitive dynamic analyses, yet is able to capture most of the important nonlinear behaviors of the wall components and the diaphragms.

4.4.2 URM Building Components

The two-dimensional analysis model for a URM building computes building response due to an earthquake input in a single horizontal direction. Building components are defined as being either in-plane or out-of-plane, depending on their orientation relative to the loading direction.

URM In-Plane Walls

Building walls that are oriented parallel to the loading direction are referred to as in-plane walls. URM walls usually develop high initial elastic stiffness in the in-plane direction resulting in a high elastic stiffness and low elastic structural period of URM buildings. The overall nonlinear behaviors of the in-plane perforated walls are dominated by behaviors of different components and their arrangement in the wall. A perforated wall can be subdivided into wall components between openings (see Figure 4.4). Each individual component (referred to as a wall pier) behaves in a similar fashion as a solid URM wall. There are four kinds of in-plane failure mode for the monolithic URM walls when subjected to lateral loadings. The type of failure mode is dependent primarily on the masonry strength, aspect ratio of the wall component, and the vertical compressive stress on the wall. The four types of in-plane failure mode can be summarized as follows [FEMA, 1997].

(a) *Rocking failure* (Figure 4.3a): As horizontal load or displacement demand increases, bed-joint cracks in tension, and shear is carried by the friction of compressed masonry at the toe. The final failure occurs the wall overturns about its toe.

(b) *Bed-joint sliding* (Figure 4.3b): Due to the formation of horizontal tensile cracks in the bed-joints, subjected to reversed seismic action, potential sliding planes can

form along the cracked bed-joints. This failure mode is possible for low levels of vertical load and/or low friction coefficients.

(c) *Diagonal tension cracking* (Figure 4.3c): Peak resistance is governed by the formation and development of inclined diagonal cracks, which may follow the path of bed and head joints in a stair-step pattern or may go through the bricks in a straight diagonal path, depending on the relative strength of mortar joints, brick-mortar interface, and bricks.

(d) *Toe crushing* (Figure 4.3d): When the strength, as limited by toe compression stress, is less than the strength determined by rocking, the wall undergoes a sudden failure due to the crushing of the toe.

Strengths of the URM wall corresponding to each failure mode are derived in FEMA [2000a] and will be discussed later in this chapter.

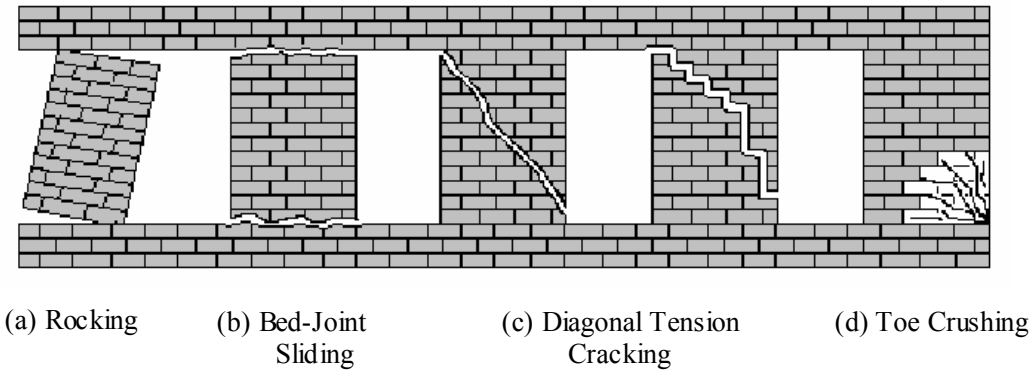

Figure 4.3: Four Failure Modes of URM In-Plane Walls [Yi, 2004]

URM Out-of-Plane Walls

Contrary to the in-plane wall, the out-of-plane wall is the building wall that is perpendicular to the direction of the earthquake inputs. Its lateral stiffness is significantly lower than that of the in-plane wall. Out-of-plane failures are generally quite brittle unless significant compressive loads are present. Failure or even collapse of the out-of-plane walls under earthquakes is imminent if the connections between the out-of-plane walls and the diaphragms and/or the in-plane walls are not well constructed.

Floor and Roof Diaphragms

The floors and roof diaphragms of a URM building in the region are typically constructed of timber sheathings and joists. The use of timber as a construction material makes the diaphragms much more flexible than the supporting masonry walls. Timber diaphragms have large deformation capacity and high strength relative to its mass [Yi, 2004]. Failure of the diaphragm itself usually has not been a major concern under earthquake loadings. However, the connection between the diaphragms and the supporting walls are sometimes the weak points. Improper design and construction of diaphragm connection can even trigger failures in other components such as out-of-plane walls. Even though it has been realized that the connections are an important issue in the URM buildings, the precise manner of this connection is often quite difficult to assess and to model. For the interest of a simpler dynamic model for the URM building, the connections between the diaphragms and the masonry walls are assumed rigid in this research.

4.4.3 Component-Level Modeling

As mentioned in section 4.4.1, this research only focuses on two-dimensional responses of the URM test structure. Earthquake loadings should be applied to the building in the direction that the three-dimensional effects are prevented. Figure 4.2 shows that the configurations of wall 1 and wall 2, which are parallel to each other, are significantly different. This indicates a major difference in terms of the lateral stiffness between the two walls. As a result, torsional effects will be developed if the seismic load is applied in the in-plane direction to wall 1 and wall 2. On the other hand, wall A and, on the opposite side, wall B are constructed with identical configuration. Lateral load applied in the in-plane direction of wall A and B is less likely to cause major torsional deformation in the URM test structure. Based on these observations, earthquake inputs are restricted only in the direction parallel to wall A and wall B in this study. With this loading direction, wall A and wall B consequently become in-plane walls, while wall 1 and wall 2 are out-of-plane walls.

In-Plane Wall Modeling

While solid URM walls exhibit a very stiff linear elastic behavior for in-plane loading, the walls will ultimately fail through a fracture process that can involve diagonal cracking or bed joint fracture and sliding. Perforated walls can exhibit much more complex behavior that is associated with localized failures in the masonry piers, lintels and spandrels. For these cases, the behavior can range from essentially ductile behavior developed through pier rocking to highly nonlinear hysteretic behavior developed through, for example, bed joint sliding.

In order to more realistically model the nonlinear in-plane wall behavior, especially for perforated walls with different kinds of openings, a simple composite nonlinear spring model was developed (Craig et al. [2002] and Park et al. [2002]). The basic approach to develop a composite spring model for the in-plane behavior of a URM wall is to first subdivide the wall into distinct areas or segments. These segments are defined as rectangular regions that can be represented using simple flexural and shear deformation models and for which a single failure mode can be specified. Each of these segments is then represented by a single elasto-plastic hysteretic spring whose elastic properties can be determined from the deformation model and whose strength and hysteretic properties can be determined from the assumed failure mode. The geometric dimensions and end conditions are used to determine the elastic properties of a segment while the failure mode is determined from empirical data [FEMA, 2000a]. Figure 4.4 shows an example perforated URM wall on the left side and the schematic view of the corresponding composite spring model on the right. In this model, each segment of the URM wall is represented by a nonlinear spring, and the springs are assembled in series and parallel arrangements to match the segment topology for the wall itself. In this figure, springs number 1 and number 8 are not representative of any wall component, but rather capture the story bending effects. The elastic properties of these two springs are defined as a function of the overall interstory wall aspect ratio and are calibrated from the finite element analysis results (Craig et al. [2002] and Park et al. [2002]).

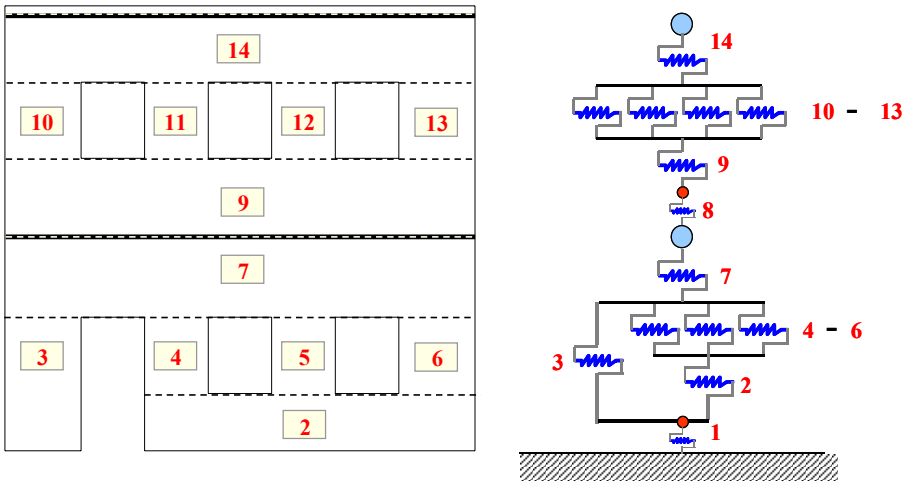

Figure 4.4: Composite Spring Model of Wall A and Wall B

In this composite spring model, each component or segment is treated individually as a solid masonry shear wall. The in-plane force-deflection behavior of unreinforced masonry shear walls is linearly elastic before net flexural tension stresses at the wall heel exceed tensile strengths, or diagonal tension, or bed-joint sliding shear stresses exceed shear strengths. FEMA-356 [FEMA, 2000a] provides formula for the calculation of the linear elastic stiffness of an URM shear wall as follows.

$$k = \frac{1}{\frac{h_{eff}^3}{3E_m I_E} + \frac{h_{eff}}{A_v G_m}} \quad \text{for a cantilever (fixed-free) shear wall} \qquad (4.1)$$

$$k = \frac{1}{\frac{h_{eff}^3}{12E_m I_E} + \frac{h_{eff}}{A_v G_m}} \quad \text{for a fixed-fixed shear wall} \qquad (4.2)$$

where

h_{eff} = Wall height

A_v = Shear area

I_g = Moment of inertia for the gross section

E_m = Masonry elastic modulus

G_m = Masonry shear modulus

These formulas are based on the classical theory of bending and shear. They are derived for different boundary conditions of the masonry shear walls. However, the masonry piers in a perforated wall are typically connected to other wall components below and above them. It is, in turn, hard to characterize the actual boundary conditions for the masonry piers as they cannot be regarded as fixed-fixed. One approach to account for boundary conditions that are less stiff than the assumed ideal fixed condition is to instead assume a finite rotational restraint at each end. Another approach is to simply increase the pier height while maintaining the ideal fixed end conditions.

For this study, the pier height is altered to account for the less than ideal end fixity. In other words, the pier height is increased by a factor, r, to create a new "effective height" [Craig et al., 2002 and Park et al., 2002]. Since this increased pier height is not real, but is used simply to compute a more accurate stiffness, it is referred to as an "effective height." Furthermore, since the end conditions may not be symmetric, the effective heights are computed separately for the upper and the lower half of the piers and added together. The r factors are determined from simple design formulas that are in turn based on correlations with detailed plane stress finite element models of the piers with a wide range of different end conditions. At the end, the initial elastic stiffness of each masonry pier is calculated using (4.2) with h_{eff} being the effective or the factored height.

The strength of the wall is different for each failure mode and must be determined separately. FEMA [2000a] provides design formulas for the strength of each failure mode of a solid wall under an in-plane force applied along its top. These empirical formulas reflect the geometry of each segment, material strengths, and the vertical compressive loads. FEMA [2000a] also notes that unreinforced masonry walls and piers should be considered as deformation-controlled components if their expected lateral strength, limited by bed-joint sliding, shear stress, or rocking, is less than the lower bound lateral strength limited by diagonal tension or toe compressive stress. Otherwise, these components should be considered as force-controlled components.

The strengths of the masonry solid walls are calculated following FEMA [2000a]. Material properties used in these formulations are based on the mean values of the test data. Strengths for the four failure modes can be calculated as follows:

(a) *Rocking failure*: The expected lateral strength of existing URM walls governed by rocking failure is

$$V_r = 0.9 \cdot \alpha \cdot P_E \cdot \left(\frac{L}{h_{eff}} \right) \tag{4.3}$$

where

α = Factor equal to 0.5 for fixed-free cantilever wall, or equal to 1.0 for fixed-fixed wall

P_E = Expected axial compressive force due to gravity loads

= $1.1 \cdot (Q_D + Q_L + Q_S)$

Q_D = Dead load

Q_L = Effective live load

Q_S = Effective snow load

L = Length of wall

h_{eff} = Height of resultant of lateral force

(b) *Bed-joint sliding failure*: When bed-joint sliding governs the wall failure, the expected strength of the wall is

$$V_{bjs} = v_{me} A_n = \frac{0.75 A_n \left(0.75 v_{te} + \frac{P_{CE}}{A_n} \right)}{1.5} \qquad (4.4)$$

where

v_{me} = Expected bed-joint sliding shear strength, psi

A_n = Area of net mortared/grouted section, in^2

v_{te} = Average bed-joint shear strength, psi

P_{CE} = Expected vertical axial compressive force (= P_E)

The 0.75 factor on the v_{te} term may be waived for single wythe masonry, or if the collar joint is known to be absent or in very poor condition. Values for the mortar shear strength, v_{te}, in (4.4) should not exceed 100 psi.

(c) *Diagonal tension cracking failure*: the strength of a solid wall governed by diagonal shear cracking is

$$V_{dt} = f'_{dt} \cdot A_n \cdot \left(\frac{L}{h_{eff}}\right) \cdot \sqrt{1 + \frac{f_a}{f'_{dt}}} \qquad (4.5)$$

where

f'_{dt} = Lower bound of masonry diagonal tension strength (may be substituted by the bed-joint shear strength, v_{me}), psi

f_a = Upper bound of vertical axial compressive stress $\left(= \frac{P_E}{A_n}\right)$, psi

This equation is only applicable for the range of L/h_{eff} between 0.67 and 1.00. As mentioned earlier, diagonal tension cracking can be divided into two different kinds, depending on the relative strength of mortar joints, brick-mortar interface, and bricks: (1) cracking that follows the path of bed- and head-joints or a stair-step pattern, and (2) cracking that goes through the bricks. Equation (4.5) above is only applicable to case (2). It would be rational to apply (4.5) for case (1), because the lateral movement of the wall can only be resisted by the friction of the bed-joints.

(d) *Toe crushing failure*: The strength of a wall governed by toe crushing is

$$V_{tc} = \alpha \cdot P_L \cdot \left(\frac{L}{h_{eff}}\right) \cdot \left(1 - \frac{f_a}{0.7 f'_m}\right) \qquad (4.6)$$

where

P_L = Lower bound of vertical compressive force

= $0.9 \cdot Q_D$

f'_m = Lower bound of masonry compressive strength, psi

For this case, the lower bound masonry compressive strength, f'_m should be taken as the expected strength, f_{me} divided by 1.6.

The strengths of each segment in an in-plane wall are computed using the above equations. The governing failure mode of each segment is determined by the lowest strength of the four failure modes. Table 4.3 shows properties of each segment in a composite spring model for wall A (and wall B) and their governing behavior calculating from FEMA guidelines. The elastic stiffness presented in this table has been adjusted for a less-than-ideal fixity by the "effective height" method.

Based on this composite spring approach, the overall elastic stiffness of wall A and wall B is found to be 1533 kips/in. For a validation of the model, the elastic stiffness of the walls that is computed by a plane-stress analysis in Yi [2004] is used as a benchmark. The benchmark stiffnesses for wall A and wall B are varied between 1100 and 1515 kips/in, depending on the location of the applied forces. It is apparent that the stiffness based on a composite spring model is only slightly higher than that from a detailed finite element analysis. This confirms the validity of the composite spring model in approximating the elastic properties of a perforated wall.

Under strong earthquake loadings, URM in-plane wall (and its components) generally deforms into an inelastic range. Hysteretic properties associated to each failure mode must be defined for the nonlinear spring elements. A number of past experimental research characterized nonlinear behaviors of different failure modes. However, since all component-level behaviors in wall A and wall B are either rocking or bed-joint sliding (Table 4.3), only the hysteretic properties of the two failure mode are used in this thesis.

Details of hysteretic behaviors of the diagonal tension cracking and toe crushing failure modes can be found elsewhere (Magenes and Calvi [1997] and FEMA [1998]).

Table 4.3: Elastic Properties and Strength of Wall Components in Wall A and Wall B

Segment	Governing Failure Mode	Elastic Stiffness* (k/in)	Strength (kips)
2	Sliding	16678.38	108.72
3	Rocking	1688.14	7.08
4	Rocking	880.73	8.60
5	Rocking	966.34	8.60
6	Rocking	1133.95	12.38
7	Sliding	13612.09	148.98
9	Sliding	21447.34	121.05
10	Rocking	1138.3	4.23
11	Rocking	970.11	2.94
12	Rocking	970.11	2.94
13	Rocking	1138.3	4.23
14	Sliding	17352.35	113.81

* Elastic stiffness is calculated using the "effective height" approach

Rocking failure: In the case of a rocking response, very large displacements can theoretically be obtained without significant loss in strength. A typical flexural response is depicted in Figure 4.5a, where a nonlinear but nearly elastic behavior with very minimal hysteretic energy dissipation is shown. A simple elasto-plastic model with a completely elastic behavior is used in the spring model in the case that rocking failure governs (Figure 4.5b).

Bed-joint sliding failure: When sliding on horizontal bed-joints occurs, a very stable mechanism is involved, since high displacements are possible without a loss of integrity of the wall. Damage is concentrated in a bed-joint, and as long as a vertical load is present, high energy dissipation is possible due to solid friction generated by a relative movement between sliding brick units. The hysteretic shape the bed-joint sliding behavior was developed from a cyclic loading test of a URM wall under constant vertical pressure [Abrams, 1992], shown in Figure 4.6a. This hysteretic behavior can be idealized with an elasto-plastic model with inelastic unloading, as shown in Figure 4.6b.

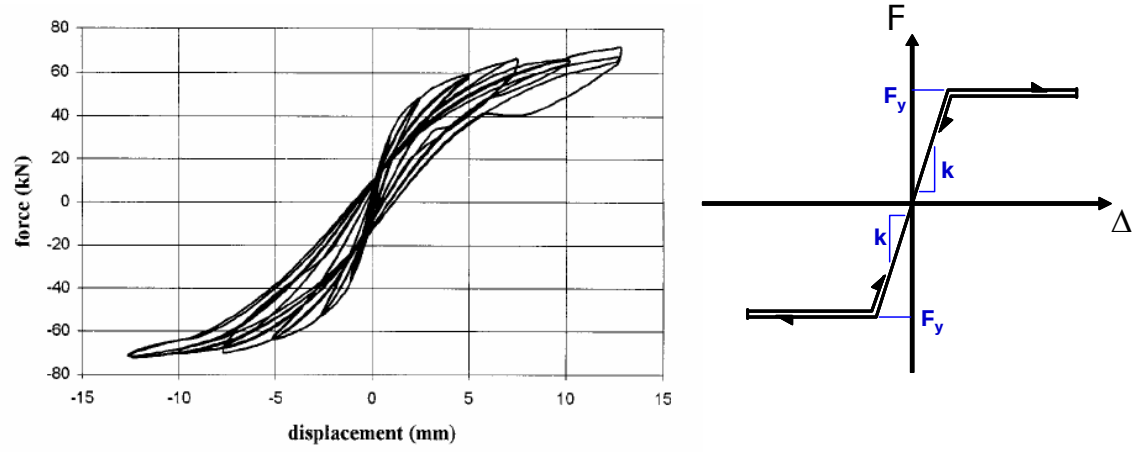

Figure 4.5: Rocking Hysteretic Behavior, (a) Experimental Results [Magenes and Calvi, 1997], and (b) Idealized model

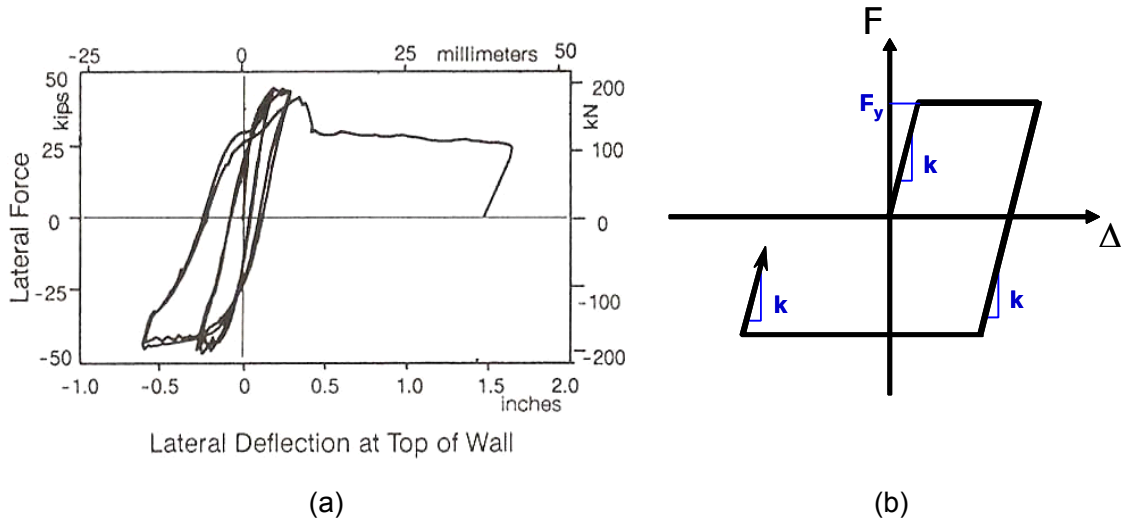

Figure 4.6: Bed-Joint Sliding Hysteretic Behavior, (a) Experimental Results {Abrams, 1992], and (b) Idealized model

Another important component of the dynamic analysis is the mass property of the URM walls. The mass of the in-plane wall is computed from the wall's self weight and, for this composite spring model, is lumped at the floor and the roof levels. Masses for wall A and wall B at floor and roof levels are computed to be 0.11 k-sec^2/in and 0.04 k-sec^2/in, respectively.

Out-of-Plane Wall Modeling

In reality, URM walls that are subjected to the out-of-plane loadings are susceptible to damage because of their relatively low out-of-plane stiffness and, more importantly, brittle failure mechanism. URM out-of plane walls are most likely the dominant cause of structural failure under earthquakes. In order to prevent the premature failure of a building, it is assumed in this research that a strengthening measure has been applied to the out-of-plane walls to ensure integrity of the walls. This also makes the

URM wall out-of-plane behavior much simpler to model as it can be assumed linear elastic.

In the simplified model, only a single linear-elastic spring is used to represent an out-of-plane stiffness between floor levels. The values for the out-of-plane stiffness of wall 1 and wall 2 are obtained from the finite element model [Yi, 2004] and are presented in Table 4.4. As expected, it should be noted that these stiffnesses are much lower than the in-plane wall stiffness and therefore contribute relatively little to the 2D response of the structure. The mass properties of wall 1 and wall 2 are calculated in a similar way as that of the in-plane walls. The mass values at each floor level are also shown in Table 4.4.

Table 4.4: Properties of the Out-of-Plane Wall 1 and Wall 2

Properties	Wall 1		Wall 2	
	1st Floor	2nd Floor	1st Floor	2nd Floor
Out-of-Plane Stiffness (k/in.)	104.4	160.9	66.4	160.9
Mass (k-sec^2/in)	0.125	0.041	0.091	0.037

Flexible Diaphragm Modeling

In 2-dimensional URM building models, floor bending is not considered, and as a result, the floors are usually considered as diaphragms with extensional and shear stiffnesses. Floors made from tongue-and-groove or plywood decking over wooden joists are quite common in old URM construction in the region although newer construction

may involve poured concrete on light steel decking. In either case, and especially for the wooden floors, the shear stiffness is much less than the extensional stiffness and usually is the defining characteristic of the floor. Laboratory tests of typical and modified wooden flooring systems [Peralta et al., 2000] confirm this behavior and provide representative stiffnesses. It should also be noted that these stiffnesses are nonlinear and are often accurately characterized by a bilinear stiffness with hysteretic behavior.

Floor and roof diaphragms for the test structure are of identical construction. Their shear and extensional stiffnesses from the experiments are found to be 4 kips/in and 870 kips/in, respectively. Mass of each diaphragm is lumped at its center and is found to be 0.06 k-sec^2/in, based on experimental study [Yi, 2004]

4.4.4 DRAIN Model for a URM building

A DRAIN-2DX [Prakash et al., 1993] is selected in this study for modeling the behavior of the URM test structure. While DRAIN-2DX does not have a straightforward means to model URM structures, it does include a versatile, zero-length spring element with a variety of possible nonlinear behaviors. As described in the previous sections, this simple nonlinear spring element can be used to develop basic nonlinear models for simple URM structures with flexible floor diaphragms. Each component in the model is constructed using the DRAIN-2DX TYPE 04 zero-length nonlinear spring element. A simple 2D model can be constructed by orienting the 2D axis system in a horizontal plane. The complete URM test structure is modeled by assembling the composite nonlinear springs for each wall with the lumped wall masses, as illustrated in Figure 4.7. For illustration purpose, the in-plane walls are represented in Figure 4.7 by a single spring in

each floor. However, the actual model incorporates the nonlinear behaviors of in-plane walls at a component-level as displayed in Figure 4.4.

Parallel research [Kim and White, 2001] has also developed a 3-dimensional nonlinear modeling tool for URM structures with flexible floor diaphragms that is based around ABAQUS. Much like the above DRAIN-2DX approach, the nonlinear URM wall behavior is modeled using simple nonlinear springs. However, the floor diaphragm is modeled with a special ABAQUS User Element developed specifically for this purpose. As a result, the ABAQUS model is capable of handling more realistic 3-dimensional models but at the expense of using a considerably more complex analysis tool. This ABAQUS model is used as a validation tool for a much simpler DRAIN-2DX composite spring model used in this study.

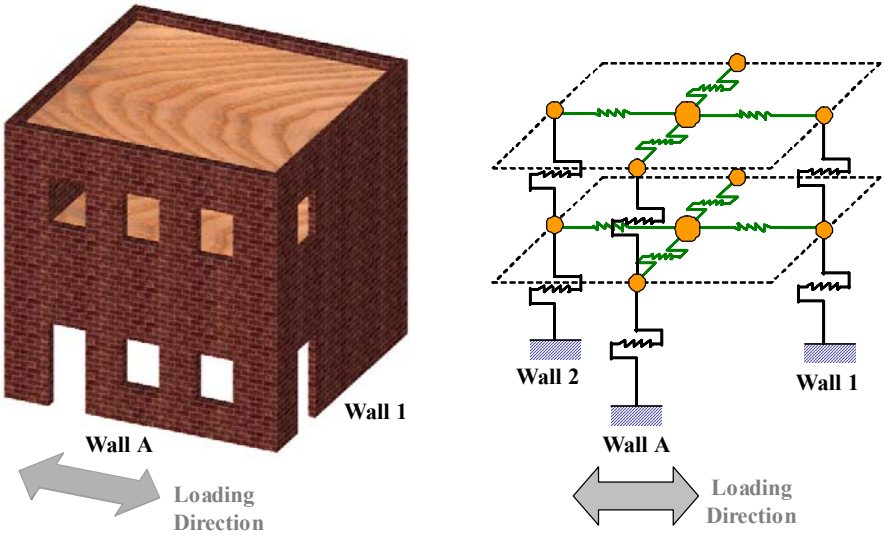

Figure 4.7: Nonlinear Spring Model Representing a URM Test Structure

Validation of the simplified DRAIN-2DX model is carried out by comparing its dynamic characteristics and responses to those computed from the finite element model [Kim and White, 2001]. It is found that the simplified model is able to capture most of the nonlinear behaviors in the walls and diaphragms and produces similar results to the more complex finite element model when the behavior is largely 2-dimensional (i.e., no torsional response). Comparisons in the building's fundamental period and maximum displacement at various locations due to a certain artificial ground motions are displayed in Table 4.5.

Table 4.5: Comparisons between Results from DRAIN-2DX and ABAQUS Models

	DRAIN-2DX Model	ABAQUS Model
Fundamental Period (sec)	0.304	0.304
Max Disp. @ Top of Wall A (in.)	0.0290	0.0263
Max Disp @ Top of Wall 1 (in.)	0.4528	0.4505
Max Disp. @ Center of Roof (in.)	0.4073	0.3930

Good agreement in the dynamic responses between the DRAIN-2DX composite spring model and the ABAQUS model provides confidence in utilizing the composite spring model in this research. It is believed that the much simpler spring model is sufficient for seismic performance assessment, and more importantly in the fragility analysis that requires a large number of analyses, of the URM structure in this study.

4.4.5 Building Model with Degraded Material Properties

The majority of the URM firehouses in Mid-America were constructed prior to 1970 [French and Olshansky, 2000]. Strength and structural integrity of these buildings

may experience some sorts of degradation over such a long period of time. In addition, construction materials (i.e., brick and mortar) that are older than 50 years did not provide as high a strength as similar materials today. In order to truly represent existing firehouses in the region, these factors must be taken into account in the structural models.

One way is to use lower values for the strength parameters of masonry to reflect the poor masonry condition. FEMA [2000a] suggests the values for compressive strength, elastic modulus, and shear strength of masonry with poor condition and they are listed in Table 4.6. These so-called degraded material properties replace those values obtained from the experimental study and are used to construct the composite spring model in this research. Consequently, the stiffness and strength properties of each wall are modified to reflect these degraded material properties.

Table 4.6: Degraded Masonry Properties

Properties	Values
Masonry Compressive Strength (psi)	300
Masonry Elastic Modulus (ksi)	165
Masonry Bed-Joint Shear Strength (psi)	13

4.5 EARTHQUAKE INPUTS

The focus of this study is to assess performance of typical firehouse in Mid-America under earthquakes. The test structure presented in the previous sections is a representation of typical URM firehouse constructions in this region. In order to be relevant, the earthquake loadings that are applied to the test structure must resemble

seismic characteristics in the same region. An ideal approach is to use ground motions recorded from historical earthquake events. However, due to the fact that the last major earthquake in this region was almost 200 years ago, the available recorded information for strong ground motions is scarce.

Wen and Wu [2001] developed a suite of synthetic ground motions for 3 cities in Mid-America. These cities include Carbondale, IL, Memphis, TN, and St. Louis, MO. Earthquakes are generated based on two hazard levels: 10% and 2% probabilities of exceeding in 50 years. Earthquake events are simulated with their epicenters uniformly distributed around the New Madrid Seismic Zone (NMSZ). The body wave magnitudes of these simulated earthquakes range between 5 and 8. Local site effects and soil amplification at the location of each city are also taken into account in the simulation process. At the end, a suite of 20 ground acceleration records are generated for each city location (10 records for 10% probability level and 10 records for 2% probability level).

In this research, focus has been placed on the area around Memphis and Shelby County. As a result, using the synthesized ground motions for Memphis is most appropriate. Both probability levels are applied in this research with the 10% exceeding probability events signifying the BSE-1 (Basic Safety Earthquake-1 defined by FEMA [2000a]) and the 2% events indicating the BSE-2. Time-history and elastic acceleration spectrum plots for each synthesized record can be found in Wen and Wu [2001].

4.6 DYNAMIC ANALYSIS OF A COMPOSITE SPRING MODEL

Performances of this URM firehouse under the earthquakes are assessed by numerical simulation of dynamic responses by DRAIN-2DX. The synthetic ground

accelerations are applied to the composite spring model and the building displacement responses are computed. Table 4.7 and Table 4.8 summarize the maximum displacements computed during the period of ground excitations. The maximum displacements displayed in these tables are computed at various locations in the building, that is Δ_{IPW} represents the maximum displacement at the top of the in-plane wall (wall A), Δ_{OPW} corresponds to the out-of-plane wall (wall 1), and Δ_{DIA} is computed at the center of the roof diaphragm.

Table 4.7: Maximum Displacements at Various Locations of the URM Structure under BSE-1 Ground Motions

Ground Motions	Δ_{IPW} (in.)	Δ_{OPW} (in.)	Δ_{DIA} (in.)
m10_01s	0.014	0.288	0.288
m10_02s	0.018	0.348	0.348
m10_03s	0.018	0.235	0.235
m10_04s	0.018	0.325	0.325
m10_05s	0.025	0.350	0.350
m10_06s	0.016	0.321	0.321
m10_07s	0.019	0.459	0.459
m10_08s	0.027	0.378	0.378
m10_09s	0.022	0.461	0.461
m10_10s	0.014	0.285	0.285

Table 4.8: Maximum Displacements at Various Locations of the URM Structure under BSE-2 Ground Motions

Ground Motions	Δ_{IPW} (in.)	Δ_{OPW} (in.)	Δ_{DIA} (in.)
m02_01s	0.501	2.122	2.124
m02_02s	0.129	1.775	1.776
m02_03s	0.354	1.770	1.771
m02_04s	0.304	2.324	2.325
m02_05s	0.454	1.776	1.777
m02_06s	0.217	2.218	2.219
m02_07s	0.182	1.713	1.714
m02_08s	0.237	2.032	2.033
m02_09s	0.358	2.096	2.097
m02_10s	0.327	2.367	2.369

Table 4.7 and Table 4.8 show that the maximum displacements due to earthquake loadings are much higher in the out-of-plane wall and the diaphragm than they are in the in-plane wall. This finding confirms that the out-of-plane walls are usually the most vulnerable component in the URM buildings. Past research on the nonlinear behaviors of the URM out-of-plane walls (Simsir et al. [2002] and Goodno et al. [2003]) also showed very low out-of-plane strengths. Had the out-of-plane walls not been strengthened, they would likely be the first point of failure due to their large lateral deformations.

The issue on the out-of-plane walls is beyond the scopes of this research. It is assumed in this research that proper mitigation has been implemented in the out-of-plane walls such that the out-of-plane walls remain elastic. A focus is made mainly on the

nonlinear behaviors and failures in the in-plane walls. Future studies should include a more detailed nonlinear behavior of the out-of-plane action in the analytical models.

The use of the building maximum displacements provides an insight on how the building performs under earthquake loadings and it may relate well to building damage. However, rather than using the maximum displacements, FEMA-356 [FEMA, 2000a] suggests the use of maximum inter-story drift as a performance measure in the URM buildings. The inter-story drift is computed as the relative lateral displacement between floors expressed as a percent of the story height at that floor. Building performance or damage levels are specified as a function of the maximum inter-story drift the building sustains during an earthquake. In the case of a URM building, three performance levels are defined. They include, Collapse Prevention (CP), Life Safety (LS), and Immediate Occupancy (IO) performance levels. Descriptions and the maximum drift limit for each building performance level are displayed in Table 4.9.

Table 4.9: Structural Performance Levels for URM Structures [FEMA, 2000a]

	Structural Performance Levels		
	Collapse Prevention S-5	Life Safety S-3	Immediate Occupancy S-1
Damage Levels	Severe	Moderate	Light
Overall Damage Descriptions	Extensive cracking. Face course and veneer may peel off. Noticeable in-plane and out-of-plane offsets.	Extensive cracking. Noticeable in-plane offsets of masonry and minor out-of-plane offsets	Minor cracking of veneers. Minor spalling in veneers at a few corner openings. No observable out-of-plane offsets.
Drift	1.0%	0.6%	0.3%

In order to assess the performance of the URM firehouse in the research, the maximum inter-story drifts are calculated from the time-history analyses of the composite spring model subjected to the suite of artificial ground motions. Both BSE-1 (10% exceedance probability) and BSE-2 (2% exceedance probability) earthquakes are applied to the structure. Table 4.10 presents the values of the maximum inter-story drift for both earthquake levels. The results obtained from the BSE-1 case are displayed on the left-hand side of the table, while those from the BSE-2 case are on the right. It is found that the building performs reasonably well under the BSE-1 earthquakes as its maximum drifts always satisfy FEMA's Immediate Occupancy (IO) criterion. On the other hand, when subjected to the stronger BSE-2 motions, the building undergo large drifts that it exceed the Collapse Prevention (CP) limit most of the time.

Table 4.10: Computed Maximum Inter-Story Drifts due to a Suite of Ground Motions

Ground Motions	Max Drift (%)	Ground Motions	Max Drift (%)
m10_01s	0.167	m02_01s	1.250
m10_02s	0.209	m02_02s	0.973
m10_03s	0.136	m02_03s	0.975
m10_04s	0.178	m02_04s	1.390
m10_05s	0.201	m02_05s	1.003
m10_06s	0.181	m02_06s	1.187
m10_07s	0.275	m02_07s	1.020
m10_08s	0.224	m02_08s	1.192
m10_09s	0.269	m02_09s	1.256
m10_10s	0.157	m02_10s	1.342
Mean	0.200	Mean	1.159
COV	0.23	COV	0.13

FEMA [2000a] defines a building performance objective that is mainly used for a rehabilitation purpose; however, the same objective can be used to assess seismic performance of existing building as well. The Basic Safety Objective (BSO) is the objective that ensures acceptable risk on a traditional life safety criterion. In order to achieve the BSO, the building must exceed the Life Safety (LS) building performance level under the BSE-1 earthquake hazard level and, at the same time, it must also exceed the Collapse Prevention (CP) building performance level under the BSE-2 hazard level.

However, in the case for an essential facility, a more stringent performance objective must be utilized. FEMA [1997] suggests an Enhanced Safety Objective for essential facilities that are critical for post-earthquake disaster response and recovery. In order to achieve this enhanced objective, the building must satisfy the Immediate Occupancy (IO) performance level under BSE-1 and the Life Safety (LS) level under BSE-2. It must be noted that this objective does not ensure that no interruptions will occur in the building function. Some cleaning or minor repair may be required in order to restore the building's original services, but it is intended that such repair can be quickly accomplished.

The maximum drift values from Table 4.10 indicate that the URM firehouse under this study does not comply with the Enhanced Safety Objective. A seismic rehabilitation is required in order to improve the building performances under future earthquakes. The thesis proposed the use of metallic damping devices for the seismic rehabilitation purpose. The details of such application are presented in Chapter 5 of this thesis.

More important point from Table 4.10 is that the computed maximum drifts vary quite significantly even in the same level of earthquakes. The primary cause of the fluctuation in the building responses is due to an inherent randomness in the seismic ground motions. Deterministic assessment of a building due to certain earthquakes may not provide an accurate insight for planning proper mitigation measures. Fragility assessment takes into account the uncertain parameters in determining the damage likelihood to the buildings. The following section presents a fragility analysis of the URM firehouse by utilizing the proposed approach developed in Chapter 3.

4.7 FRAGILITY ASSESSMENT OF THE URM BUILDING

It is discovered that significant variation in building responses may exist when the building is subjected to various ground motions. This is due to the inherent random characteristics of the earthquake events. In addition, the construction materials also exhibit uncertain properties that by using their mean values in the response computation alone may be misleading. As a result, an assessment that takes into account the uncertainty issue must be implemented. It is particularly useful for the decision-makers to be able to assess the likelihood of seismic damage and plan for proper actions. Fragility curves are a common tool in this regard as it describes the probabilities of damage to a building due to different levels of earthquake intensity.

In this research, the seismic responses and, consequently, damage are estimated through an explicit response surface metamodel. Uncertainties that exist in the problem are taken into account by simulating a large number of possibilities and calculating probabilities that damage may take place. The process for generating fragility curves for this URM building follows what has been presented in Chapter 3 for a SDOF system.

4.7.1 Damage Measure and Limit States

The first step in the process (Figure 3.3 and Figure 3.6) is to define a response measure that is suitable for quantification of seismic damage. A number of researchers have proposed the damage measures for buildings subjected to earthquake loadings. Some utilized a displacement-based measure such as a maximum roof drift ratio to quantify damage [Rodriguez and Aristizabal, 1999]. Some used energy-based criteria that relate the amount of hysteretic energy to the levels of damage [Wong and Wang, 2001]. Some researchers combined the two parts and derived unique measures (Park and Ang [1985] and Rodriguez and Aristizabal [1999]). However, there has been little consistency on the most appropriate measure to quantify the seismic damage. In light of these available damage measures, FEMA [2000a] proposed the use of the maximum drifts to assess building performance and levels of damage to structural components. In the case for unreinforced masonry walls, certain values of drift are defined for three performance or damage levels, as shown in Table 4.9. This simpler damage measure is used for assessing damage potential in the URM firehouse under investigation.

4.7.2 Uncertainties in Structural Parameters

Past investigations (Abrams and Shinozuka [1997], Schueremans and Gemert [1999], and JCSS [2001]) suggest a number of the URM material properties that exhibit uncertain properties. In this study, it is assumed that masonry density, elastic modulus, compressive strength, bed-joint shear strength, tensile strength and damping ratio are major sources of structural uncertainty for the URM structures. Statistical descriptions of the structural parameters are presented in Table 4.11. The mean values of the random parameters are obtained from the experimental study [Yi, 2004] and FEMA [2000a];

while the parameters' probability distribution and their dispersion measures are collected from several research in the past (Abrams and Shinozuka [1997], Schueremans and Gemert [1999], and JCSS [2001]).

Table 4.11: Structural Uncertainties for URM Structures

Random Parameters	Distribution	Mean	COV
Masonry Density (lb/in^3)	Lognormal	0.06944	0.05
Masonry Elastic Modulus (ksi)	Uniform	165.0	0.20
Masonry Compressive Strength (psi)	Lognormal	300.0	0.25
Masonry Tensile Strength (psi)	Lognormal	10.0	0.44
Masonry Bed-Joint Shear Strength (psi)	Lognormal	13.0	0.20
Damping (%)	Uniform	5.0	0.10

4.7.3 Uncertainties in Earthquake Loadings

This chapter continues to use a set of artificial ground motions generated for Memphis, Tennessee [Wen and Wu, 2001] for fragility analysis. The earthquakes in this suite were generated with variability in magnitudes and hypocentral distances from Memphis. Local site effects and soil amplification were also taken into consideration. Twenty synthetic ground acceleration records for Memphis are selected, as it is found in the preliminary study on the SDOF system that using a suite of 20 ground motions provides comparable results to a much larger suite.

A measure of earthquake intensity must also be identified. Initial investigation of the SDOF system (Chapter 3) shows that the use of spectral ordinate of the earthquakes provides better correlation to the displacement-based damage measure. In particular, the

spectral acceleration value at the fundamental period of the building is considered as an earthquake intensity measure.

Since fragility describes the damage probability conditional on a specific level of earthquake intensity, all ground acceleration records in the suite are scaled, according to (3.27), such that all have the same spectral acceleration values.

4.7.4 Response Surface Parameters

The main purpose of fragility is to describe the probabilistic response or damage of a structure with uncertain properties subjected to random excitations. A response surface model is defined in a way that it relates the damage measure to a set of random variables consisting of structural and seismic uncertainty parameters. The research proposed 3 approaches for constructing fragility curves. For this particular example, Approach 3 (see Chapter 3 for details), which incorporates the seismic parameter in the metamodel, is implemented because it provides the least computational expense (Table 3.9) while maintaining prediction accuracy. In this case the output parameters for the response surface are the mean values (y_μ) and the standard deviation (y_σ) of the maximum drifts (in percents) in the URM building computed from a suite of ground motions. The input parameters for the response surface are the material properties (random variables) and the seismic intensity measure (control variable).

The random input variables for constructing the response surface must be those structural uncertainty parameters (Table 4.11) that possess significant contributions to the computation of the response. The preliminary step is to perform a screening test for this set of input variables. It is found that the masonry tensile strength is largely unimportant and can be omitted from the response surface model derivation. The remaining random

parameters include the masonry density, the masonry compressive strength, the elastic modulus, the bed-joint shear strength, and the damping ratio. However, the elastic modulus and the compressive strength are perfectly dependent to each other (i.e., knowing one parameter means knowing the other) which violate the rule that states that the input variables for the response surface must be independent [Khuri and Cornell, 1987]. As a result, only the elastic modulus is used as one of the input variables for the response surface metamodel. Finally, this set of 4 random variables (density, elastic modulus, bed-joint shear strength, and damping) is joined by a control variable describing the level of earthquake intensity. Parameter space or ranges of input variables are specified for generating a response surface. Each input variable range is set such that it covers most (if not all) of the area under the probability density of the input. In the case when the input variables are described by the uniform distribution (i.e., masonry elastic modulus and damping ratio), their ranges are identical to the distribution limits. For cases other than the uniform distribution (i.e., lognormally distributed masonry density and bed-joint shear strength), the input parameters' lower and upper bounds for the response surface are set at -3σ and $+3\sigma$ from the means, respectively.

Table 4.12 summarizes the response surface input variables and their ranges. It can be seen that each input variable is normalized (3.4) such that its values lie between -1 and +1. The spectral acceleration level is assumed to vary between 0.1g to 1.9g. Three levels of the spectral acceleration are used for generating the response surface model. These levels correspond to three batches of scaled ground motions; that is batch 1, 2, and 3 contain the Memphis ground acceleration records that are scaled to 0.1g S_a, 1.0g S_a, and 1.9g S_a, respectively.

Table 4.12: Input Variables for a Response Surface Model

Random Structural Parameters	Input Variables	Lower Bounds	Center Points	Upper Bounds	Units
Masonry Density	ξ_1	0.0592	0.06944	0.07986	lb/in^3
	x_1	-1	0	+1	-
Masonry Elastic Modulus	ξ_2	108.0	165.0	222.0	ksi
	x_2	-1	0	+1	-
Masonry Bed-Joint Shear Strength	ξ_3	5.2	13.0	20.8	psi
	x_3	-1	0	+1	-
Damping	ξ_4	4.0	5.0	6.0	%
	x_4	-1	0	+1	-
Spectral Acceleration (S_a)	ξ_5	0.1	1.0	1.9	g
	x_5	-1	0	+1	-

4.7.5 Design of Experiments

JMP [1995] is a versatile statistical software package that is employed extensively in this research. It can be used in an initial step of formulating the DOE tables, fitting the response surface models, and finally performing statistical diagnosis on the derived models. In this part, JMP is used to form a DOE table based on the CCD. For this particular case of 5 input variables, 43 combinations of input variables are employed. Table 4.13 shows a Design of Experiments (DOE) table utilizing a scheme with reduced number of runs on the CCD. Each case or combination is composed of values -1, 0, or +1 of the input variables signifying the lower bounds, center, and upper bounds values, respectively.

Table 4.13: Design of Experiments Table of Input and Output Variables

Case	x_1	x_2	x_3	x_4	x_5	Mean (y_μ)	Std Dev (y_σ)
1	-1	-1	-1	-1	-1	0.064	0.011
2	-1	-1	-1	-1	1	1.201	0.229
3	-1	-1	-1	1	-1	0.056	0.010
4	-1	-1	-1	1	1	1.058	0.204
5	-1	-1	1	-1	-1	0.064	0.011
6	-1	-1	1	-1	1	1.205	0.231
7	-1	-1	1	1	-1	0.056	0.010
8	-1	-1	1	1	1	1.060	0.204
9	-1	0	0	0	0	0.458	0.075
10	-1	1	-1	-1	-1	0.042	0.010
11	-1	1	-1	-1	1	0.772	0.179
12	-1	1	-1	1	-1	0.036	0.009
13	-1	1	-1	1	1	0.690	0.162
⋮	⋮	⋮	⋮	⋮	⋮	⋮	⋮
40	1	1	1	-1	-1	0.051	0.006
41	1	1	1	-1	1	1.015	0.109
42	1	1	1	1	-1	0.047	0.005
43	1	1	1	1	1	0.850	0.102

The input parameters x_1 through x_4 describe the random material properties for constructing the composite spring models. The input parameter x_5 indicates the level of earthquake intensity a particular building is subjected to, which corresponds to the 3 batches of scaled earthquakes. In the end, there are 860 structure-earthquake combinations resulting from 43 unique building models with each subjected to 20 ground motions. Nonlinear time-history analysis is performed on each of the structure-earthquake combination and the maximum inter-story drift is extracted. The mean values and standard deviation of maximum drifts are computed with the normality assumption at each DOE case and recorded in the DOE table, as shown in Table 4.13.

4.7.6 Response Surface Model Fitting

The response surface models approximate the mean and standard deviation of maximum drifts by means of simple polynomial functions. A second-degree polynomial function is deemed appropriate in this study since the building responses are computed with nonlinear behaviors. A typical second-degree response surface function for 5 input variables is in the form of

$$\begin{aligned}\hat{y} = {} & b_0 + b_1x_1 + b_2x_2 + b_3x_3 + b_4x_4 + b_5x_5 + b_{11}x_1^2 + b_{21}x_2x_1 + b_{22}x_2^2 + \\ & b_{31}x_3x_1 + b_{32}x_3x_2 + b_{33}x_3^2 + b_{41}x_4x_1 + b_{42}x_4x_2 + b_{43}x_4x_3 + b_{44}x_4^2 + \\ & b_{51}x_5x_1 + b_{52}x_5x_2 + b_{53}x_5x_3 + b_{54}x_5x_4 + b_{55}x_5^2\end{aligned} \quad (4.7)$$

Least-square regression analyses between the input variables (x_1 to x_5) and the output variables (y_μ and y_σ) result in a matrix of the polynomial coefficient estimates (**b**). In particular, the coefficients of the polynomial are derived by (3.13) and the response surface models for the mean ($\hat{y}_\mu$) and standard deviation ($\hat{y}_\sigma$) of the maximum drifts are expressed as follows:

$$\hat{y}_{\mu} = 0.55 + 0.06x_1 - 0.103x_2 + 0.001x_3 - 0.034x_4 + 0.495x_5 - 0.023x_1^2 + 0.001x_2x_1 - 0.004x_2^2 - 0.007x_3x_1 + 0.003x_3x_2 + 0.008x_3^2 - 0.004x_4x_1 + 0.008x_4x_2 - 0.001x_4x_3 + 0.011x_4^2 + 0.053x_5x_1 - 0.094x_5x_2 + 0.001x_5x_3 - 0.03x_5x_4 + 0.008x_5^2 \quad (4.8)$$

and

$$\hat{y}_{\sigma} = 0.055 + 0.02x_1 - 0.0491x_2 - 0.002x_3 - 0.006x_4 + 0.102x_5 + 0.039x_1^2 - 0.037x_2x_1 + 0.066x_2^2 - 0.004x_3x_1 + 0.001x_3x_2 - 0.012x_3^2 - 0.002x_4x_1 + 0.004x_4x_2 + 0.033x_4x_3 - 0.014x_4^2 + 0.018x_5x_1 - 0.045x_5x_2 - 0.003x_5x_3 - 0.007x_5x_4 - 0.012x_5^2 \quad (4.9)$$

A two-dimensional or a so-called prediction profiler plots [JMP, 1995] are shown in Figure 4.8 and Figure 4.9, for the mean and standard deviation of the maximum drifts, respectively. In the prediction profiler plot, the response is plotted against each of the input variables, while other input variables are fixed at their center point values. The purpose of this plot is to observe the trend of the response due to an effect from a single input variable.

It is apparent from Figure 4.8 that the earthquake intensity level (x_5) has much more influence than the URM material properties on the calculation of the maximum inter-story drift of the URM building. Figure 4.9 also reveals that variability in the maximum drifts from a suite of earthquakes is more pronounced as the earthquake intensity increases.

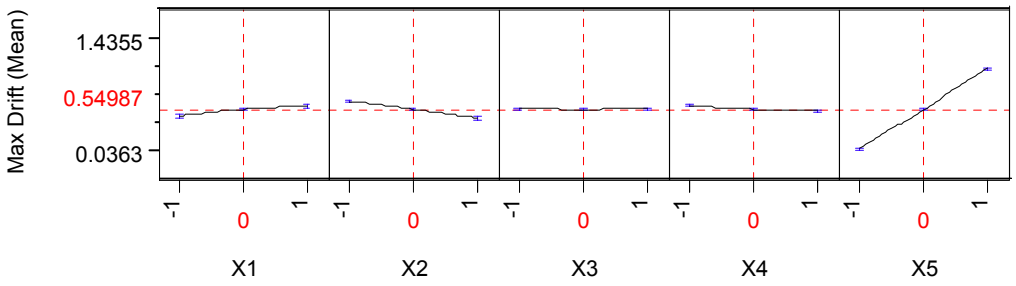

Figure 4.8: Prediction Profiler Plot of the Mean of Maximum Drifts

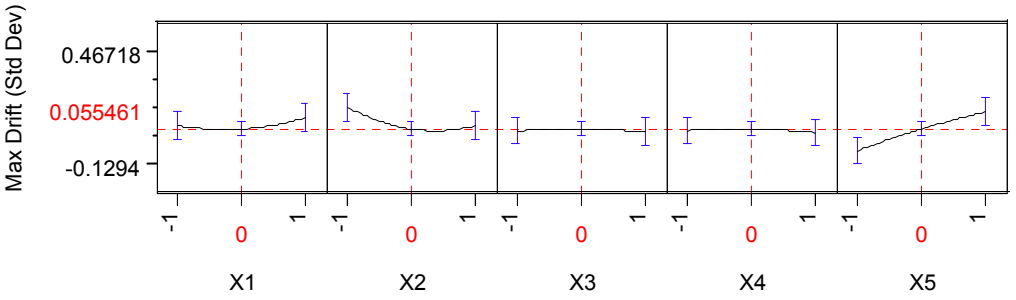

Figure 4.9: Prediction Profiler Plot of the Standard Deviation of Maximum Drifts

4.7.7 Statistical Validation of the Response Surface Models

The simplest step to check the response surface models is through the R^2 and R_A^2 values computed from (3.15) and (3.16), respectively. The model for the mean response has R^2 and R_A^2 of 0.9999 and 0.9996, while the model for the standard deviation has R^2 and R_A^2 of 0.9743 and 0.8885, respectively. Both models exhibit high correlation between the actual responses and those that are approximated by the

metamodels. However, these overly optimistic indications may be the result of the number of experiments compared to the numbers of degree of freedom in the model. The next step to verify the overall prediction accuracy of the response surface models require a model testing at additional and random combinations of the inputs. [Venter et al., 1997] suggested the use of the Average Absolute Error (%AvgErr), the Maximum Absolute Error (%MaxErr), and the Root Mean Square Error (%RMSE) for testing response surface model accuracy. For the purpose of these statistical tests, 100 additional combinations of input variables are generated at random. Actual (y_i) and predicted ($\hat{y}_i$) maximum inter-story drifts are calculated for each combination and those statistical measures are computed as follows:

$$\%\text{AvgErr} = 100 \cdot \frac{\frac{1}{N} \cdot \sum_{i=1}^{N} |y_i - \hat{y}_i|}{\frac{1}{N} \cdot \sum_{i=1}^{N} y_i} = 2.96\%$$

$$\%\text{MaxErr} = \underset{i}{\text{Max}} \left[100 \cdot \frac{|y_i - \hat{y}_i|}{\frac{1}{N} \cdot \sum_{j=1}^{N} y_j} \right] = 8.73\%$$

$$\%\text{RMSE} = 100 \cdot \frac{\sqrt{\frac{1}{N} \cdot \sum_{i=1}^{N} (y_i - \hat{y}_i)^2}}{\frac{1}{N} \cdot \sum_{i=1}^{N} y_i} = 3.58\%$$

The above measures quantify the error, in percentage, that the predicted maximum drifts from the response surface model depart from the actual values. It can be

seen that the level of error in the model is extremely low indicating the prediction accuracy of the response surface model.

Figure 4.10 displays a plot of actual drifts from the time-history analyses versus the drifts predicted by the response surface models. The diagonal line represents a perfect fir between the actual and the predicted values. It is apparent from the figure that the majority of the points lie within a close proximity of this line. This plot confirms that the response surface metamodel provide good approximation to the much more complex nonlinear dynamic analysis.

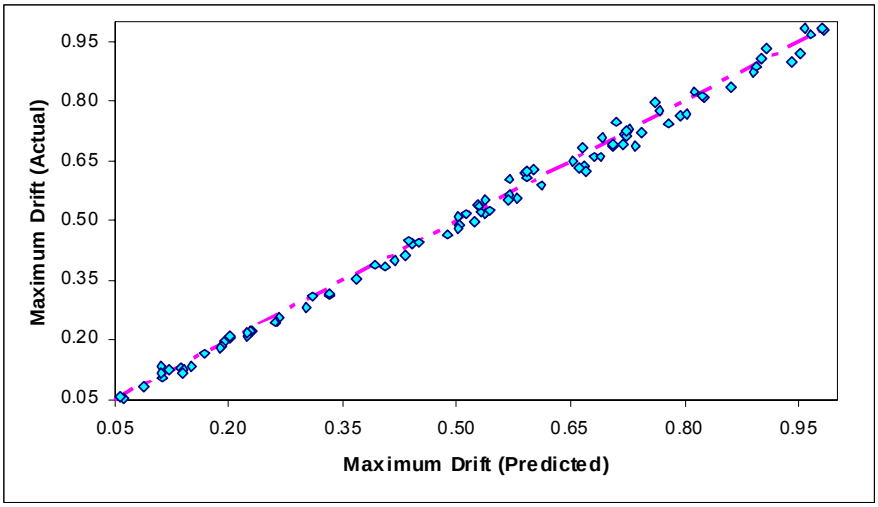

Figure 4.10: Plot of Actual Versus Predicted Maximum Drifts

4.7.8 Response Simulation

The response surface model generated by Approach 3 predicts the maximum drifts in the URM building subjected to earthquake with various intensities. In order to compute the building fragilities, the response surface must be evaluated at specific

intensity levels, creating metamodels that are conditioned on specific levels of earthquake intensity. The overall response surface in this case is evaluated at every 0.1g increment of the spectral acceleration (from 0.1g to 1.9g). The process creates 19 distinct polynomial models for predicting maximum drifts conditioning on specific intensity levels. For example, in the case of $S_a = 0.9g$, the value for the input parameter x_5 is derived from the normalization of the parameter according to (3.4) as follow.

$$x_5 = \frac{0.9g - \frac{1.9g + 0.1g}{2}}{\frac{1.9g - 0.1g}{2}} = -0.11 \tag{4.10}$$

Consequently, the response surface models of a mean and standard deviation of maximum drifts for a spectral acceleration of 0.9g are obtained by substituting $x_5 = -0.11$ in (4.8) and (4.9) and, hence, they become

$$\begin{aligned}\hat{y}_{\mu|S_a=0.9g} = {} & 0.495 + 0.054x_1 - 0.093x_2 + 0.001x_3 - 0.031x_4 - \\ & 0.023x_1^2 + 0.001x_2x_1 - 0.004x_2^2 - 0.007x_3x_1 + 0.003x_3x_2 + \\ & 0.008x_3^2 - 0.004x_4x_1 + 0.008x_4x_2 - 0.001x_4x_3 + 0.011x_4^2\end{aligned} \tag{4.11}$$

and

$$\begin{aligned}\hat{y}_{\sigma|S_a=0.9g} = {} & 0.044 + 0.018x_1 - 0.044x_2 - 0.002x_3 - 0.005x_4 + \\ & 0.039x_1^2 - 0.037x_2x_1 + 0.066x_2^2 - 0.004x_3x_1 + 0.001x_3x_2 - \\ & 0.012x_3^2 - 0.002x_4x_1 + 0.004x_4x_2 + 0.033x_4x_3 - 0.014x_4^2\end{aligned} \tag{4.12}$$

The overall metamodel takes the following form

$$\hat{y}_{S_a=0.9g} = \hat{y}_{\mu|S_a=0.9g} + N\left[0, \hat{y}_{\sigma|S_a=0.9g}\right] \tag{4.13}$$

in which a normality assumption (see Chapter 3 for validation) on the distribution of maximum drifts is exercised. Monte Carlo simulation is performed on (4.13) by randomly selecting, for a large numbers of time, values for input variables under their probability density assumptions (Table 4.11) and calculating responses from the metamodels.

Further validation of the outcomes from simulating the response surface metamodels is performed. A conventional approach that utilizes the Latin Hypercube Sampling (LHS) technique is used as a benchmark. The LHS divides the probability densities of the structural uncertainty parameters into 20 segments of equal probability. A random pairing process of structural parameters and earthquakes generates 20 structure-earthquake systems for dynamic analyses. Twenty discrete values of maximum drifts obtained form the dynamic analyses are rank-ordered and their cumulative probability values are computed according to Ang and Tang [1975]. Figure 4.11 compares these discrete probability values with the continuous cumulative density plot derived from the simulation of the response surface models. The figure shows consistent outcomes from both approaches.

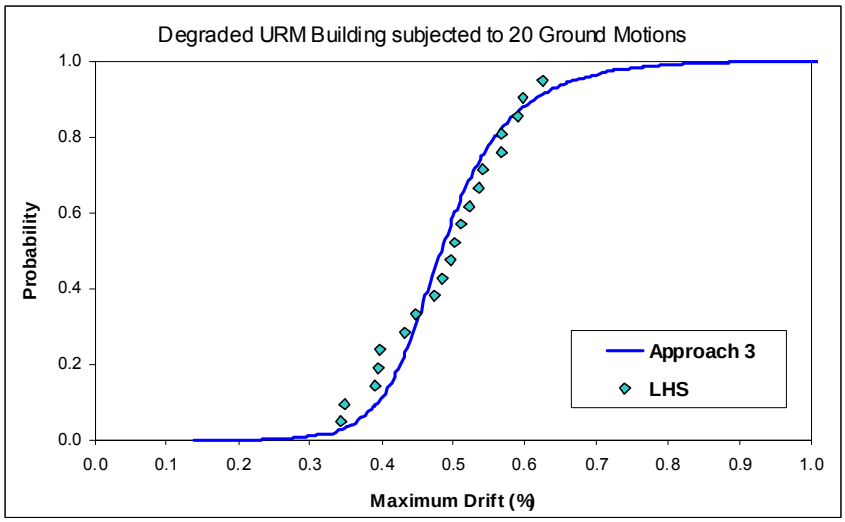

Figure 4.11: Cumulative Probability Plot of Maximum Drifts Conditioning to Sa =0.9g

The probabilities that the computed maximum drifts exceed the predefined limit states (Table 4.9) are computed from ten-thousand outcomes of the simulated response surface model as follows:

$$PE_{IO|Sa=0.9g} = \frac{1}{10{,}000} \cdot \sum_{i=1}^{10{,}000} I(Drift_i \geq 0.3\%) = \frac{9911}{10000} = 0.9911$$

$$PE_{LS|Sa=0.9g} = \frac{1}{10{,}000} \cdot \sum_{i=1}^{10{,}000} I(Drift_i \geq 0.6\%) = \frac{1216}{10000} = 0.1216$$

$$PE_{CP|Sa=0.9g} = \frac{1}{10{,}000} \cdot \sum_{i=1}^{10{,}000} I(Drift_i \geq 1.0\%) = \frac{5}{10000} = 0.0005$$

where $PE_{IO|Sa=0.9g}$, $PE_{LS|Sa=0.9g}$, and $PE_{CP|Sa=0.9g}$ are, respectively, the probabilities of exceeding the IO, LS, and CP limit states conditioning on the intensity level of 0.4g S_a. $I(\cdot)$ is an indicator function giving a value of 1 if the condition is met, and 0 otherwise.

Repetition of the process for all earthquake intensity levels (0.1g to 1.9g) gives a damage probability matrix, as shown in Table 4.14.

Table 4.14: Conditional Probabilities of Exceedance for the URM Building

S_a (g)	Probability of Exceedance		
	IO	LS	CP
0.1	0.0002	0.0000	0.0000
0.2	0.0001	0.0000	0.0000
0.3	0.0019	0.0000	0.0000
0.4	0.0312	0.0000	0.0000
0.5	0.2517	0.0006	0.0000
0.6	0.7456	0.0019	0.0000
0.7	0.9318	0.0115	0.0000
0.8	0.9764	0.0469	0.0001
0.9	0.9911	0.1216	0.0005
1.0	0.9951	0.2634	0.0016
1.1	0.9979	0.4603	0.0075
1.2	0.9987	0.6581	0.0179
1.3	0.9986	0.7955	0.0439
1.4	0.9995	0.8947	0.0829
1.5	0.9996	0.9429	0.1414
1.6	1.0000	0.9693	0.2260
1.7	0.9999	0.9831	0.3248
1.8	0.9999	0.9908	0.4250
1.9	0.9998	0.9954	0.5544

Plotting these probability values against the corresponding intensity level produces fragility curves for this URM building (Figure 4.12). Each curve is specific to a limit state or performance level. These curves depict the likelihood of damage corresponding to specific damage states with increasing levels of earthquake intensity.

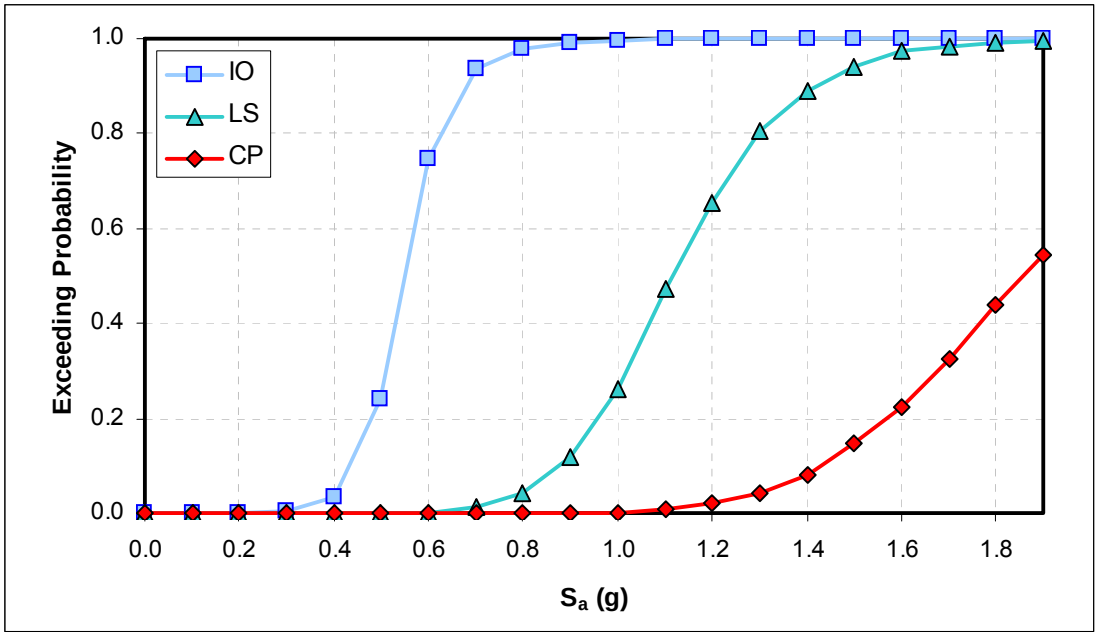

Figure 4.12: Fragility Curves of a Typical URM Firehouse in Mid-America

It is found, however, that these curves are generally different from those obtained from HAZUS [NIBS, 1999], especially for the higher damage levels (i.e. LS and CP). HAZUS fragility curves are generated based on subjective assessment of the states of damage and are not expected to provide reliable results for a particular building. The approach in this research is viewed as advancement from HAZUS methodology in

computing fragilities and could potentially be implemented in the loss estimation package in the future.

4.7.9 Evaluation of Building Fragilities

In order to evaluate the fragilities of the URM building under investigation, the seismic hazard information at the site of the building is required. In this study, the URM building is assumed to be located in Memphis, TN (35.172 Latitude and -90.016 Longitude). U.S. Geological Survey (USGS) provides the spectral acceleration values at short and long structural periods at locations throughout the United States. The values at the assumed location of the URM building are extracted from the 2002 USGS hazard maps. FEMA [2000a] guidelines are used to construct acceleration spectra for both BSE-1 (10% in 50 years) and BSE-2 (2% in 50 years) as shown, respectively, in Figure 4.13 and Figure 4.14.

Expected values for the spectral acceleration corresponding to the building fundamental period can be obtained directly from these spectra. For this URM firehouse, with a fundamental period of approximately 0.5 second, the corresponding spectral acceleration values from the spectral plots are approximately 0.4g and 1.2g for the BSE-1 and the BSE-2 hazard levels, respectively.

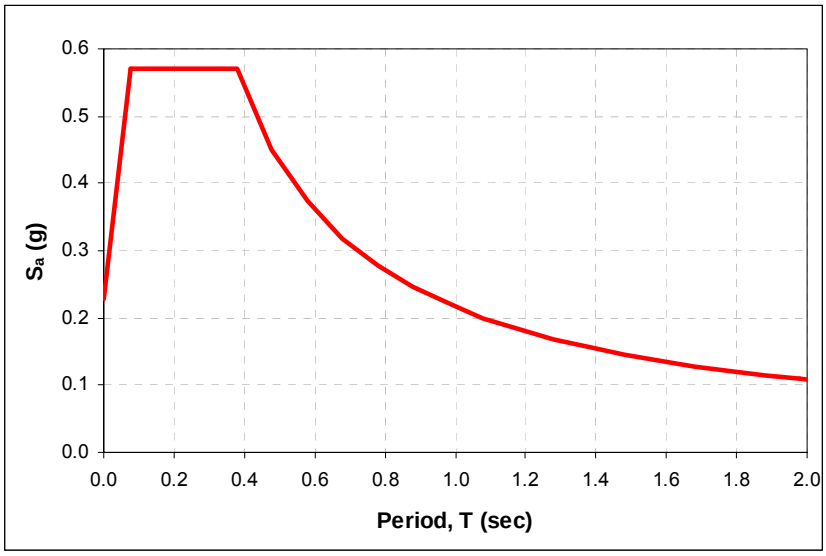

Figure 4.13: Acceleration Spectrum corresponding to BSE-1 Hazard Level for a Site in Memphis, TN [FEMA, 2000a]

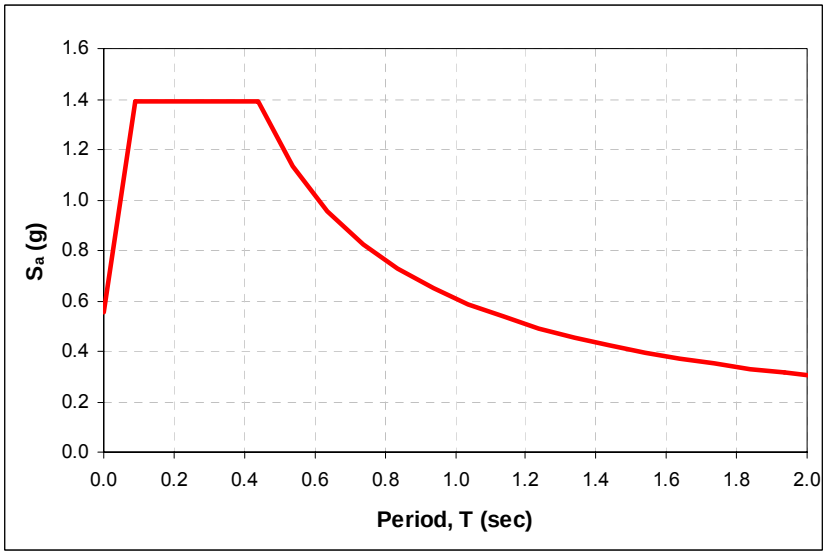

Figure 4.14: Acceleration Spectrum corresponding to BSE-2 Hazard Level for a Site in Memphis, TN [FEMA, 2000a]

As mentioned previously, the Enhanced Safety Objective [FEMA, 1997] requires that the essential facilities satisfy the Immediate Occupancy (IO) performance level under BSE-1 and the Life Safety (LS) level under BSE-2. Based on the spectral acceleration values for the BSE-1 and the BSE-2 hazard levels specific to the site, it is found from the fragility curves (Figure 4.12) that there is approximately 3% chance that the building damage exceeds the IO performance level given that the BSE-1 event were to occur. However, there is 66% chance that this URM building is damaged beyond the LS limit under the BSE-2 earthquake.

An appropriate rehabilitation option may be implemented to reduce the damage probabilities to a more desirable level. Chapter 5 presents the rehabilitation proposal for this URM firehouse using the metallic dampers. Deterministic and probabilistic assessments are performed.

CHAPTER 5

FRAGILITY ASSESSMENT OF A REHABILITATED URM BUILDING

In chapter 4, seismic assessment of an unreinforced masonry building typical of firehouse construction in Mid-America has led to a conclusion that the building is susceptible to future earthquakes and may not satisfy the performance criterion defined by FEMA [1997]. An appropriate rehabilitation should be employed in order to upgrade the building to the desired levels of performance. In this chapter, innovative rehabilitation schemes using a simple metallic damping device are proposed. Seismic fragility of the rehabilitated URM building is assessed using the response surface approach. Resulting fragility curves display significant reduction to damage potential over that of the baseline URM building.

5.1 PASSIVE ENERGY DISSIPATION CONCEPT

It is usually not practical to design building structures to withstand a maximum credible earthquake while maintaining purely elastic structural response. Conventional seismic design is based, instead, on the concept of ductility where structural members undergo large inelastic deformation and hence dissipate seismic input energy. This large

and repetitive inelastic deformation could result in damage in those structural members. However, the structure is pre-designed such that damage is concentrated only in the area where structural integrity would not be affected. This design philosophy focuses on preventing structural collapse, but the inter-story drifts required to achieve significant energy dissipation are often large and result in severe damage to nonstructural components. Substantial damage in both structural and nonstructural components could affect the overall functionalities of the structures. This is particularly important for essential facilities, which must be designed to maintain operational capabilities during and after an earthquake.

Supplemental energy dissipation systems are one way of addressing these problems in the seismic rehabilitation applications. The basic role of the energy dissipation devices is to absorb a significant portion of the seismic energy imparted to the building from an earthquake, reducing energy dissipation demand in the primary structural elements. As a result, damage in the main structural elements is minimal. Another benefit from incorporating the energy dissipation devices appears in the reduction in the dynamic responses of the buildings. The energy dissipation systems that are widely used as the structural protective systems can be divided into 3 groups. They include (1) the seismic isolation system, (2) the passive energy dissipation system, and (3) the active and semi-active control system [Soong and Dargush, 1997]. While all the protective systems mentioned herein can be effectively used for the seismic rehabilitation application, the focus of this research is on an implementation of a specific type of the passive energy dissipation devices.

For roughly 25 years, it has been recognized by both researchers and practitioners that incorporation of passive energy dissipation (PED) devices into buildings would improve their dynamic responses (i.e., reduce displacements, accelerations, etc.) Different types of passive energy dissipation devices have been used in seismic protection application for buildings. Metallic energy dissipation devices are based on the plastic deformation of metallic materials, such as mild steel. Friction dampers dissipate energy through the friction that develops between two solid bodies sliding relative to each other. Viscoelastic dampers use highly dissipative polymeric materials, which dissipate energy when subjected to shear deformations. Other forms of passive energy dissipation devices include viscous fluid dampers, tuned mass dampers, tuned liquid dampers, and metal extrusion.

5.2 METALLIC HYSTERETIC DAMPERS

As noted previously, the earthquake hazard in Mid-America, particularly in the NMSZ, is characterized by seismic events with very large magnitudes but relatively long recurrence intervals. As a result, much higher levels of reliability and higher resistance to aging must be assured for any technology used to reduce this hazard.

Passive energy dissipation systems using metallic hysteretic dampers are attractive for seismic protection systems under these conditions because they offer good long-term reliability, modest cost and relatively simple design. As a result, this research focuses only on the metallic energy dissipation devices as an innovative way of rehabilitating URM buildings in this region.

In recent years, extensive efforts have been carried out on the application of metallic hysteretic dampers for rehabilitation and retrofit purposes. A large number of PED devices using metallic hysteresis have been successfully installed in structures in high seismic regions throughout the world. Development of the metallic hysteretic energy dissipation systems will be described in the following sections.

5.2.1 Past Development

The idea of utilizing metallic hysteretic dampers to dissipate portion of the input energy in the structures began in early 1970s. Kelly, Skinner, and Heine [1972], and Skinner, Kelly, and Heine [1973, 1975] reported on the conceptual and experimental development of three special mechanical devices to be incorporated into a structure specifically to passively absorb energy generated by an earthquake. These devices included the rolling-bending of thin U-shaped strips, torsional energy absorbers, and flexural energy absorbers.

The U-shaped steel strips interact between adjacent surfaces whose relative movement is directed parallel to each other. The plastic deformation occurs when the strip changes from straight to curved. Different specimens were tested under controlled cyclic displacements. The peak load, dissipated energy and the total number of cycles to failure depended upon the thickness, radius and width of the device. The torsional bar utilizes a combination of torsion and bending, and therefore can be designed for use between surfaces moving away from each other in foundations or shear wall systems. The flexural device utilizes bending of short rectangular beams, and can be designed for use in a number of different situations.

A concept of triangular plate damper was originally developed in New Zealand by Tyler [1978]. This device, which consists of some identical triangular structural steel plates positioned in parallel, is typically installed within a frame bay between chevron braces and the overlying beam. The base of each triangular plate is welded into a rigid base plate to approximate a fixed end condition. As a result of this configuration, the damper primarily resists horizontal forces, associated with an interstory drift, via uniform flexural deformation of the individual plate.

Following the triangular plate energy dissipators, Scholl [1988] reported on the development of a tapered steel X-plate (so-called added damping and stiffness element or ADAS) and its applications as an energy dissipation device. ADAS elements (Figure 5.1) consist of multiple X-shaped mild steel plates connected in parallel to each other. Whittaker et al. [1991] investigated the use of ADAS elements in the retrofit of moment resisting frames. They showed that these energy dissipation devices could successfully reduce the dynamic response of a moment resisting frame, and they proposed to extend their use to other types of structural systems.

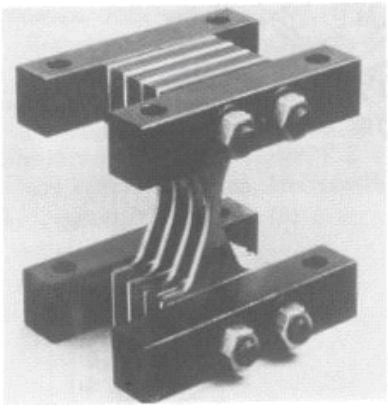

Figure 5.1: Scaled Model of ADAS Element [Perry et al., 1993]

At Georgia Tech, Pinelli [1992] and Pinelli et al. [1993] analytically and experimentally investigated the use of tapered energy dissipation device as cladding connections in buildings. The particular device they proposed consists of a section of a square tube, cut away as shown in Figure 5.2 to create two tapered beams for which the plastification will occur over the greater portion of materials and ensure that the tapered beams will deform with double curvature.

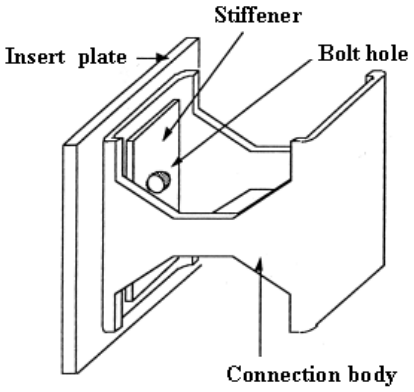

Figure 5.2: Tapered Energy Dissipation Device [Pinelli et al., 1993]

The test results showed that these tapered devices provided large and stable hysteretic loops without stiffness degradation and strength deterioration (Figure 5.3). The plastic deformations were distributed uniformly throughout the tapered beams maximizing the amount of energy dissipated. The device also sustained a large number of cyclic load reversals (as high as 37 cycles) before failure presenting a good fatigue behavior of the tapered device.

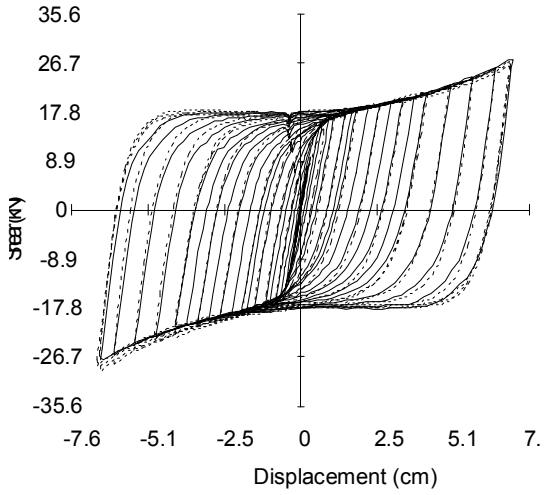

Figure 5.3: Hysteretic Loops for Tested Tapered Device [Pinelli et al., 1993]

5.2.2 Structural Applications

Having gained some confidence from experimental results of the metallic damper, researchers and practitioners turned their interests to its applications. This part of the thesis summarizes the applications of the metallic damping devices in the real structures.

Martinez-Romero [1993] reported on the implementations of the metallic damping devices in 3 buildings in Mexico City including the Izazaga building, the Cardiology Hospital buildings, and the Reforma buildings. The 3 buildings experienced structural damage from the 1985 Mexico earthquake to various degrees. The buildings were retrofitted with the application of the ADAS systems. Computer simulations of the retrofitted buildings showed that the buildings would perform well under future major earthquakes.

Perry et al. [1993] summarized the seismic upgrade of the Wells Fargo Bank building in San Francisco. The building is a two-story non-ductile concrete frame

structure. The building experienced structural and nonstructural damage from the 1989 Loma Prieta earthquake. The retrofit plan was to add some steel chevron-braced frames connected to the existing concrete frames by the ADAS devices. A series of X-shaped mild steel plates was used for this system. The use of the ADAS devices in this building was the first structural application of these devices in the United States. The nonlinear time-history analyses confirmed that the maximum displacement of the retrofitted building was within the acceptable limits under severe earthquakes.

Goodno et al. [1998] investigated the application of cladding connectors using tapered energy dissipation devices developed by Pinelli [1993]. A 20-story steel frame building located in Oakland was selected to carry out computational analyses and check the performance of the tapered connectors. DRAIN-2DX, which can perform nonlinear time-history dynamic analysis, was used. Over a thousand of tapered energy dissipative cladding connectors were added to the building model. The simulations indicated a reduction in top floor displacement of up to 40 percent when the tapered connectors were included. Further investigation included a redesign process that concentrated on the reduction in seismic demand of the primary structures while maintaining the same level of baseline building response. It was concluded that by installing the tapered cladding connectors in a new design, the primary structural member sizes could be reduced by up to 17 percent in weight compared to the baseline building.

5.3 PROPOSED REHABILITATION SCHEMES

Normally, passive energy dissipation systems are not considered for unreinforced masonry applications because it is difficult to realize sufficient deformation in these relatively stiff structures to activate typical devices. However, the vast majority of URM

essential facilities in the NMSZ are one or two story structures with wooden floor and roof diaphragms. For such buildings, the flexibility of the floor diaphragm and its interaction with the walls in a building with fairly regular floor plan may provide sufficient deformation to activate inelastic deformation, and hence develop energy dissipation, in appropriately configured passive devices.

The hysteretic damper considered in this research is a tapered ductile metal flexural device similar to the ADAS device [Perry et al., 1993] presented in section 5.2.1. Such devices, even those fabricated from mild steel, are capable of developing large and stable hysteresis loops under cyclic loads and are capable of providing good and predictable energy dissipation.

Initial analysis of the 2-story URM model with square floor plan shows that the relative displacement between the center of the floor diaphragm and the top of the in-plane wall is in the order of 6 times greater than that between the diaphragm center and the out-of-plane wall. This suggests the possible use of PED devices, perhaps in connection with floor stiffening, to reduce this flexibility and therefore stabilize the out-of-plane walls. On this basis, the devices considered in this study are activated using the flexibility in the floor diaphragm. One configuration makes use of relative displacement between flexible floor diaphragms and the in-plane walls. Another potential configuration is to utilize the relative displacement between the center of the flexible diaphragm and the ground or the floor below. These implementations are called Type 1 and Type 2 rehabilitation schemes, respectively.

5.3.1 Type 1 Rehabilitation Scheme

The concept behind the Type 1 rehabilitation scheme is to utilize the differential displacement between the flexible floor (or roof) diaphragm and the much stiffer in-plane walls to activate the hysteretic devices. The actual application could be in a number of different forms involving either distributed deformation or transfer (via braces or link beams) to a localized device. An implementation of the devices using a link beam and localized PED device is shown in Figure 5.4. In this figure, wall 2 of the URM building is removed from the view in order to better see the implementation of the PED devices. It is assumed that the device will respond only to seismic input in a direction perpendicular to the link beam. A relatively stiff link beam is used to connect between the two in-plane walls (wall A and wall B). The PED device is then attached between the middle of the link beam and center of the diaphragm. Provided that the lateral stiffness (and possibly the torsional stiffness for eccentric connections) of the link beam is relatively high, the displacement at the middle of the link beam is comparable to that of the in-plane walls. The PED device then sustains relative displacement between center of the diaphragm and the in-plane walls, and energy dissipation is developed when the device deforms inelastically.

5.3.2 Type 2 Rehabilitation Scheme

Because of the flexibility of the diaphragm, high differential displacement between the center of the diaphragm and the ground is also expected. The Type 2 scheme makes use of this differential movement directly to trigger inelastic deformation and, consequently, energy dissipation in a PED device connected between the floor diaphragm and the ground. The second floor implementation may be less effective, but

definitely is possible. In order to capture this differential displacement, a simple chevron-brace frame is used to support the PED device relative to the floor diaphragm. A very stiff chevron-brace system is desirable in such a scheme, and it seems reasonable to think that such a design could be incorporated in a rehabilitation project. Figure 5.5 illustrates the application of a Type 2 rehabilitation scheme in unreinforced masonry building. Wall A and wall 2 are omitted from the URM building in the figure for better view of the PED devices. In this illustration it is assumed that the device will respond to seismic input in the direction of the chevron-brace plane.

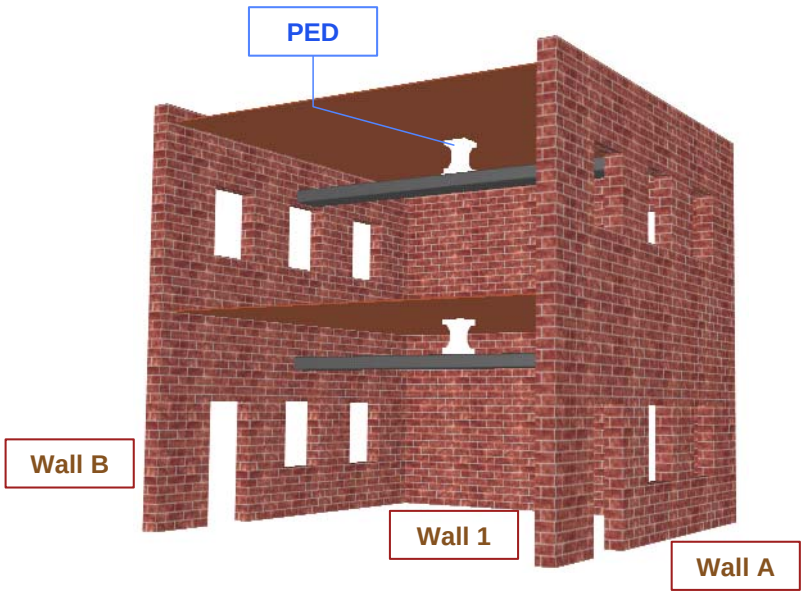

Figure 5.4: Type 1 Rehabilitation Scheme

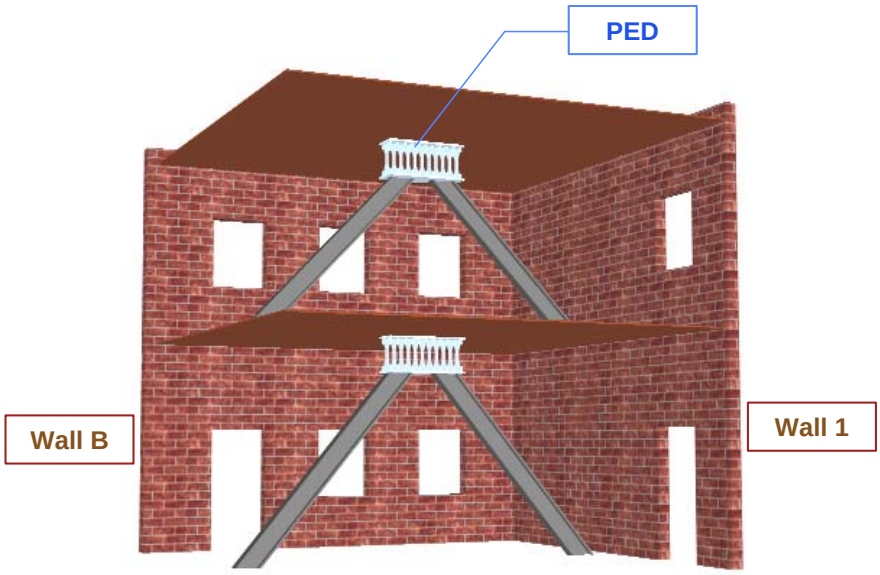

Figure 5.5: Type 2 Rehabilitation Scheme

5.3.3 Analytical Models

Chapter 4 of this thesis has presented the use of DRAIN-2DX spring elements to construct models of the URM building with nonlinear behaviors. The model is constructed using the DRAIN TYPE 04 zero-length nonlinear spring. Figure 5.6 shows a schematic of this simple spring model in which the zero-length springs and nodes are separated in order to show the model topology. Wall A and, on the opposite side, wall B represent the in-plane walls, while wall 1 and wall 2 represent the out-of-plane walls. The masses of the in-plane walls, out-of-plane walls, and diaphragms are lumped at the floor level, as shown in Figure 5.6.

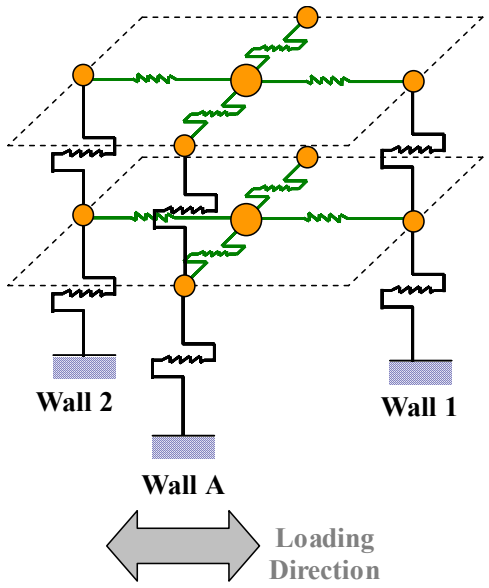

Figure 5.6: Simplified Composite Spring Model for the URM Test Structure

The basic well-designed hysteretic metallic PED device can be represented by a nonlinear spring element. As a result, it is a relatively simple matter to introduce the PED device into the building model simply by adding another TYPE 04 spring in the appropriate place(s). For a Type 1 PED device design, this spring is introduced between the in-plane wall and diaphragm masses as shown in Figure 5.7a. For the Type 2 PED device design, the spring is introduced between the diaphragm mass and the ground as shown in Figure 5.7b. For clarification purpose, only the first story parts of the model are shown in these figures. In addition, since there is no explicit interaction between the out-of-plane walls and the PED devices, the representation of the out-of-plane walls is also omitted from the figures. The two in-plane walls are connected to each other through the springs representing the shear stiffness of the diaphragm (DIA_S).

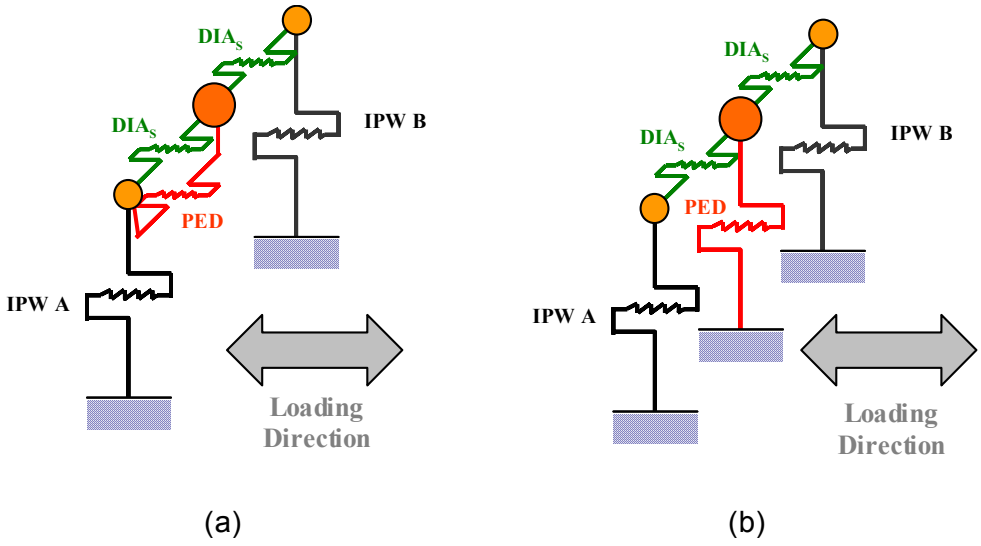

Figure 5.7: Part of the Composite Spring Model with (a) Type 1 Rehabilitation Scheme, and (b) Type 2 Rehabilitation Scheme

The stiffness of the link beam used with the Type 1 design or the stiffness of the brace used to support the Type 2 design will clearly reduce the available differential displacement across the PED device and therefore reduce its potential performance capability. However, this less-than-ideal behavior is not taken into consideration in the current study.

5.3.4 Hysteretic Model of Metallic Dampers

As previously mentioned, the energy dissipation mechanism in the metallic dampers results from their inelastic deformations. Numerous mathematical models have been proposed to simplify the force-displacement relationship of the metallic substances. Two of the simplest and most well-known models are the elastic-perfectly plastic model (Figure 5.8a) and the elastic-linear strain hardening model (Figure 5.8b). These models

present reasonably good comparisons with the experimental results for well-designed PED devices.

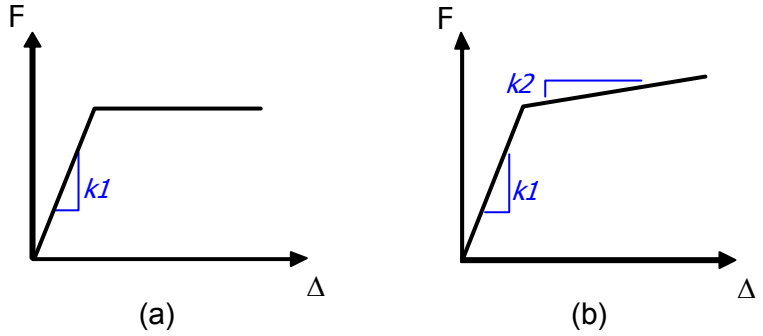

Figure 5.8: Force-Displacement Relationship with (a) Elastic-Perfectly Plastic Behavior, and (b) Elastic-Linear Strain Hardening Behavior

Furthermore, in order to develop the hysteretic model for the metallic dampers, material behavior under load reversals must be considered. The unloading branch of the force-displacement curve is assumed parallel to the initial loading path until it reaches another yield point in the reversed direction. The loading-unloading process will be repeated as the external cyclic loading continues.

An experimental result by Pinelli et al. [1993] (Figure 5.3) displays the hysteretic loops of the metallic tapered devices. An occurrence of the strain hardening behavior is obvious in the post yield region. As a result, this hysteretic behavior is best modeled by the elastic-linear strain hardening model. Figure 5.9 illustrates a typical metallic damper hysteretic model in this research. This kind of behavior is easily modeled using the DRAIN-2DX TYPE 04 nonlinear zero-length spring element.

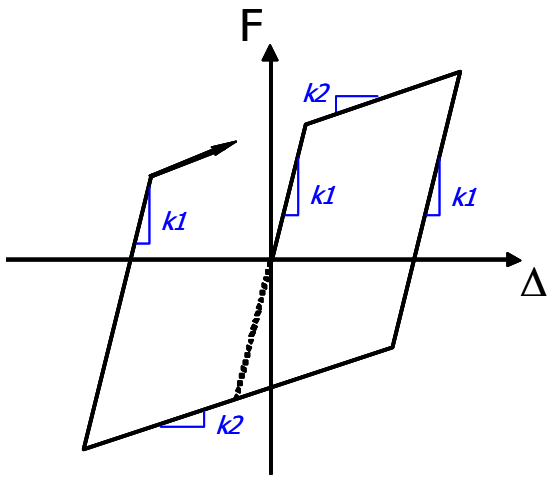

Figure 5.9: Idealized Bilinear Force-Displacement Relationship with

5.4 EFFECT OF DIAPHRAGM STIFFNESS

As mentioned previously, the flexibility of the floor diaphragms is a key issue in the utilization of a passive rehabilitation system. Further investigations on the effects of diaphragm stiffness are performed. The ratio of the energy dissipated in the PED device to the total input seismic energy (labeled as the "energy ratio") is computed as the shear stiffness of the floor diaphragm is varied. Figure 5.10 shows the relationship between the energy ratio and the shear stiffness of the floor diaphragm normalized to the stiffness of the in-plane wall. The vertical lines (error bars) capture a variation due to different ground motion inputs. This figure shows a rapid decrease in the energy dissipation ratio as the diaphragm shear stiffness gets higher. The curve confirms our early assumption that the energy dissipation capability of the PED devices will be more promising when the floor diaphragm is more flexible.

Generally, the maximum displacements (or drifts) are of interest in the case of unreinforced masonry structures. Figure 5.11 demonstrates how the diaphragm shear stiffness affects the maximum displacement at the diaphragm center under a suite of ground motions. Both displacements from the existing and rehabilitated structures are plotted against the diaphragm shear stiffness ratio. The maximum displacement from the existing structure is shown with a darker line, while that of a rehabilitated one is shown with a lighter line. The maximum displacements for both cases are almost identical when the stiffness ratio is relatively high (the diaphragm shear stiffness is around 20% or more of in-plane wall elastic stiffness). This means the passive control system is not effective. On the other hand, the maximum diaphragm displacement for the rehabilitated structure is much lower than that of the existing building when the diaphragm stiffness is significantly less than the in-plane wall elastic stiffness. This indicates a greater response reduction can be achieved in the rehabilitated structure, in addition to more energy dissipation, when the diaphragm is more flexible. For the URM building in this research, the diaphragm shear stiffness is approximately 1% of the elastic stiffness of the in-plane wall confirming great benefits from implementing the PED device.

Stiffening of the diaphragms is one of the typical ways for diaphragm rehabilitation. Results from a relevant research on diaphragm rehabilitation shows that typical stiffening methods would not increase the stiffness of the diaphragm beyond a few percents of the in-plane wall stiffness. This indicates that the application of a passive energy dissipation system in conjunction with diaphragm stiffening technique is also plausible.

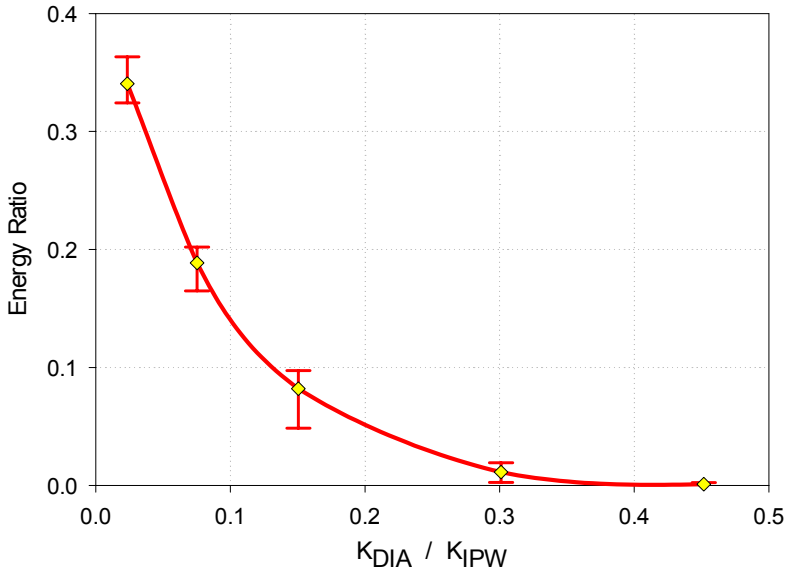

Figure 5.10: Effects of Diaphragm Shear Stiffness on the Energy Dissipation Ratio Considering a Suite of Ground Motions

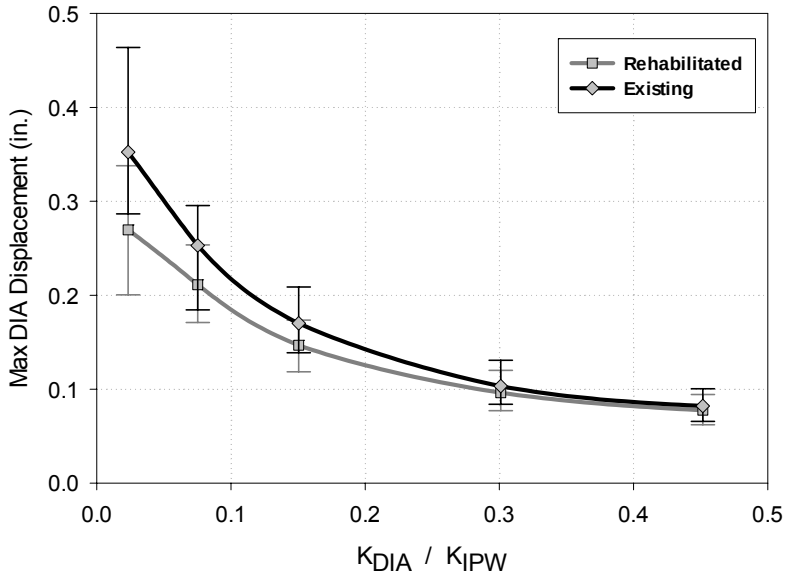

Figure 5.11: Effects of Diaphragm Shear Stiffness on the Diaphragm Maximum Displacement Considering a Suite of Ground Motions

5.5 DESIGN OF THE HYSTERETIC DEVICES

The approach for designing the hysteretic dampers in this research follows the works done by Pinelli et al. [1993], Goodno et al. [1998], and Craig et al. [2002]. The PED device itself is designed using an energy-based formulation. In this approach, the system is designed such that it maximizes the amount of the energy dissipation in the devices and, hence, minimizes the demand in the primary structural elements.

5.5.1 Design Objectives and Constraints

For a structure to resist an earthquake excitation in an economical and feasible way, part of the energy must be dissipated through viscous or hysteretic damping. However, hysteretic damping is often associated with yielding and damage to the structural members, formation of plastic hinges, and possibly collapse of the structure. Alternatively, many of the so-called energy dissipators developed in recent years aim at concentrating the dissipation, either viscous or hysteretic, away from the structural members, in a few pre-engineered elements. This is exactly the idea behind the tapered PED device.

In order to identify the best possible design for a PED device, the following criterion is adopted [Pinelli et al., 1996]:

The best design will be the one that provides the highest ratio E_C/E_i,

where E_c is the total hysteretic energy dissipated in all the devices, and E_i is the relative energy input to the structure at the end of the motion. The term E_c/E_i is referred to as an "energy ratio" or a "dissipating energy ratio" in this research.

The design process can easily be cast into the form of a simple nonlinear optimization process with the energy ratio as the objective function and appropriate constraints added for the maximum force in the PED device, stiffness and dynamic ductility, for example:

(1) The ductility demand on any of the PED devices should not exceed an allowable value defined for each particular energy dissipator (e.g., based on laboratory tests);

(2) PED device physical geometry and fabrication constraints (these are not explicitly considered in the present study).

The E_c/E_i criterion takes the fullest advantage of the energy dissipation property of the PED devices. Pinelli et al. [1996] showed that satisfaction of this design criterion would ensure that little hysteretic energy was dissipated in the structural members, and that the overall seismic response of the building was reduced.

A critical issue in the design of the PED device is the definition of ductility. The traditional definition of ductility, as the ratio of maximum displacement to yield displacement, provides only limited information to designers in the case of systems subjected to random vibrations with varying amplitudes. It overlooks important parameters like the number of cyclic reversals and the energy dissipated by the system. Here, a more comprehensive definition of ductility due to McCabe and Hall [1989] has been adopted.

McCabe and Hall [1989] assumed that the damage suffered by an elasto-plastic structural steel system during an earthquake is similar to a low cycle fatigue phenomenon.

Based on their work, it is possible to predict an equivalent monotonic ductility, μ_p, for a system subjected to an arbitrary cyclic loading. This equivalent monotonic plastic ductility, or ductility demand, is the maximum plastic ductility that the system should exhibit in a monotonic loading test in order to dissipate the same amount of energy as that obtained during the cyclic loading. The equivalent monotonic plastic ductility demand on the system can be evaluated in terms of energy, and load reversals, as:

$$\mu_p = \frac{H_t}{f_y u_y (2N_f)^{0.4}} \tag{5.1}$$

where H_t is the total hysteretic energy dissipated in the system during N_f load reversals; and f_y and u_y are the yield load and yield displacement of the system.

5.5.2 Design Variables

The design criterion as stated above is, in fact, a classical constrained optimization problem. The objective function to be optimized (or maximized in this case) is the energy ratio E_c/E_i. The design variables for the present optimization process are direct properties of the PED device, and they include, (a) the elastic stiffness, and (b) the yield capacity of the metallic devices. The use of only 2 design variables makes it somewhat easier to graphically describe the design space since a simple Cartesian 3-dimensional surface or a 2-dimensional contour plot can be used to describe the objective function, and the constraints can be readily superposed. It should be noted that for more complicated cases involving more design variables, a numerical optimization procedure could also be employed to compute the design parameters directly. However, in most cases little or no information about the design space itself is revealed. For the present

study, a grid of values of the objective (energy ratio) and constraint (dynamic ductility demand) functions are computed and plotted as superposed contour plots.

Based on the energy ratio criterion, the damage in the main structural components, if at all occurs, is minimal. Instead, damages will be concentrated in the pre-designed hysteretic devices where most of the hysteretic energy takes place. In terms of performances, rehabilitated URM buildings are expected to experience less response (i.e., displacement, acceleration) due to an earthquake. The following sections describe the design process and outcomes for both Type 1 and Type 2 rehabilitation schemes in details.

5.5.3 Design Optimization

The design process can be formulated as a straightforward numerical optimization process in which an objective function (E_c/E_i) as computed using DRAIN-2DX must be maximized with respect to PED device design variables, elastic stiffness (k) and yield force (f_y), and with constraints on the maximum allowable dynamic ductility. A number of powerful, versatile, and widely available numerical methods could be used but are not in this study. Rather, a purely graphical process is manually implemented in which the objective function is numerically evaluated for a tabular array of different design variables (PED device elastic stiffness and yield force) spanning the design space under investigation. In addition, the resulting dynamic ductility demand for each case is also computed and recorded. The result of these calculations is a grid of values of the objective function and constraint values (dynamic ductility demand) that could be plotted as superposed 2-dimensional contour plots.

Type 1 Rehabilitation Scheme

A number of test cases are investigated using the Type 1 PED device model subjected to a reference suite of ground accelerations. In the case of an essential facility, it is more appropriate that the protective system is designed based on the maximum credible earthquakes (BSE-2 level earthquakes based on FEMA [2000a]). A suite of the Memphis synthetic ground motions [Wen and Wu, 2001] with 2% probability of exceedance in 50 years is considered in the design of the PED devices. A contour plot for determining an optimal design of the PED devices is generated specific to each ground motions in the suite.

The yield force and elastic stiffness of the PED devices are varied from 1 to 15 kips and from 10 to 120 kips/in, respectively, resulting in a total of 345 analysis cases. DRAIN-2DX computes the objective energy ratio and the constraint dynamic ductility for each analysis case. An example of the resulting contour plot from a particular earthquake is shown in Figure 5.12. Contour lines of the energy ratios and dynamic ductility demand are superimposed over the design space. The contour lines for the energy ratio are shown as solid gray lines while the contour lines for the plastic ductility demand are shown as solid black lines.

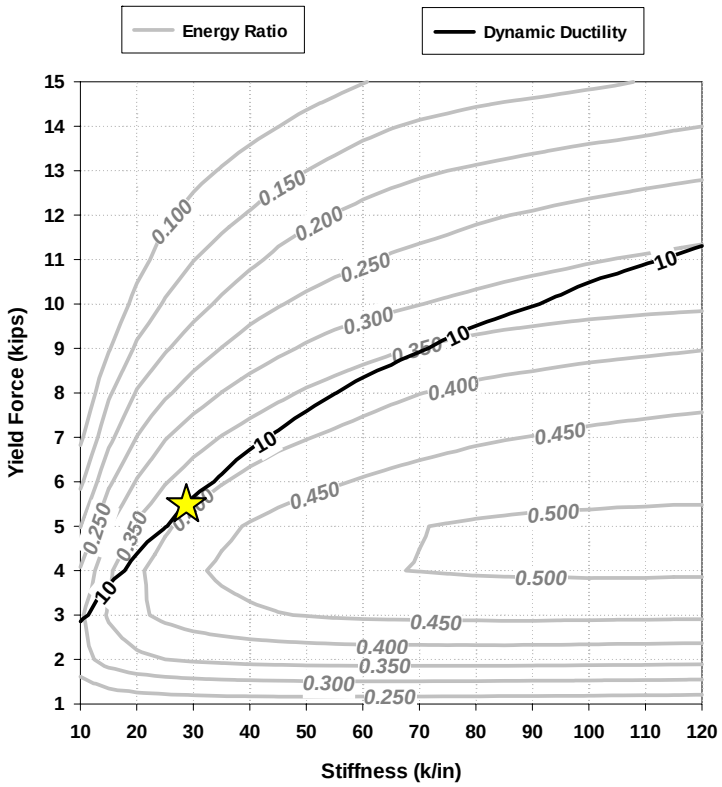

Figure 5.12: Example Contour Plots of the Energy Ratio and Dynamic Ductility

When the dynamic ductility is considered as a constraint in order to represent the finite deformation capacity of the devices (before fracture), the optimal solutions can be limited by the superposed dashed curves. Based on a laboratory test of tapered flexure PED devices [Pinelli et al. 1996] similar to the ones considered in this research, it is reasonable to allow dynamic ductility demands of no greater than about 10. Using this constraint value, the optimal design can be found along the ductility constraint line where the highest energy ratio presents. A star in Figure 5.12 shows the optimal design point of the PED devices for this particular ground motion. The objective contours indicate that by adding the PED devices with their properties corresponding to the optimal values into the existing structure, approximately 40% of the input seismic energy can be dissipated.

For better visualization of the optimal design of the PED devices, the 2-dimensional contour plot is converted to a design curve. This design curve is constructed by reading the values for the energy ratio and the elastic stiffness along the constraint curve at each increasing discrete levels of the yield force. Next, a plot of the energy ratio versus the corresponding elastic stiffness can be drawn for increasing levels of the yield force. The optimal design is defined at the peak of the curve where the energy ratio reaches its maximum. An example of the design curve can be seen from Figure 5.13.

Another important point is that the optimal solution of the PED device design is dependent of the earthquake ground motion used in the analysis. A straightforward solution is to design the PED devices corresponding to all of the earthquakes in a suite and evaluate the building performances when subjected to all other earthquakes. The final design is selected from the design that provides the best overall building performances. However, this is a very time-consuming process, and it may also be possible that no single design provides the "best" performance when earthquakes with various characteristics are considered. This research takes a simpler step by pre-selecting a few earthquakes from the suite that are believed to cause the most damage to the structure and using them as a basis in the design. The earthquakes are selected based on various intensity measures that have been found to correlate well with structural damage [Kramer, 1996]. These intensity parameters include the peak ground acceleration (PGA), the effective duration of (T), the ratio between the peak velocity and the peak acceleration (V/A), and the spectral acceleration at the fundamental period of the structure (S_a). Table 5.1 lists the Memphis synthetic earthquakes with their intensity parameters with the maximum values in each category underlined. From this table, it

appears that 3 ground motions (m02_05s, m02_08s, and m02_10s) may be appropriate as design earthquakes.

The design curves for these 3 particular earthquakes are constructed and are displayed in Figure 5.13. The optimal solution of the design is obtained from the peak of each curve. For conservatism, the lowest curve is used for selecting the optimal design. In this case the optimal design is found to be 6 kips and 19 kips/inch for the yield force and elastic stiffness of the PED devices, respectively.

Table 5.1: Memphis Synthetic Ground motions and their Intensity Measures

Earthquakes	PGA (in/s^2)	V/A (sec)	Duration (sec)	S_a @ 0.52 sec (g)
m02_01s	430	0.1352	30.67	3.04
m02_02s	326	0.1327	21.46	2.41
m02_03s	353	0.1381	20.24	1.95
m02_04s	317	0.1347	55.32	2.76
m02_05s	466	0.1400	57.82	2.52
m02_06s	408	0.1539	43.51	2.77
m02_07s	358	0.1429	23.01	2.29
m02_08s	286	0.2255	18.04	2.71
m02_09s	328	0.1286	22.18	2.18
m02_10s	405	0.1364	19.68	3.74

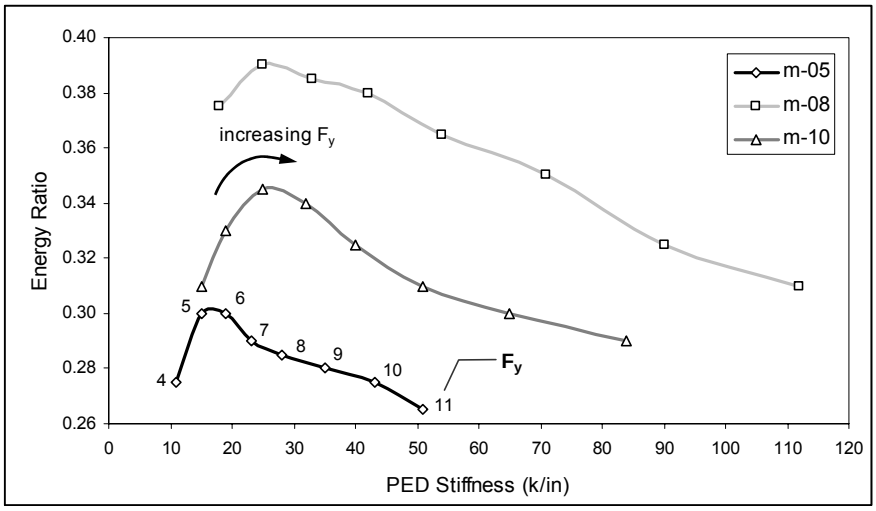

Figure 5.13: Design Curves for the Type 1 PED Device with Ductility Demand Constraint of 10

Type 2 Rehabilitation Scheme

A design process for the Type 2 scheme is similar to that of the Type 1 scheme. A grid of energy ratio and dynamic ductility demand values computed from over 300 cases is used to construct the superimposed contour plots. Similar to the Type 1 scheme, the ductility constraint of 10 is implemented for the Type 2 scheme as well. The resulting design curves for the Type 2 scheme are presented in Figure 5.14.

The optimal design for the PED devices with Type 2 configuration is found to be 13 kips and 86 kips/inch for the yield force and elastic stiffness of the PED devices, respectively.

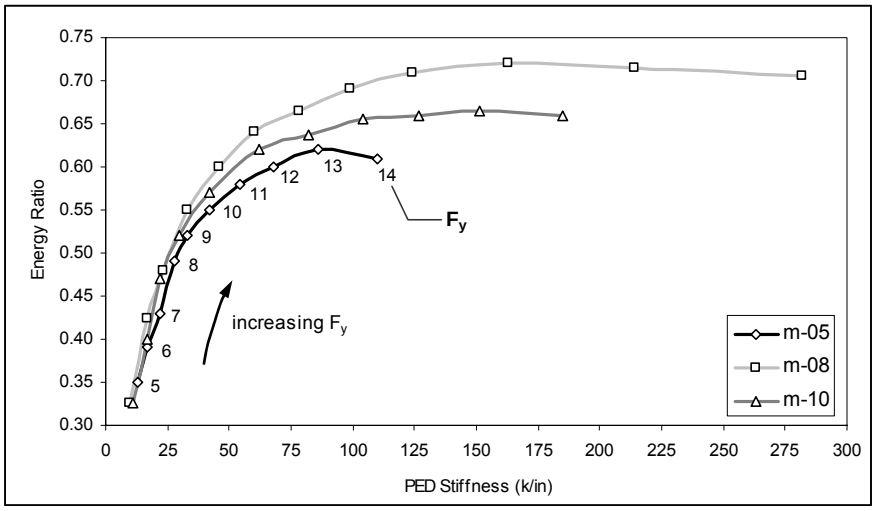

Figure 5.14: Design Curves for the Type 2 PED Device with Ductility Demand Constraint of 10

5.6 SEISMIC RESPONSE OF THE REHABILITATED BUILDING

The energy-based design criterion ensures that a large portion of the seismic input energy is absorbed by the supplemental energy dissipation devices and, hence, reducing energy dissipation demand and possible damage in the main structural components. In addition, an increase in supplemental damping and stiffness from the added devices may also help in improving building seismic responses (i.e., displacements or accelerations). Evaluation of the rehabilitated URM building subjected to potential earthquakes is presented in this section.

As presented in Chapter 4, the maximum inter-story drift is used for quantifying levels of damage according to FEMA [2000a]. Maximum drifts from the URM building that incorporates the optimal PED device designs are computed for every Memphis

artificial ground motions and are listed in Table 5.2 and Table 5.3 for the Type 1 and Type 2 rehabilitation schemes, respectively.

A comparison between the maximum drifts obtained from the existing building and the building rehabilitated with the PED devices reveals that the addition of the PED devices not only reduces the energy dissipation demands in the primary structures, it also has an effect on reducing the drift responses in the URM building under investigation.

The case with Type 2 rehabilitation scheme shows better performance than that of Type 1 scheme. The building's maximum drift demands, in most of the time, conform to the enhanced objective for essential facilities. On the other hand, the Type 1 scheme, even though achieving a major improvement, still fails to fulfill the Life Safety requirement under strong earthquakes (BSE-2 with 2% probability of exceedance in 50 years). Fluctuation in the computed building drifts is considerably high as due primarily on the random characteristics of the earthquakes. Fragility assessment of these Type 1 and Type 2 rehabilitated buildings takes into account the uncertainties in both earthquakes and structure and, consequently, provides the likelihood of damage as will be shown in subsequent sections.

Table 5.2: Comparison of the Computed Maximum Inter-Story Drifts for Existing and Type 1 Rehabilitated URM Buildings

Ground Motions	Maximum Drift (%)		Percent Reduction	Ground Motions	Maximum Drift (%)		Percent Reduction
	Rehabilitated	Existing			Rehabilitated	Existing	
m10_01s	0.142	0.167	14.7	m02_01s	0.840	1.250	32.8
m10_02s	0.167	0.209	20.0	m02_02s	0.709	0.973	27.1
m10_03s	0.100	0.136	26.3	m02_03s	0.815	0.975	16.3
m10_04s	0.165	0.178	7.5	m02_04s	0.945	1.390	32.0
m10_05s	0.193	0.201	4.2	m02_05s	0.737	1.003	26.5
m10_06s	0.140	0.181	22.8	m02_06s	0.944	1.187	20.5
m10_07s	0.152	0.275	44.5	m02_07s	0.652	1.020	36.1
m10_08s	0.191	0.224	14.7	m02_08s	0.747	1.192	37.3
m10_09s	0.246	0.269	8.5	m02_09s	0.876	1.256	30.3
m10_10s	0.108	0.157	31.2	m02_10s	0.921	1.342	31.4
Mean	0.160	0.200	19.5	Mean	0.819	1.159	29.0
COV	0.27	0.23	0.63	COV	0.13	0.13	0.23

Table 5.3: Comparison of the Computed Maximum Inter-Story Drifts for Existing and Type 2 Rehabilitated URM Buildings

Ground Motions	Maximum Drift (%)		Percent Reduction	Ground Motions	Maximum Drift (%)		Percent Reduction
	Rehabilitated	Existing			Rehabilitated	Existing	
m10_01s	0.112	0.167	32.9	m02_01s	0.508	1.250	59.3
m10_02s	0.094	0.209	55.1	m02_02s	0.424	0.973	56.4
m10_03s	0.096	0.136	29.6	m02_03s	0.447	0.975	54.2
m10_04s	0.105	0.178	41.4	m02_04s	0.466	1.390	66.5
m10_05s	0.098	0.201	51.2	m02_05s	0.451	1.003	55.1
m10_06s	0.090	0.181	50.0	m02_06s	0.610	1.187	48.6
m10_07s	0.119	0.275	56.7	m02_07s	0.431	1.020	57.8
m10_08s	0.148	0.224	33.8	m02_08s	0.462	1.192	61.2
m10_09s	0.079	0.269	70.8	m02_09s	0.466	1.256	62.9
m10_10s	0.070	0.157	55.0	m02_10s	0.512	1.342	61.9
Mean	0.101	0.200	47.7	Mean	0.478	1.159	58.4
COV	0.22	0.23	0.27	COV	0.12	0.13	0.10

5.7 FRAGILITY ASSESSMENT

As randomness is inherent in the problem, a deterministic assessment of building's seismic performances may not be sufficient. As a result, probabilistic description of the URM buildings with hysteretic damping devices would be more appropriate. The proposed approach of using the response surface metamodels is again implemented for fragility computation. Fragility curves can be used as an indicator for assessing an improvement on the damage likelihood in the URM firehouse when the metallic PED devices are implemented.

The structural uncertainties follow those defined for the existing building in Chapter 4 (Table 4.11). They include the masonry density, elastic modulus, shear strength, and the building's damping ratio. It is assumed that the PED system is well constructed that the level of uncertainty in its properties is statistically insignificant compared to those of the earthquakes and the URM material properties. As a result, the properties of the PED device are assumed to remain deterministic in this research. In terms of seismic uncertainty, it is taken into consideration by utilizing a suite of artificial earthquakes. The ground motions generated specifically for Memphis, TN are used in the same way as in Chapter 4 for the existing URM building.

5.7.1 Response Surface Model Generation

The maximum inter-story drift that the building experiences over the duration of an earthquake defines the level of damage. Response surface models are sought to relate this damage measure to those structural uncertainty parameters as well as the earthquake intensity parameter. It was obvious that Approach 3 (see details in Chapter 3) provides comparable outcomes while only requiring a fraction of the computational expenses

compared to the other 2 approaches. In Approach 3, the response surfaces for the mean (y_μ) and the standard deviation (y_σ) of the maximum drifts due to a suite of earthquakes are constructed. The input variables for the response surface polynomial and their ranges are described in Table 4.12. Note that in this chapter, the range of the spectral acceleration (S_a) is expanded (0.1g to 2.9g) in order to accommodate the potentially shift-to-the-right fragility curves. All other parameters (structural uncertainties) remain the same as those for the existing building.

The special scheme of the Central Composite Design (CCD) is then used to assemble combinations of input variables. Nonlinear time-history analyses are performed on the rehabilitated buildings (both with Type 1 and Type 2 schemes) for each combination to complete the DOE table (Table 5.4 and Table 5.5 for Type 1 and Type 2 Rehabilitation schemes, respectively).

Table 5.4: Design of Experiments Table for the Type 1 Rehabilitated Building

Case	x_1	x_2	x_3	x_4	x_5	Mean (y_μ)	Std Dev (y_σ)
1	-1	-1	-1	-1	-1	0.045	0.011
2	-1	-1	-1	1	1	1.026	0.212
3	-1	-1	1	-1	1	1.130	0.264
4	-1	-1	1	1	-1	0.041	0.010
5	-1	0	0	0	0	0.461	0.096
6	-1	1	-1	-1	1	0.808	0.201
7	-1	1	-1	1	-1	0.028	0.007
8	-1	1	1	-1	-1	0.032	0.008
9	-1	1	1	1	1	0.775	0.202
10	0	-1	0	0	0	0.609	0.109
11	0	0	-1	0	0	0.535	0.112
12	0	0	0	-1	0	0.554	0.116
13	0	0	0	0	-1	0.039	0.010
14	0	0	0	0	0	0.536	0.113
15	0	0	0	0	1	1.039	0.233
16	0	0	0	1	0	0.519	0.110
17	0	0	1	0	0	0.536	0.112
18	0	1	0	0	0	0.460	0.095
19	1	-1	-1	-1	1	1.425	0.430
20	1	-1	-1	1	-1	0.053	0.007
21	1	-1	1	-1	-1	0.059	0.009
22	1	-1	1	1	1	1.368	0.385
23	1	0	0	0	0	0.579	0.111
24	1	1	-1	-1	-1	0.040	0.010
25	1	1	-1	1	1	1.007	0.225
26	1	1	1	-1	1	1.086	0.239
27	1	1	1	1	-1	0.036	0.009

Table 5.5: Design of Experiments Table for the Type 2 Rehabilitated Building

Case	x_1	x_2	x_3	x_4	x_5	Mean (y_μ)	Std Dev (y_σ)
1	-1	-1	-1	-1	-1	0.024	0.007
2	-1	-1	-1	1	1	0.616	0.176
3	-1	-1	1	-1	1	0.662	0.216
4	-1	-1	1	1	-1	0.022	0.006
5	-1	0	0	0	0	0.236	0.054
6	-1	1	-1	-1	1	0.456	0.128
7	-1	1	-1	1	-1	0.016	0.005
8	-1	1	1	-1	-1	0.018	0.006
9	-1	1	1	1	1	0.445	0.130
10	0	-1	0	0	0	0.333	0.083
11	0	0	-1	0	0	0.277	0.064
12	0	0	0	-1	0	0.280	0.064
13	0	0	0	0	-1	0.024	0.007
14	0	0	0	0	0	0.275	0.063
15	0	0	0	0	1	0.629	0.180
16	0	0	0	1	0	0.272	0.061
17	0	0	1	0	0	0.275	0.063
18	0	1	0	0	0	0.252	0.056
19	1	-1	-1	-1	1	0.832	0.214
20	1	-1	-1	1	-1	0.032	0.010
21	1	-1	1	-1	-1	0.035	0.011
22	1	-1	1	1	1	0.801	0.203
23	1	0	0	0	0	0.317	0.078
24	1	1	-1	-1	-1	0.025	0.007
25	1	1	-1	1	1	0.645	0.186
26	1	1	1	-1	1	0.677	0.206
27	1	1	1	1	-1	0.023	0.006

The response surface models are represented by simple polynomial functions. A least-square regression technique is used to derive the polynomial coefficients. The response surface models for the mean ($\hat{y}_\mu$) and standard deviation ($\hat{y}_\sigma$) of the maximum drifts in the URM building rehabilitated with the Type 1 scheme are expressed as follows:

$$\begin{aligned}\hat{y}_\mu = {} & 0.528 + 0.073x_1 - 0.082x_2 + 0.005x_3 - 0.018x_4 + 0.516x_5 - \\ & 0.007x_1^2 - 0.009x_2x_1 + 0.008x_2^2 - 0.003x_3x_1 + 0.001x_3x_2 + \\ & 0.009x_3^2 - 0.001x_4x_1 + 0.003x_4x_2 + 0.007x_4x_3 + 0.01x_4^2 + \\ & 0.069x_5x_1 - 0.076x_5x_2 + 0.006x_5x_3 - 0.016x_5x_4 + 0.012x_5^2\end{aligned} \tag{5.2}$$

and

$$\begin{aligned}\hat{y}_\sigma = {} & 0.104 + 0.023x_1 - 0.025x_2 + 0.001x_3 - 0.007x_4 + 0.128x_5 + \\ & 0.001x_1^2 - 0.017x_2x_1 - 0.002x_2^2 - 0.005x_3x_1 + 0.001x_3x_2 + \\ & 0.009x_3^2 - 0.001x_4x_1 + 0.005x_4x_2 + 0.018x_4x_3 + 0.009x_4^2 + \\ & 0.025x_5x_1 - 0.026x_5x_2 + 0.001x_5x_3 - 0.007x_5x_4 + 0.018x_5^2\end{aligned} \tag{5.3}$$

Similarly, the least-square regression analysis derives the response surface polynomial functions for the Type 2 rehabilitation scheme based on Table 5.5. The models are presented as follows:

$$\begin{aligned}\hat{y}_\mu = {} & 0.278 + 0.05x_1 - 0.044x_2 + 0.002x_3 - 0.008x_4 + 0.308x_5 - \\ & 0.002x_1^2 + 0.004x_2x_1 + 0.014x_2^2 - 0.002x_3x_1 + 0.001x_3x_2 - \\ & 0.002x_3^2 + 0.001x_4x_1 + 0.002x_4x_2 - 0.005x_4x_3 - 0.002x_4^2 + \\ & 0.046x_5x_1 - 0.041x_5x_2 + 0.002x_5x_3 - 0.007x_5x_4 + 0.048x_5^2\end{aligned} \tag{5.4}$$

and

$$\hat{y}_{\sigma} = 0.065 + 0.011x_1 - 0.011x_2 + 0.003x_3 - 0.004x_4 + 0.087x_5 + 0.001x_1^2 + 0.006x_2x_1 + 0.004x_2^2 - 0.002x_3x_1 - 0.001x_3x_2 - 0.002x_3^2 + 0.001x_4x_1 + 0.002x_4x_2 - 0.007x_4x_3 - 0.002x_4^2 + 0.009x_5x_1 - 0.009x_5x_2 + 0.003x_5x_3 - 0.004x_5x_4 + 0.028x_5^2 \quad (5.5)$$

5.7.2 Response Surface Model Validation

In order to examine the prediction accuracy of the response surface models, 100 additional random combinations of the input variables are generated. The maximum drifts are computed by DRAIN-2DX nonlinear dynamic analysis (y_i) and the response surface model ($\hat{y}_i$) for each combination of inputs. A graphical comparison is obtained by plotting the actual values (DRAIN-2DX) against the predicted values (response surface) as shown in Figure 5.15 and Figure 5.16. It is apparent from those comparisons that the response surface models are able to predict the maximum drifts well. Furthermore, Venter et al. [1997] suggested the use of 3 quantitative measures to test the models. These measures quantify the level of error (in percentage) that the predicted responses depart from the actual ones. The expressions for the 3 measures can be found in (3.17), (3.18), and (3.19). Table 5.6 summarizes these statistical measures for both Type 1 and Type 2 rehabilitated buildings. The percentages of error in all measures are small, indicating high prediction accuracy of the response surface metamodels.

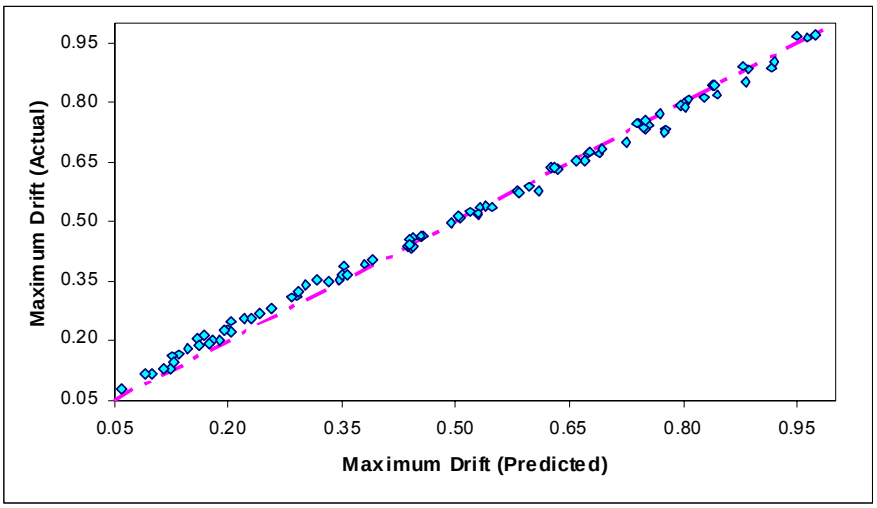

Figure 5.15: Plot of Actual Versus Predicted Maximum Drifts for the Type 1 Rehabilitated Building

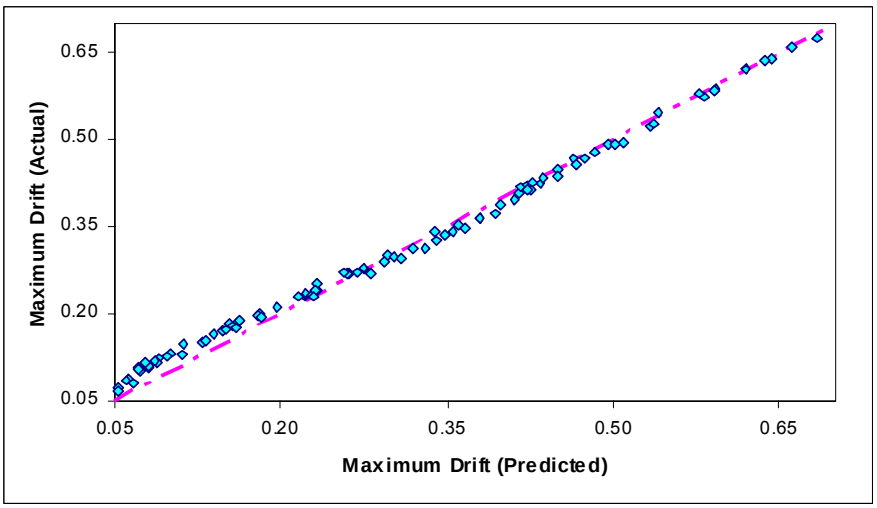

Figure 5.16: Plot of Actual Versus Predicted Maximum Drifts for the Type 2 Rehabilitated Building

Table 5.6: Computed Measures of Modeling Error

Measures	Type 1 Scheme	Type 2 Scheme
%AvgErr	3.2	4.5
%MaxErr	9.3	12.8
%RMSE	4.0	5.6

5.7.3 Response Simulation and Fragility Curves

The response surface models are evaluated at discrete levels of S_a from 0.1g to 2.9g. This process essentially produces new response surface models specific to certain values of S_a. The response surface models for the mean and the standard deviation of the maximum drifts are combined with an assumption that the drifts due to various ground motions are normally distributed. Monte Carlo simulation is performed at a specific level of earthquake intensity S_a and the fragilities or the conditional probabilities of damage are extracted. The plot of the damage probability values against the corresponding spectral acceleration values yields fragility curves for the rehabilitated URM buildings. Note that the detailed description of the process is given in Chapter 4.

The fragility curves for the IO, LS, and CP performance levels for the buildings with Type 1 and Type 2 rehabilitation schemes are presented in Figure 5.17 and Figure 5.18, respectively.

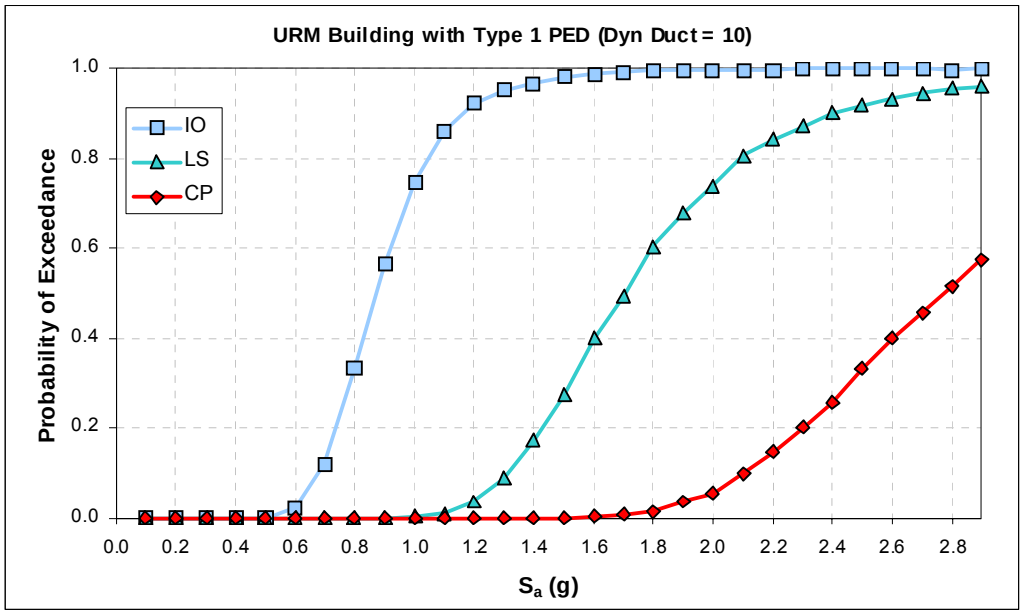

Figure 5.17: Fragility Curves of a Type 1 Rehabilitated URM Firehouse in Mid-America

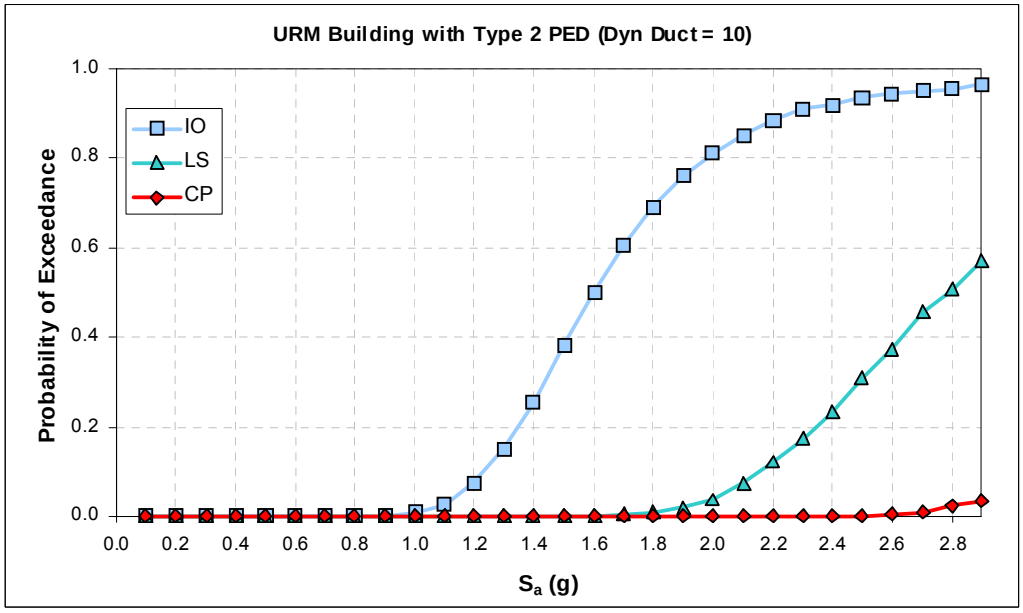

Figure 5.18: Fragility Curves of a Type 2 Rehabilitated URM Firehouse in Mid-America

5.7.4 Evaluation of Building Fragilities

For the URM building located in Memphis, TN (35.172 Latitude and -90.016 Longitude), the expected spectral acceleration values for the BSE-1 and BSE-2 earthquakes can be read from the USGS site-specific acceleration spectra (Figure 4.13 and Figure 4.14). In the case of the URM building with the Type 1 rehabilitation scheme, the fundamental period of the building is approximately at 0.4 second. As a result, the expected S_a values for the BSE-1 and BSE-2 earthquake events are 0.55g and 1.4g, respectively. FEMA [1997] stated that the building must conform to the Immediate Occupancy (IO) performance level under the BSE-1 events and, at the same time, to the Life Safety (LS) performance level under the BSE-2 earthquakes. In this regard, the fragility curves for the URM building with Type 1 rehabilitation scheme (Figure 5.17) are examined. It was found that there is virtually no chance that the building will be damaged beyond the IO level under the BSE-1 earthquakes. However, there exists 17% chance that the building drift will go in excess to the LS limit if the BSE-2 earthquakes were to happen. Even though the Type 1 scheme does not guarantee buildings' operability under stronger earthquakes, it still provides a significant improvement in building performance over that of the existing building in Memphis.

For the Type 2 rehabilitation scheme, the building has a fundamental period of 0.27 second resulting in the spectral acceleration of 0.57g and 1.4g for BSE-1 and BSE-2 earthquakes, respectively. The fragility curves for the Type 2 scheme (Figure 5.18) reveal that it is statistically likely that the rehabilitated URM building will perform well and achieve the enhanced safety objective under future earthquakes.

In conclusion, it is found in this research that the use of the metallic tapered energy dissipation devices, which was once thought inappropriate, can be a viable option for seismically upgrading URM low-rise buildings. The devices not only lessen the seismic energy dissipation demand in the structures, but they are also effective in reducing the seismic response such as story drifts in the buildings.

However, there are several practicality issues that should be stated. Significant improvement in building seismic performance in this research may be due largely to the assumptions of an ideal condition such as the perfect connectivity of the PED device to the URM wall and diaphragm components or the infinitely rigid link beams and the chevron-braces, which may be impossible or impractical in real-building implementations. In addition, caution must be placed in an actual attachment of PED devices to the timber diaphragms. Significant amount of lateral force is required in order to achieve sufficient deformation in the metallic device. This force will be transferred to the timber diaphragm and could cause a localized damage to timber at the attached points. Nonetheless, these practicality issues are not the main focus of this feasibility-type investigation. Further analytical and experimental studies are required in the future for such connection details to ensure most benefit from the implementation of PED devices.

CHAPTER 6

RAPID FRAGILITY ASSESSMENT OF A BUILDING PORTFOLIO

The proposed approach of using a response surface methodology (RSM) in conjunction with a simple Monte Carlo simulation has been shown to be effective and quite accurate in deriving the seismic fragility curves for a representative unreinforced masonry (URM) building. The current chapter takes a step further in utilizing the proposed approach. The approach is viewed as an efficient tool for a rapid fragility assessment of a particular building portfolio. The main idea is to explicitly include broader macro-level building parameters that describe different building physical characteristics in a response surface metamodel. Fragility estimation of buildings in a hypothetical portfolio is presented as an example in this chapter.

6.1 PORTFOLIO FRAGILITY ASSESSMENT

Seismic fragility describes a likelihood of damage to building(s) due to future earthquakes. Fragility relations specific to a building or a building portfolio is an important component in the loss estimation process. It is usually of interest to governmental agencies or building owners who are responsible for developing effective

mitigation measures for their building portfolios. The fragility must be consistently derived as inaccurate fragility computation could leads to erratic portfolio loss estimation.

6.1.1 Conventional Approach

Conventional loss assessment package [NIBS, 1999] makes use of the fragility curves that are generated for a representative building (called generic fragility curves hereafter) in a loss estimation computation for a population of building with similar classification in a region (i.e., low-rise URM buildings in Mid-America). It is not intended that these generic fragility curves be used for evaluating individual buildings in a community, but rather, they are more appropriate for assessing fragility and losses at a regional level.

Even though the perspective of using generic curves is widely acceptable among many practitioners, it is doubtful that different buildings would share the same fragility relation even if they are considered in the same classification. The building configurations and many other non-physics parameters (e.g., age, maintenance, etc.) also play an important role in the dynamic responses of the buildings. The conventional approach tends to ignore this fact and assumes that the buildings with similar construction type would produce the same level of damage under an earthquake regardless of their geometries. This could lead to an inaccurate estimation of building portfolio losses. As a result, building-specific fragility relations that take into account building physical characteristics are needed for better estimation of the loss. While building-specific fragility curves can be determined from brute-force simulations based on complex structural analyses on each building, for portfolio assessment, it becomes

impractical to produce a large number of seismic response analyses. Instead, some sort of rapid assessment may be more appropriate at the portfolio level.

6.1.2 Proposed Use of the RSM

This research extends the use of the response surface metamodel to include broader macro-level building parameters for estimating the damage levels. The approach in this chapter takes into account not only uncertainties in material properties but it also considers variability in building geometry as well as the age of the buildings. By this way, the structural variability in a region is explicitly incorporated in the development of the damage estimation model for a certain building type.

A benefit of using the closed-form response surface model to approximate the degree of damage is realized when a fragility or loss assessment of a particular building or building portfolio is of interest. The use of the readily developed generic fragility curves does not provide accurate results to specific buildings [NIBS, 1999] and, on the other end, a detailed building-by-building fragility analysis may be prohibitively expensive. The response surface model, when incorporating the geometric parameters, can be utilized for a rapid fragility assessment of specific building or building portfolio in a specific region. The response surface in this case can be regarded as a damage prediction model for a certain type of building construction in a particular region. The level of damage to a specific building can be quickly estimated based on the building geometry (and possibly other) parameters. Randomness that exists in the material properties and seismic inputs are used as a basis for simulating probabilistic distribution of damage and, hence, deriving fragility curves specific to a particular building.

A detailed example application of the proposed approach for computing portfolio-specific fragilities is presented in this chapter. The approach presents a good compromise between the use of the rather inaccurate generic curves and the time-consuming building-by-building assessment.

6.2 REGION OF INTEREST

The first step is to define the region of interest. As mentioned previously, the New Madrid Seismic Zone (NMSZ) is regarded as one of the most hazardous seismic region in the US. However, due to the infrequent nature of earthquake events in the region, most building owners believe that a stringent seismic design is not an economical solution for their buildings. The city of Memphis, as one of the major cities close to the NMSZ, could be susceptible to consequence following an earthquake event if a suitable mitigation is not in place. Fragility analysis of a building portfolio in Memphis can provide an insight into the level of damage that might be expected if an earthquake were to happen in the region.

It is assumed in this study that a suitable database or building inventory is available to describe the portfolio of interest. For example, research at the Mid America Earthquake Center [French, 2003] has yielded a building inventory database of over 280,000 buildings in Memphis. Results from this study are essential in defining the parameters and their applicable ranges for use in the response surface models. At this point, however, the database is still under development and does not include all the needed information. As a result, appropriate assumptions must be made in the development to bridge these gaps.

6.3 BUILDING PARAMETERS

In reality, a building portfolio will typically consist of building constructions that belong to several classifications and the buildings from different classifications will likely respond differently to earthquakes. As a result, a response surface model is needed for each building class for its damage prediction. It is assumed in this study, however, that only a class of the low-rise steel moment resisting frame construction (S1-L according to HAZUS building classification) represents all buildings in the example portfolio. This simplified problem is viewed as a first step with a purpose of showing an applicability of the method.

The benefit of using the metamodel is an ability to rapidly predict the response and damage to any particular building given its geometric characteristics, but such characteristics must be defined. Building parameters that should be included in the model are the ones that affect the response computation. In addition, the parameters must be largely independent of each other. The initial step in the input parameter selection process is to identify all possible building parameters and then some parameters with little effect will be eliminated in the screening process.

While the direction of an earthquake and the 3-dimensional building characteristics can cause significant impact to the building responses, the scope of this research is limited only to the 2-dimensional aspect of the building. This will make the problem more tractable and appropriate for the proof-of-concept type of investigation.

In order to further limit the extent of the problem to a manageable level, the initial study assumes that the S1-L buildings in the region are regularly constructed without structural discontinuity (e.g., missing columns or beams, etc.). Furthermore, assumptions

on the variation of the building overall dimensions have to be made because the detailed building inventory data for the region is lacking at the time of this research. The buildings in the region are assumed to have their overall length (along the direction of the applied earthquakes) varying between 96 ft and 144 ft and the overall height ranging from 29 ft to 39 ft. In this first study, a general bay and story arrangement is assumed invariable. It is defined following the 3-story-4-bay steel moment frame building model from the SAC project [FEMA, 2000b]. The variability in the building overall length and overall height is taken into account by adjusting the width of each bay and the story heights. This may not be sensible to the normal design practice in which the bay width does not vary by much and the length of a building is increased by adding new bays. However, following a design practice is not as important an issue in this research as showing the applicability of the approach. It is believed that it would be more appropriate for future research to address this issue.

In addition to the configuration parameters, the mass (reflecting dead and live loads in a building) at each story is also incorporated as the input variables. Material property parameters, even though are expected to have much less significance in the response computation, represent uncertainty in the model and must still be incorporated for probabilistic assessment of damage. Table 6.1 presents all possible input parameters for the response surface generation. These parameters can be divided into 2 groups: geometric variability parameters that are used to characterize individual buildings, so-called macro-level parameters (ξ_1 to ξ_6) and random parameters for material properties, so-called micro-level parameters (ξ_7 to ξ_{11}).

Information on the regional variability (i.e., bounds of each parameter) can be obtained from an actual field survey or building inventory data. However, resources are not available to develop the necessary survey of the structural characteristics in the target region and, as noted previously, the available inventory data is not complete. As a result, in this study, variability of building characteristics must be assumed. Table 6.1 shows the assumed lower and upper bounds of the input parameters for the specified region. Bounds are given to each parameter to define range of parameters applicable to a specific building class in the Memphis area.

Table 6.1: Potential Building Parameters for Response Surface Model Generation

	Building Parameters	Lower Bounds	Center Points	Upper Bounds
ξ_1	Bottom Floor Height (ft)	11.2	14.0	16.8
ξ_2	Typical Floor Height (ft)	9.0	10.0	11.0
ξ_3	Bay Width (ft)	24.0	30.0	36.0
ξ_4	2nd Floor Mass (kips-sec^2/ft)	26.21	32.76	39.32
ξ_5	3rd Floor Mass (kips-sec^2/ft)	26.21	32.76	39.32
ξ_6	Roof Mass (kips-sec^2/ft)	28.36	35.45	42.54
ξ_7	Column Yield Strength (ksi)	44.0	55.0	66.0
ξ_8	Beam Yield Strength (ksi)	44.0	55.0	66.0
ξ_9	Column Young's Modulus (ksi)	27550	29000	30450
ξ_{10}	Beam Young's Modulus (ksi)	27550	29000	30450
ξ_{11}	Damping Ratio	2%	3%	4%

6.4 RESPONSE MEASURES AND DAMAGE CRITERIA

Quantification of damage from a seismic event to a building is based primarily on overall response of the buildings. Maximum inter-story drift is one of the simplest parameters and has been known to provide a good correlation to connection damage in steel frame structures [Kircher, 2003]. FEMA-356 [FEMA, 2000a] also suggests the use of maximum inter-story drift as a performance measure in the steel moment frame buildings. The inter-story drift is computed by dividing the relative lateral displacement between floors with the corresponding height between the two floors. The peak value at any location in a frame and at any time instance is termed peak or maximum inter-story drift. Similar to the case of the URM structures, three building performance levels are defined. They include Collapse Prevention (CP), Life Safety (LS), and Immediate Occupancy (IO) performance levels. Descriptions and the maximum drift limit for each building performance level are displayed in Table 6.2.

Table 6.2: Structural Performance Levels for Steel Moment Frames [FEMA, 2000a]

	Structural Performance Levels		
	Collapse Prevention S-5	Life Safety S-3	Immediate Occupancy S-1
Damage Levels	Severe	Moderate	Light
Overall Damage Descriptions	Extensive distortion of beams and column panels. Many fractures at moment connections, but shear connections remain intact.	Hinges form. Local buckling of some beam elements. Severe joint distortion; isolated moment connection fractures, but shear connections remain intact.	Minor local yielding at a few places. No fractures. Minor buckling or observable permanent distortion of members.
Drift	5%	2.5%	0.7%

6.5 GROUND MOTION AND INTENSITY MEASURE

A suite of the synthesized accelerograms for Memphis, TN [Wen and Wu, 2001] is used again in this chapter. The earthquakes in the suite are generated with randomness in the characteristics of source, site, and magnitude of the earthquake as well as the local soil conditions. As a result, the use of an ensemble of earthquakes indirectly incorporates seismic uncertainty in the fragility assessment.

A simple parameter that characterizes earthquake intensity must be defined. It was shown in Chapter 3 that the use of the spectral acceleration as an earthquake intensity measure is more appropriate than the use of the peak accelerations. The spectral acceleration at the fundamental period of the building has been used extensively in the previous chapters. However, in this chapter, the damage prediction response surface model also takes into consideration the variability in building geometrical parameters. As a result, the building configuration and, consequently, the building's fundamental period can be varied over the parameter space. The use of the spectral acceleration at a specific period as the intensity measure becomes inappropriate in this case.

Dimova and Elenas [2002] suggested the use of an average spectral acceleration (S_{am}) as a measure of seismic intensity in the case that involves the fragility analysis of several buildings with different periods. It is an average value of S_a between the minimum (T_i) and the maximum periods (T_j) of those buildings. The concept of the average spectral acceleration is presented graphically in Figure 6.1. The study by Dimova and Elenas [2002] also suggested high correlation between this intensity measure and structural damage.

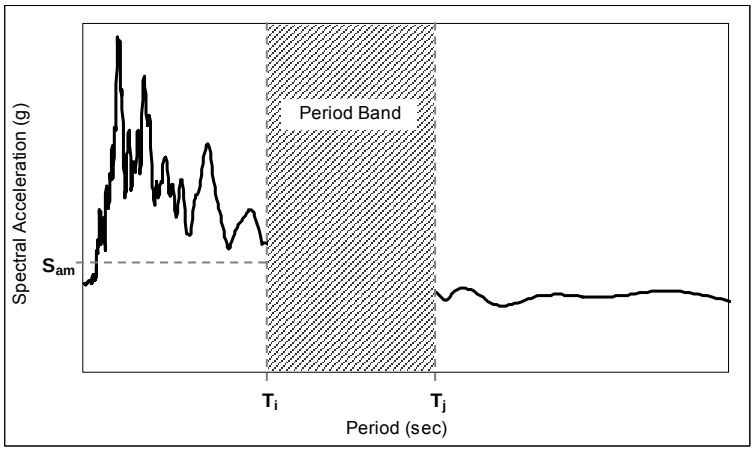

Figure 6.1: Concept of Average Spectral Acceleration (S_{am})

In this investigation, the earthquakes in the suite are scaled such that they have the same value of S_{am}. The same scaling scheme (3.27) as in the case of S_a can be utilized.

6.6 BUILDING MODEL

The low-rise moment-resisting steel frame (S1-L) in Memphis is assumed to have a general configuration similar to the model building from the SAC report [FEMA, 2000b]. The building is 3-story in height with 4 bays in the east-west direction and 6 bays in the north-south direction (Figure 6.2a). All bays are assumed to be of equal width. Discontinuity in structural elements (i.e., beams and columns) is not presented in this building. The seismic response analysis in this study is limited only to the 2-dimensional aspects and, as a result, the earthquake is assumed to arrive at the structure only in the east-west direction. Figure 6.2a also shows the position of moment-resisting frames in the plan view (shown as bold lines). Figure 6.2b shows an elevation view of the moment resisting frame that is used in the response analysis. In this study, the dynamic analysis is performed on the 2-dimesional moment-resisting frame model generated by DRAIN-

2DX. Element type 2 (beam-column element) is used to assemble the frame models. Plasticity in any element that may occur is concentrated at the end of each element. A simple bilinear force-displacement relationship with an inelastic unloading branch is assumed for the element's hysteretic property. The gravity loads used in the design of the building as well as in the calculation of masses follow FEMA [2000b] and are listed in the following section. The masses are lumped at the frame nodes. Connections between the beams and the columns, however, are assumed to be rigid. The columns in the moment-resisting frame bend about their strong axes and the column based are considered fixed. The P-Δ effects are ignored in this study.

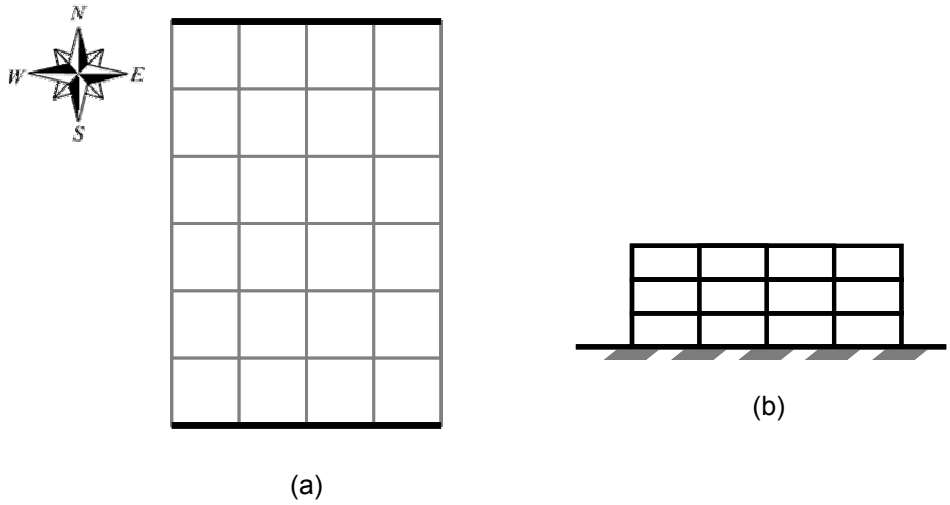

Figure 6.2: General Building Configuration with (a) Plan View showing Moment-Resisting Frames, and (b) Elevation View of a Moment-Resisting Frame

6.7 BUILDING DESIGNS FOR LATERAL LOADS

Buildings in a region, even though they are in the same class, are designed differently. Some are designed without a consideration of seismic effects. On the other hand, some are designed to the most stringent level. The seismic design provision to which a particular building conforms also plays a very important role on how the building would respond to an earthquake. However, it is hard to derive a consistent criterion for characterizing the building design provision for each building. For simplicity, it is assumed that the construction year of the buildings reflect the seismic design provision that the buildings conform to. It is further assumed that all the low-rise steel moment-resisting frame buildings (S1-L) in Memphis can be categorized into three different design provisions as follows:

- The 2000 International Building Code (IBC2000) represents the most stringent design (so-called high seismic design) and is applicable to the buildings constructed after the year 2001.
- The 1991 Standard Building Code (SBC1991) represents the less stringent design (so-called a low seismic design) in the region and is applicable to the buildings constructed between 1992 and 2001.
- Lastly, the non-seismic design follows the design provision for wind loads and is applicable to the buildings in the region that are constructed prior to 1992.

A brief summary of design criteria and results for each design level is presented as follow.

6.7.1 IBC2000 Design

IBC2000 code [ICC, 2000] represents the most stringent seismic design provision that is assumed to be applicable for the recently constructed buildings in the region. For such a low-rise and regularly constructed frame, the equivalent lateral force procedure is used for the purpose of designing the moment-resisting frame. The following design criteria are adopted for the design of the steel moment frame building in Memphis.

- A572 steel for both columns and beams
- Nominal steel yield strength of 50 ksi
- Steel Young's modulus of 29,000 ksi
- Site class D for Memphis [Williams et al., 2003]
- Spectral acceleration for short period (S_S) of 1.12 second
- Spectral acceleration for a 1-second period (S_1) of 0.33 second
- Seismic use group I
- Seismic occupancy importance factor (I_E) of 1.0
- Response modification coefficient (R) of 4.0 (for ordinary steel moment frames)
- Floor dead load of 96 psf [FEMA, 2000b]
- Roof dead load of 83 psf [FEMA, 2000b]
- Reduced floor and roof live load of 20 psf

In this equivalent lateral force procedure, the seismic base shear is calculated as a fraction of the total weight of the building in accordance to the following equation.

$$V = C_s W \tag{6.1}$$

The multiplier C_s or the seismic response coefficient is determined from the building characteristics, the site-specific design spectral responses, the building classification and its occupancy. The total base shear is then vertically distributed as nodal forces acting on the moment-resisting frames at each floor level. The amount of force acting on each floor is determined primarily by the floor weight and its height from the ground.

IBC2000 also indicates that the building must be designed to resist the following load combinations when earthquake actions are considered. Note that wind load is not taken into consideration since earthquake effect is expected to govern in the design.

(1) D

(2) D + L

(3) $D + L + L_r$

(4) $D + 0.7E + L + L_r$

(5) $0.6D + 0.7E$

where D, L and L_r are the dead loads, the floor live loads and the roof live loads, respectively. E is the combined effect of horizontal and vertical earthquake induced forces.

GTSTRUDL [1999] is used in selecting the structural members for the building that is design based on the Allowable Stress Design (ASD). The member selection criteria are specified such that the beams are of the same section in each floor and, at the same time, the columns are of the same section for all interior columns (and same for the exterior columns). Table 6.3 shows an example of the beam and column sections in a particular building design (the building with mean geometries).

Table 6.3: Beam and Column Sections for a Building Designed with IBC2000

Floor	Columns		Beams
	Exterior	Interior	
1/2	W14x211	W14x283	W24x104
2/3	W14x211	W14x283	W27x146
3/Roof	W14x211	W14x283	W24x131

6.7.2 SBC1991 Design

Most of the designs of the low-rise building in Memphis and its vicinity had not considered the effect from an earthquake until the early 90s. The 1991 Standard Building Code [SBCCI, 1991] has pioneered the seismic design procedure in this region. In this study, it is used as a basis for the less stringent design (compare to the more recent IBC2000) that is applicable for the buildings constructed on or after the early 90s but before the IBC2000 is adopted.

Similar to the general concept in IBC2000, the equivalent lateral load procedure is implemented. The total shear at the base of a building that is resulted from seismic forces is determined as a fraction of the weight of the building. The formulation in (6.1) also applies in this case; however, the derivation of the factor C_s is quite different. The following design data are used for designing a building in Memphis.

- Peak velocity-related acceleration coefficient (A_v) of 0.2
- Peak acceleration coefficient (A_a) of 0.2
- Seismic hazard exposure group I

- Seismic performance category C
- Soil profile type S_4 (site coefficient, S = 2.0)
- Response modification factor (R) of 4.5 (for ordinary steel moment frames)

The distribution of the lateral loads is similar to that defined in IBC2000. They are determined based on the weight and elevation of the floor. The gravity loads follow the information provided in FEMA [2000b], which is also presented in 6.7.1. Load combinations that are defined in SBC1991 are slightly different from those of IBC2000. They are presented as follows:

(1) Dead + Floor Live + Roof Live

(2) Dead + Floor Live + Seismic

(3) $(1.1 + 0.5A_v)$ Dead + Floor Live + Seismic

(4) $(0.9 - 0.5A_v)$ Dead + Seismic

It is also assumed for this design that the A572 steel with nominal strength of 50 ksi and Young's modulus of 29,000 ksi is used for both beams and columns. Similar criteria for selecting beam and column sections are implemented in the GTSTRUDL design procedure and the resulting selection of steel sections of a particular building (the building with mean geometries) is shown in Table 6.4.

Table 6.4: Beam and Column Sections for a Building Designed with SBC1991

Floor	Columns		Beams
	Exterior	Interior	
1/2	W14x159	W14x193	W18x97
2/3	W14x159	W14x193	W24x104
3/Roof	W14x159	W14x193	W18x86

6.7.3 Wind Load Design

For older buildings or those buildings in the region that are constructed prior to the point when the seismic provision is adopted, it is assumed that they are designed to withstand the effects from the gravity and wind loads only. For this matter, the recommendation for the wind load design from the 1969 edition of the Southern Standard Building Code [SBCC, 1969] is adopted in designing the steel moment frame buildings that are associated to the non-seismic design level.

The minimum design wind pressure for an inland location (more than 125 miles from the coast) varies with the height of the building. For the height zone that is less than 30 feet from the ground level, the wind pressure is 10 psf. For the height zone between 31 feet and 50 feet, the design wind pressure becomes 20 psf. The wind pressure in each height zone is assumed to be uniformly distributed over the building side. Nodal forces are computed for each floor of the moment-resisting frames based on the tributary area. GTSTRUDL is again used in selecting the appropriate steel sections. In this case, which represents older constructions in the region, A36 steel is assumed for the beams while A572 steel is used for the columns. Table 6.5 shows an example of beam and column sections in a particular design (the building with mean geometries).

Table 6.5: Beam and Column Sections for a Building Designed to the Non-Seismic Code Level

Floor	Columns		Beams
	Exterior	Interior	
1/2	W12x40	W12x53	W14x68
2/3	W12x40	W12x53	W14x68
3/Roof	W12x40	W12x53	W14x61

6.8 PARAMETER SCREENING

One disadvantage of the response surface model is the limitation on the number of independent input variables. In general, for standard Design of Experiment (DOE) designs, less than 8 input parameters are allowed for a response surface metamodel. The structural parameters to be included in the metamodels should be those that have greatest impact on the output or response calculation (maximum inter-story drift), but the selection is not always obvious for complex problems. As a result, a screening process is employed to identify the contribution of each parameter to the response of the system. One of the simplest methods is to systematically make reasonable increments in each input variable and compute the response for each case. A rank-ordered output yields what is often called a Pareto optimal solution [Montgomery, 1997].

As mentioned previously, 11 input parameters (Figure 6.1) are preliminarily chosen to capture basic structural characteristics that could affect peak inter-story drift calculations. A Design of Experiment (DOE) technique is used to generate an 11-dimensional experimental space composing of different levels of each input parameter. For the purpose of screening test, a 2-level fractional factorial design [JMP, 1995] is

employed in this study. Two-level design only uses minima and maxima of input variables to form design (or experimental) space. Sixteen experimental cases based on fractional factorial design [JMP, 1995] for the 11 input parameters are shown in Table 6.6. The values of -1 and +1 denote minima and maxima of input variables, respectively. Sixteen detailed structural analysis models are generated corresponding to the combination of input parameter levels in the DOE table. For example, case #1 is constructed by using minimum values for bottom floor height (x_1), typical floor height (x_2), bay width (x_3), 2nd floor mass, (x_4) roof mass (x_6), column yield strength (x_7) and modulus (x_9) and using maximum values for 3rd floor mass (x_5), damping ratio (x_{11}), beam yield strength (x_8) and modulus (x_{10}). The output variables (y) are those maximum inter-story drift values (in percents) obtained from the nonlinear time-history analyses, which are performed over each building model.

A first order regression model (6.1) is generated for identifying an influence each input parameter has to the output calculation.

$$y = \beta_0 + \beta_1 x_1 + \beta_2 x_2 + \cdots + \beta_{11} x_{11} \tag{6.2}$$

where y = output variable or maximum inter-story drift (%)

x_i's = input parameters

β_i's = coefficient estimates

The scaled estimates are those coefficient estimates multiplied by the standard deviation of the input parameter such that the estimates can be reasonably compared with each other. The Pareto plot is a plot showing composition of an absolute value of each scaled estimate normalized to the sum. Parameter with highest scaled estimate represents

the most influential parameter as minor change in the value of input produces major influence in the output calculation given that all other input parameters remain constant. Figure 6.3 shows a plot of the scaled estimates for each input parameters (so-called Pareto plot). The solid curve in the figure indicates the cumulative contribution to the overall response while the individual contribution or scaled estimate is indicated by the horizontal bar.

Another way to obtain a qualitative impression of the significance of each input variable is through the prediction profiler plots (Figure 6.4). The prediction profiler plot is a plot between the output variable (y) and each of the input variables (x's) while other inputs are held at their center point or mean values. The influence of each input variable can be inferred from the steepness of the line as a steeper line over the variable range means that the input variable is more influential to the output calculation than the others. It is obvious from Figure 6.3 that the first 5 parameters (x_3, x_7, x_1, x_9, and x_{11}) contribute to almost 80% of the overall response. Thus, these 5 parameters can be used as the input variables in the response surface while fixing the remaining parameters to their best estimated values and still be assured of reasonable data fit.

Table 6.6: Design of Experiments Table based on the 2-Level Fractional Factorial Design for 11 Input Variables

Case	x_1	x_2	x_3	x_4	x_5	x_6	x_7	x_8	x_9	x_{10}	x_{11}	y (%)
1	-1	-1	-1	-1	+1	-1	-1	+1	-1	+1	+1	2.46
2	-1	-1	-1	+1	-1	+1	+1	-1	+1	-1	-1	2.61
3	-1	-1	+1	-1	-1	+1	+1	-1	-1	+1	+1	2.18
4	-1	-1	+1	+1	+1	-1	-1	+1	+1	-1	-1	2.20
5	-1	+1	-1	-1	-1	+1	-1	+1	+1	-1	+1	2.16
6	-1	+1	-1	+1	+1	-1	+1	-1	-1	+1	-1	2.64
7	-1	+1	+1	-1	+1	-1	+1	-1	+1	-1	+1	2.15
8	-1	+1	+1	+1	-1	+1	-1	+1	-1	+1	-1	2.20
9	+1	-1	-1	-1	-1	-1	+1	+1	+1	+1	-1	2.29
10	+1	-1	-1	+1	+1	+1	-1	-1	-1	-1	+1	2.27
11	+1	-1	+1	-1	+1	+1	-1	-1	+1	+1	-1	2.01
12	+1	-1	+1	+1	-1	-1	+1	+1	-1	-1	+1	2.22
13	+1	+1	-1	-1	+1	+1	+1	+1	-1	-1	-1	2.59
14	+1	+1	-1	+1	-1	-1	-1	-1	+1	+1	+1	2.10
15	+1	+1	+1	-1	-1	-1	-1	-1	-1	-1	-1	2.01
16	+1	+1	+1	+1	+1	+1	+1	+1	+1	+1	+1	2.03

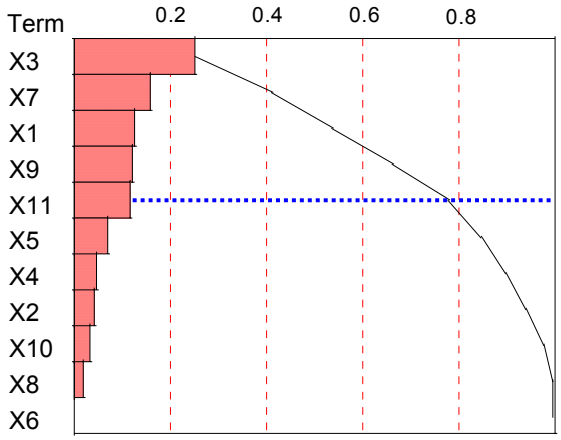

Figure 6.3: Pareto Plot of Input Parameters

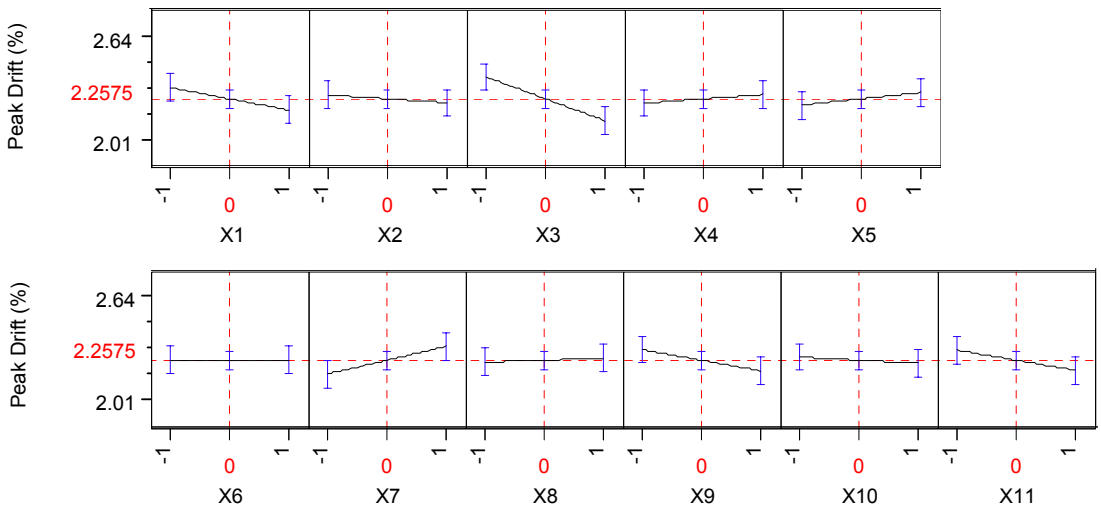

Figure 6.4: Prediction Profiler Plot

6.9 RESPONSE SURFACE MODEL GENERATION

An initial goal of this study is to develop the damage prediction response surface model specific for each design level (i.e., high-, low-, and non-seismic designs). The 5 most influential structural parameters, including the bottom floor height (ξ_1), the bay width (ξ_3), the column yield strength (ξ_7), the column Young's modulus (ξ_9), and the damping ratio (ξ_{11}) are used in combination with the earthquake intensity parameter (ξ_{EQ}) to formulate the response surface models according to the proposed Approach 3 in this study (see chapter 3 for details). The parameters' lower bound, center point, and upper bound values along with their normalized values are displayed in Table 6.7. Note that the 3 levels of the average spectral acceleration dictate the way the earthquake records are scaled. For example, in the case where $\xi_{EQ} = 0$, each of the earthquakes that is used for the response computation is scaled such that the S_{am} of 1.0g is achieved. A similar concept applies to the case of $\xi_{EQ} = -1$ and $\xi_{EQ} = +1$.

The Design of Experiments technique (i.e., a reduced Central Composite Design in particular) is utilized to formulate combinations of input variables for response computation. In this case that the building geometries are also varied in the DOE table, the buildings must be redesigned according to its geometric parameters defined for each combination. In the initial study, each combination of building parameters is designed to the 3 design levels. Maximum inter-story drifts are computed from the nonlinear dynamic analyses and recorded in the DOE table for each design level. Finally, 3 sets of matrices of input variables and the corresponding computed responses are formulated.

Table 6.7: Screened Input Parameters for Response Surface Models

Input Parameters	Input Variables	Lower Bounds	Center Points	Upper Bounds	Units
Bottom Floor Height	ξ_1	11.2	14.0	16.8	ft
	x_1	-1	0	+1	-
Bay Width	ξ_3	24.0	30.0	36.0	ft
	x_3	-1	0	+1	-
Column Yield Strength	ξ_7	44.0	55.0	66.0	ksi
	x_7	-1	0	+1	-
Column Young's Modulus	ξ_9	27550.0	29000.0	30450.0	ksi
	x_9	-1	0	+1	-
Damping	ξ_{11}	2.0	3.0	4.0	%
	x_{11}	-1	0	+1	-
Average Spectral Acceleration (S_{am})	ξ_{EQ}	0.1	1.0	1.9	g
	x_{EQ}	-1	0	+1	-

The least-square regression technique is used in deriving the coefficient estimates of the response surface functions. The response surface or the maximum drift prediction models is generated for each seismic design level (i.e., non-, low-, and high-seismic designs). They can be shown symbolically as follows:

$$\hat{y}_{non} = \hat{y}_{\mu|non} + N\left[0, \hat{y}_{\sigma|non}\right] \tag{6.3}$$

$$\hat{y}_{low} = \hat{y}_{\mu|low} + N\left[0, \hat{y}_{\sigma|low}\right] \tag{6.4}$$

$$\hat{y}_{high} = \hat{y}_{\mu|high} + N\left[0, \hat{y}_{\sigma|high}\right] \tag{6.5}$$

The response functions for the mean drift are plotted against each of the building parameters in Figure 6.5. The two extreme cases for the design levels, non-seismic and high-seismic, are plotted together for comparison. It is as expected that the maximum drifts predicted from the non-seismic design case are significantly higher. Note that the level of seismic intensity is fixed at its central value of 1.0g in these plots.

It is found that the process may not be completely efficient since the damage prediction model is dependent of the seismic design levels. Further investigation is made in order to incorporate the design levels into the response surface model and, as a consequence, merges the 3 models into a single response prediction model. In this regard, the design parameters can be thought of as an indicator or a categorical variable that determines whether the building design is non-seismic, low-seismic, or high-seismic. For the response surface models, the normalized variable (x_{DES}) has its values discretely described by –1, 0, and +1. The value –1 represents the case of the non-seismic design, while the value 0 and +1 stand for the low- and high-seismic designs, respectively. It is obvious from Figure 6.5 that the difference in the response due to distinct design levels is far greater than the variation of the responses within the same design level. This interprets as the level of the seismic design has much more influence on the computation of the maximum drifts than any other building parameters. As a result, in order to limit the number of input parameters to six, the damping ratio (that is the least influential parameter) is eliminated from a set of input variables and it is replaced by the design level parameters (ξ_{DES}) as can be seen in Table 6.8 for the new set of the response surface input variables.

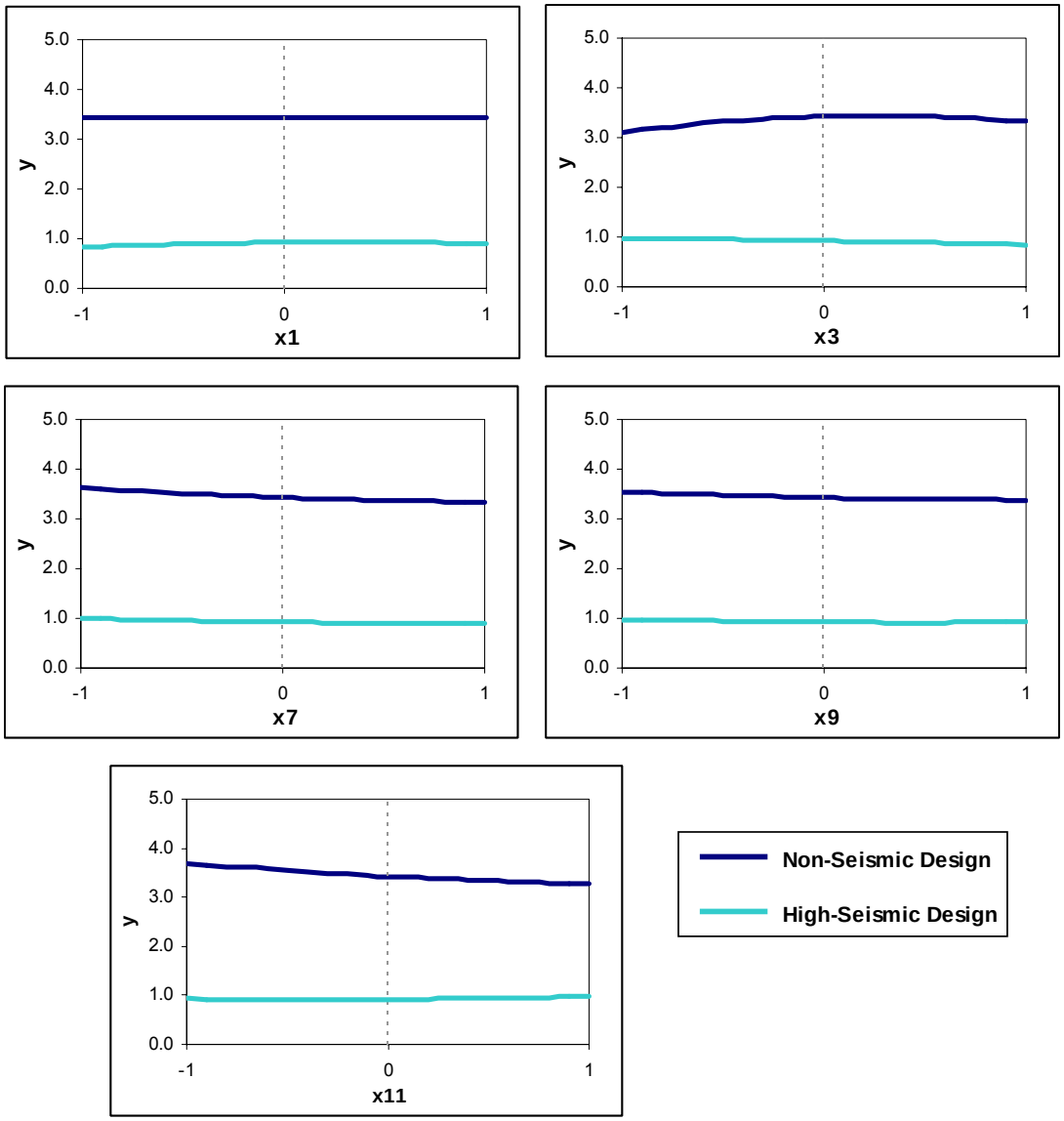

Figure 6.5: Plot of Response Surfaces with respect to Individual Input Variables

Table 6.8: Input Parameters for Response Surface Models including the Seismic Design Level Parameter

Input Parameters	Input Variables	Lower Bounds	Center Points	Upper Bounds	Units
Bottom Floor Height	ξ_1	11.2	14.0	16.8	ft
	x_1	-1	0	+1	-
Bay Width	ξ_3	24.0	30.0	36.0	ft
	x_3	-1	0	+1	-
Column Yield Strength	ξ_7	44.0	55.0	66.0	ksi
	x_7	-1	0	+1	-
Column Young's Modulus	ξ_9	27550.0	29000.0	30450.0	ksi
	x_9	-1	0	+1	-
Design Level	ξ_{DES}	Non-Seismic	Low-Seismic	High-Seismic	-
	x_{DES}	-1	0	+1	-
Average Spectral Acceleration (S_{am})	ξ_{EQ}	0.1	1.0	1.9	g
	x_{EQ}	-1	0	+1	-

The DOE table is again constructed for this new set of input parameters. Forty five combinations of input variables are defined following the reduced Central Composite Design [JMP, 1995]. It is worth showing an example of how the response computation is achieved in each of the DOE case. A specific case contains the following combination of the input variables: $x_1 = -1$, $x_3 = -1$, $x_7 = -1$, $x_9 = +1$, $x_{DES} = +1$, and $x_{EQ} = +1$. This set of variable is interpreted as a building with a bottom floor height of 11.2 feet, a bay width of 24 feet, a column yield strength of 44 ksi, and a column Young's modulus of 27550 ksi. All other building parameters that are deemed less influential are fixed at their center point or mean values. This particular building is then designed to resist the lateral loads based on the high-seismic level or the IBC2000. A suite of earthquakes that each has been scaled to have an average spectral acceleration (S_{am}) of 1.9g is applied to the

building and the maximum inter-story drifts are extracted from the nonlinear dynamic analysis of the building subjected to each earthquake. Finally, the mean and the standard deviation of the maximum drifts are computed and recorded in the DOE table. Repetition of the procedure, using the same idea, for other 44 input variable combinations results in the matrices of input and output variables.

The resulting response surface polynomial models are derived based on the least-square criterion and are shown below.

$$\begin{aligned}\hat{y}_{\mu} = {} & 1.118 - 1.278x_{DES} + 0.003x_3 - 0.100x_7 - 0.026x_9 - 0.083x_1 + \\ & 2.206x_{EQ} + 1.085x_{DES}^2 - 0.051x_3x_{DES} + 0.014x_3^2 + 0.015x_7x_{DES} + \\ & 0.005x_7x_3 + 0.007x_7^2 + 0.004x_9x_{DES} + 0.023x_9x_3 - 0.003x_9x_7 - \\ & 0.002x_9^2 + 0.064x_1x_{DES} + 0.022x_1x_3 + 0.051x_1x_7 + 0.001x_1x_9 - \\ & 0.006x_1^2 - 1.186x_{EQ}x_{DES} + 0.003x_{EQ}x_3 - 0.103x_{EQ}x_7 - 0.019x_{EQ}x_9 - \\ & 0.121x_{EQ}x_1 + 0.229x_{EQ}^2\end{aligned} \tag{6.6}$$

and

$$\begin{aligned}\hat{y}_{\sigma} = {} & 0.512 - 0.466x_{DES} + 0.041x_3 - 0.052x_7 + 0.005x_9 - 0.099x_1 + \\ & 1.003x_{EQ} + 0.415x_{DES}^2 - 0.05x_3x_{DES} + 0.168x_3^2 + 0.083x_7x_{DES} + \\ & 0.009x_7x_3 - 0.011x_7^2 - 0.017x_9x_{DES} + 0.026x_9x_3 + 0.017x_9x_7 + \\ & 0.015x_9^2 + 0.036x_1x_{DES} + 0.023x_1x_3 + 0.019x_1x_7 - 0.001x_1x_9 + \\ & 0.042x_1^2 - 0.456x_{EQ}x_{DES} + 0.042x_{EQ}x_3 - 0.052x_{EQ}x_7 + 0.008x_{EQ}x_9 - \\ & 0.118x_{EQ}x_1 - 0.037x_{EQ}^2\end{aligned} \tag{6.7}$$

The response prediction model for a building designed to a particular design level is derived by evaluating the above functions at x_{DES} = -1, 0, and +1.

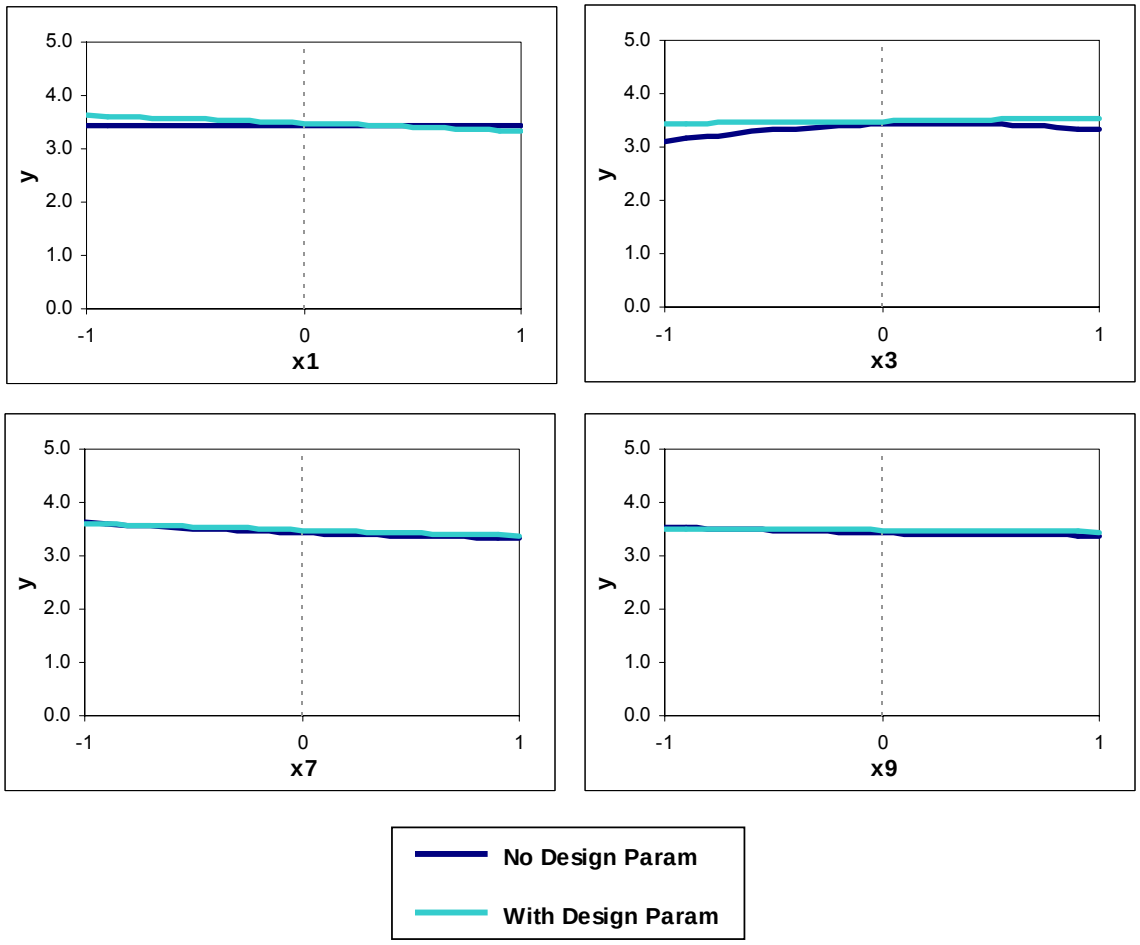

Figure 6.6: Response Surface Plots for Buildings with Non-Seismic Design

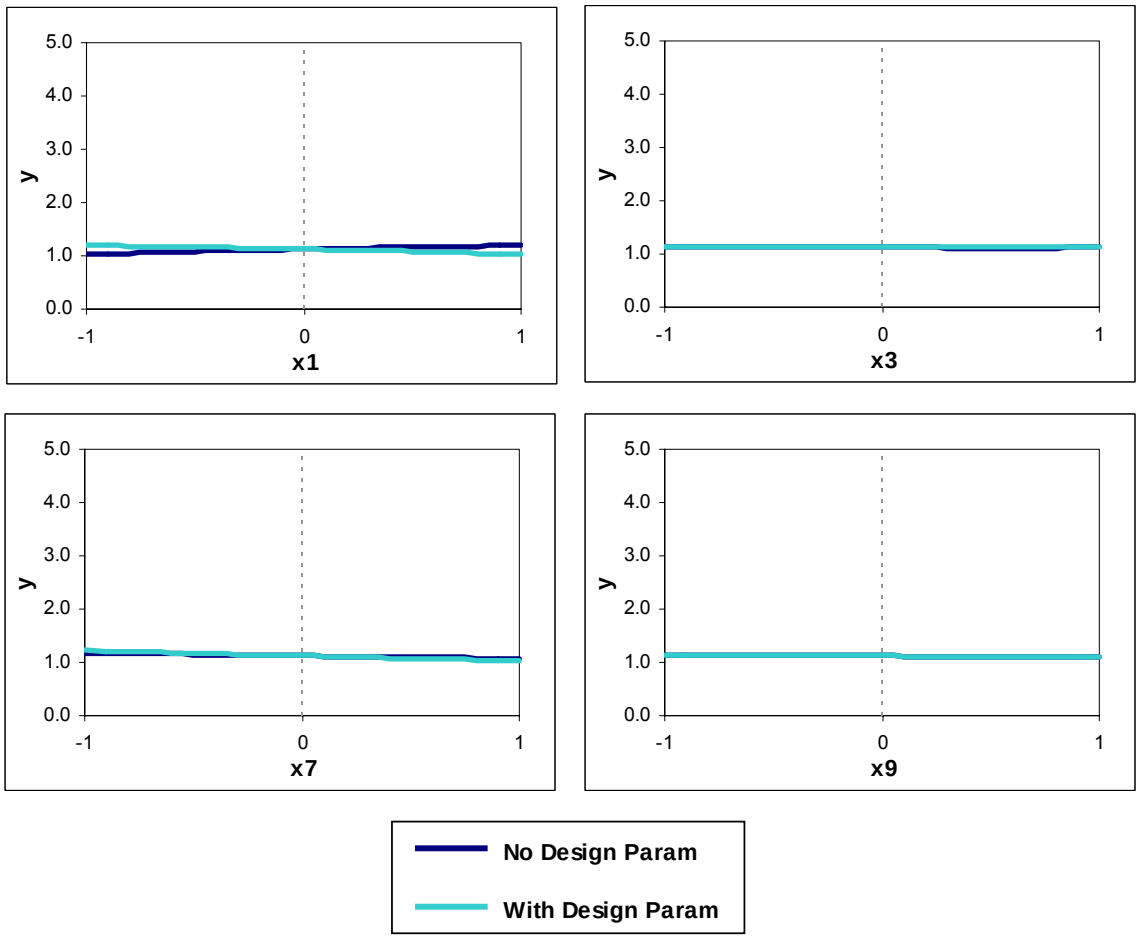

Figure 6.7: Response Surface Plots for Buildings with Low-Seismic Design

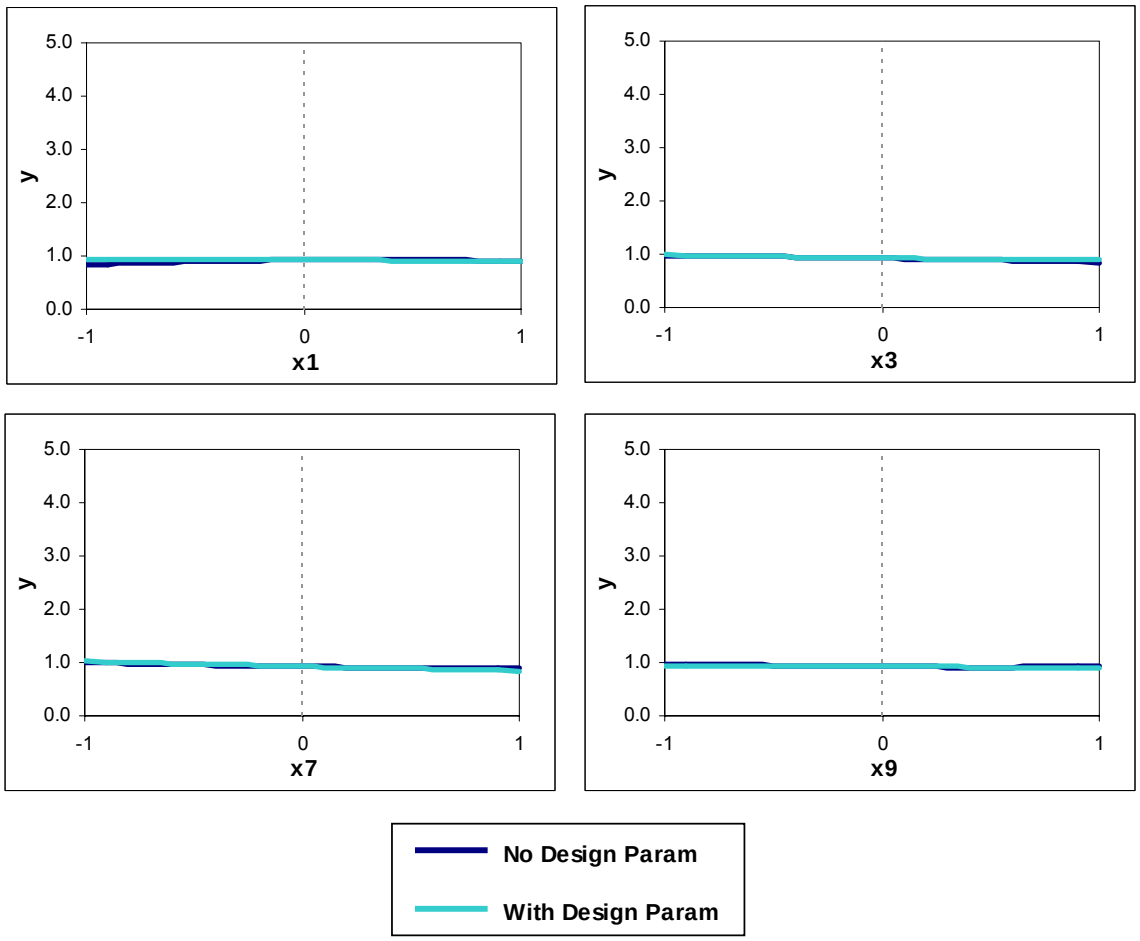

Figure 6.8: Response Surface Plots for Buildings with High-Seismic Design

The response surfaces for the mean value of the maximum drifts are plotted against each of the building parameters. For a comparison purpose, the polynomial function in (6.6) is evaluated at $x_{EQ} = 0$ (representing the case with $S_{am} = 1.0g$) and $x_{DES} = -1$, 0, and +1 (for non-, low-, and high-seismic designs), essentially creating 3 response functions. Their plots are compared with those generated from the response surface specific to each code level (i.e., $\hat{y}_{\mu|non}$, $\hat{y}_{\mu|low}$, and $\hat{y}_{\mu|high}$,) in Figure 6.6, Figure 6.7, and Figure 6.8, respectively. It can be seen from these plots that the current approach that incorporates the design level parameter directly as the response surface input variable yields comparable outcomes, but is greatly more efficient.

Diagnosis of the response surface models using the %AvgErr (3.17), %MaxErr (3.18), and %RMSE (3.19) may not be appropriate in this case. These tests require that a relatively large number of additional input variable combinations are used as a basis in performing the tests. However, for this case, the input variables include those geometric parameters as well as the design level parameters and, as a result, modifying those parameters involves in redesigning the new buildings. It would not be economical to design other 100 or more buildings for this purpose. As a consequence, only the R_A^2 value is used to validate the models at this model-level. The validation of the resulting fragility curve as an outcome of the models is performed in the subsequent section.

The R_A^2 of the response surface models for the mean and standard deviation of the maximum drifts are calculated to be 0.978 and 0.943, respectively. These high values of R_A^2 indicate a strong association between the actual and the predicted responses.

The response surface model presented in (6.6) is essentially a damage prediction model. It can be used in a rapid deterministic assessment of an individual building. The level of the maximum inter-story drift can be predicted given the building properties, the design level, and the intensity of an earthquake. However, the benefit of the proposed approach is more prominent as a tool in a portfolio loss estimation process.

6.10 HYPOTHESIZED BUILDING PORTFOLIO

In order to present the use of the response surface models as a tool in the seismic loss estimation of a building portfolio, a group of four buildings is hypothetically selected. This assumed portfolio is composed solely of low-rise steel moment-resisting frame buildings and they are all located in Memphis, TN. All buildings are different in basic properties and geometric configuration as well as the year that the buildings were constructed. Note that this less-than-realistic portfolio is used for the purpose of showing an application of the response surface models and is not intended to represent any real buildings. Description of the buildings in this portfolio is displayed in Table 6.9.

Table 6.9: Characteristics of Buildings from the Hypothesized Portfolio

Building Name	Class	Year Built	Number of Story	Typical Floor Height (ft)	Bottom Floor Height (ft)	Bay Width (ft)	Steel Yield Strength (ksi)	Steel Young's Modulus (ksi)
AAA	S1-L	1974	3	9.0	11.2	24.0	50	28000
BBB	S1-L	1993	3	10.0	14.0	30.0	55	29000
CCC	S1-L	2002	3	10.0	14.0	30.0	60	29000
DDD	S1-L	1972	3	11.0	16.8	36.0	48	28000

The response surface functions (6.6 and 6.7) obtained from the previous steps is appropriate for predicting maximum drifts for an aggregation of low-rise steel moment frame buildings. Modification is needed in order to convert to a response surface applicable to a specific building. Control variables are the variables that dictate how a metamodel for one building differs from the others. In this study, the control variables include the bottom floor height (x_1), the bay width (x_3), and the design level (x_{DES}). Building-specific response prediction model is derived by substituting values of the control variables specific for that building in the response surface of an aggregation (6.6 and 6.7).

As an example, the derivation of the damage prediction model for building AAA is shown. Building AAA was constructed in 1974 and, based on the design level criterion in 6.7, was designed according to the non-seismic design level. The value for x_{DES} of -1 is applicable for building AAA. The actual values for the bottom floor height and the bay width of building AAA are converted to the normalized values according to (3.4) as follows:

$$x_1 = \frac{11.2\text{ft} - \frac{16.8\text{ft} + 11.2\text{ft}}{2}}{\frac{16.8\text{ft} - 11.2\text{ft}}{2}} = -1$$

$$x_3 = \frac{24\text{ft} - \frac{36\text{ft} + 24\text{ft}}{2}}{\frac{36\text{ft} - 24\text{ft}}{2}} = -1$$

By substituting the specific values of the control variables into the response surface functions (6.6 and 6.7), these response surfaces then become response or damage prediction functions for Building AAA.

$$(\hat{y}_{\mu})_{AAA} = 3.607 - 0.171x_7 - 0.052x_9 + 3.510x_{EQ} - 0.003x_7x_9 - 0.103x_7x_{EQ} - 0.019x_9x_{EQ} + 0.007x_7^2 - 0.002x_9^2 + 0.229x_{EQ}^2 \quad (6.8)$$

$$(\hat{y}_{\sigma})_{AAA} = 1.67 - 0.163x_7 - 0.003x_9 + 1.534x_{EQ} + 0.017x_7x_9 - 0.052x_7x_{EQ} + 0.008x_9x_{EQ} - 0.011x_7^2 + 0.015x_9^2 - 0.037x_{EQ}^2 \quad (6.9)$$

and finally, the overall response surface model becomes

$$(\hat{y})_{AAA} = (\hat{y}_{\mu})_{AAA} + N[0,(\hat{y}_{\sigma})_{AAA}] \quad (6.10)$$

The micro-level material property parameters remain in the response functions and are treated as random variables for simulating probabilistic responses. Probability density functions of the random variables are introduced into the model. Lognormal and uniform probability distributions are assumed for the column yield strength and Young's modulus, respectively [Song and Ellingwood, 1999]. The mean values for the yield strength and the modulus can be obtained directly from the design documents of the building (also shown in Table 6.9). The Coefficient of Variation (COV), which is a measure of dispersion, is assumed to be 0.12 and 0.06 for the yield strength and the modulus, respectively.

Monte Carlo simulations are then carried out on the functions of random variables for increasing values of earthquake intensity (x_{EQ}). Probability of response exceeding certain limit states (Table 6.2) can be computed from a suitably large number of outputs

obtained from the simulation at each intensity level. This, in the same fashion as in 4.7.8, yields plots of fragility curves for building AAA as shown in Figure 6.9.

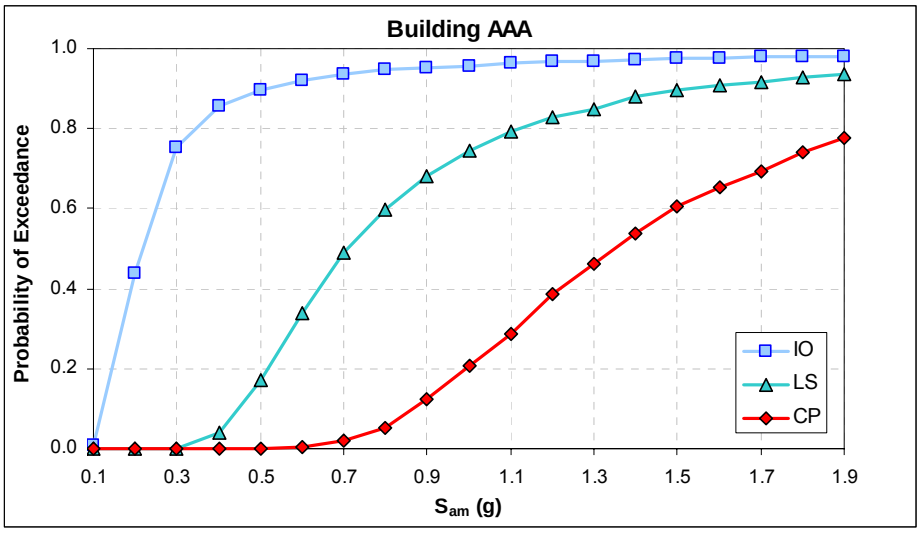

Figure 6.9: Fragility Curves for Building AAA

Fragility curves that are specific to the other 3 buildings in the hypothetical portfolio are derived in a similar fashion as that is for building AAA. They are depicted in Figure 6.10 to Figure 6.12.

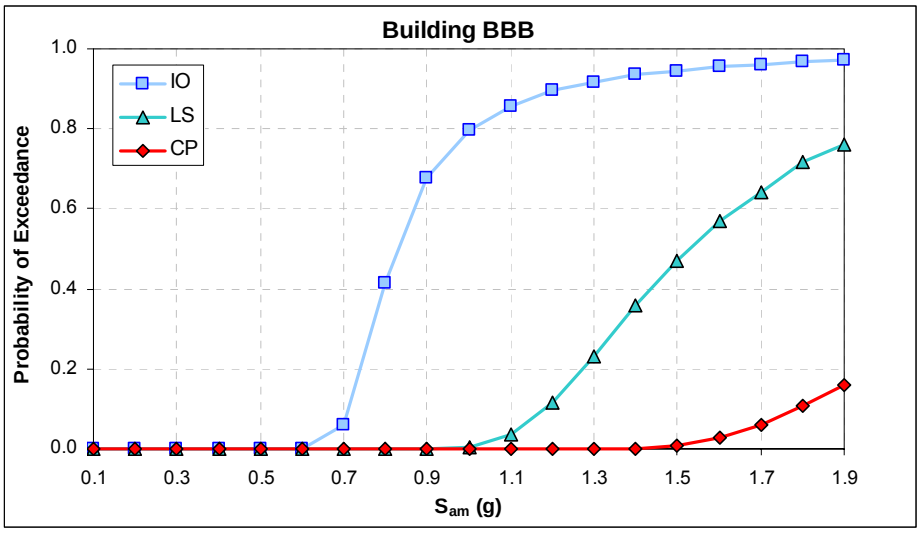

Figure 6.10: Fragility Curves for Building BBB

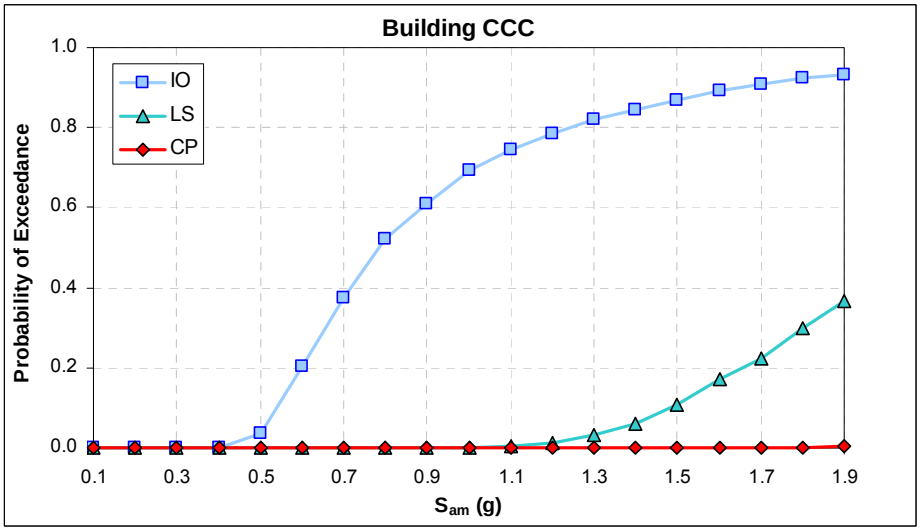

Figure 6.11: Fragility Curves for Building CCC

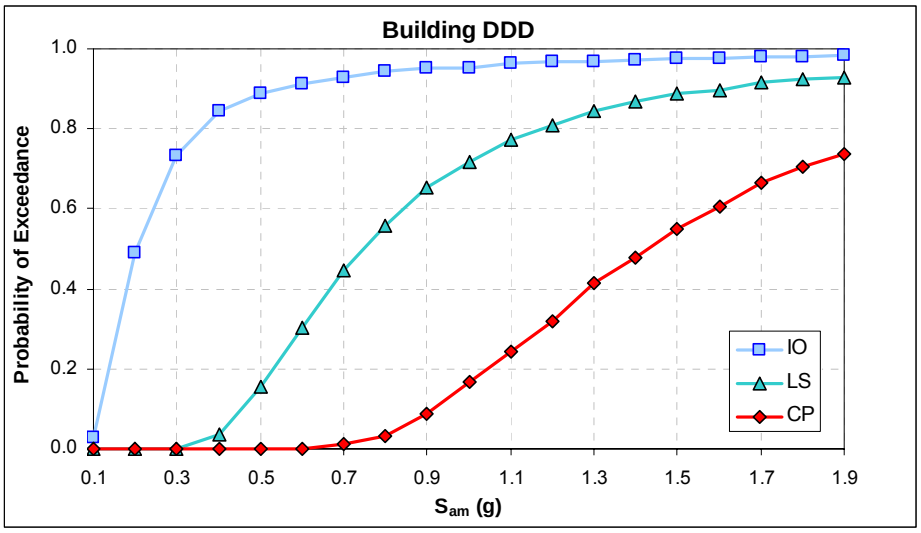

Figure 6.12: Fragility Curves for Building DDD

It is obvious that, even though all 4 buildings are in the same classification, they exhibit different seismic fragility relations. The use of generic fragility curves for all buildings in the same class may lead to an erroneous estimate of potential seismic loss to the portfolio. It can be concluded further that the geometric configurations of the building have little influence on the building fragilities as the curves for building AAA (Figure 6.9) are just slightly different from those of building DDD (Figure 6.12). This can partly due to the fact that the responses are only limited the 2-dimensional aspect. An ongoing study is investigating buildings with 3-dimensional responses and its preliminary results are showing that the parameters characterizing the plan-form configurations are much more influential than those in this study. It must also be noted that the spatial correlation of the damage may exist as the buildings in close proximity are more likely to have similar level of damage than the ones that are far apart. However, this correlation is assumed to be absent in this study.

In order to validate this rapid approach of deriving the building-specific fragility curves, a detailed building-by-building analysis is performed building AAA. The process is much like that presented in Chapters 4 and 5 where only the parameters that define the material properties are used in the response surface model. The resulting fragility curves are plotted as dashed lines along with those solid lines from the rapid assessment in Figure 6.13. The figure confirms an accuracy of the rapid fragility assessment using the response surface metamodels.

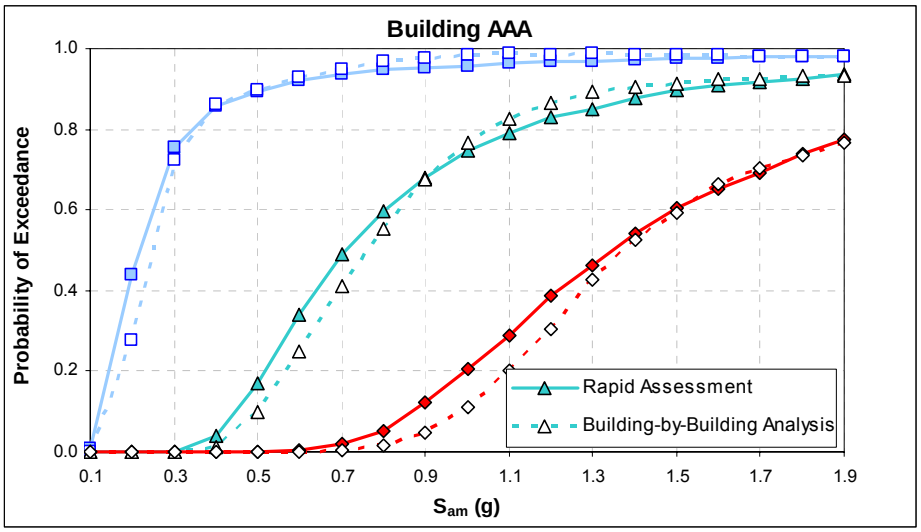

Figure 6.13: Validation of the Fragility Curves by Rapid Assessment Approach

The ability to quickly estimate a fragility relation for an individual building in a target portfolio is a step toward more accurate seismic loss estimation. Nevertheless, the hypothetical building portfolio presented in this study is composed of only a single building structural classification. This may be unrealistic because an actual portfolio of interest will likely contain buildings of several structural classifications. Ultimately,

regionally derived metamodels for every major building classification must be formulated based on the building inventory data. A similar process to that used in this study for the S1-L classification can be utilized to generate metamodels for all other building classes.

The greatest benefits from using metamodels are their computational efficiency and versatility. Considerable computational cost may be necessary in the process of actually generating the global metamodels, but utilizing them in the loss estimation process requires relatively little computational effort, even for Monte Carlo simulation. After metamodels applicable for building inventory in a geographical region are developed, they can be implemented for any portfolio of interest located within the same region.

In summary, this chapter presents a means for a rapid fragility computation. Response surface metamodels are applied in the prediction of seismic response for an aggregation of buildings. Results from the simulations can provide the seismic fragility of an individual building in a portfolio. However, the results from this paper must be considered hypothetical at this point, but the method is shown to be effective and can be directly applied to some of the available data sets.

CHAPTER 7

CONCLUSIONS AND RECOMMENDATIONS FOR FUTURE RESEARCH

Building performance under future earthquakes is largely unknown and cannot be predicted with certainty. This is primarily due to the fact that an earthquake is a random phenomenon in nature such that no two earthquakes are alike. Another source of uncertainty comes from the building itself, as the construction material properties can exhibit deviation from their designed or expected values. Performance assessment based only on deterministic response analyses may be misleading and probabilistic assessment is often more appropriate. Building seismic fragility is utilized as a probabilistic measure of the damage likelihood in a building subjected to future seismic events with specified intensity.

The conventional approaches develop building fragilities through simulation of seismic responses. However, simulation normally requires a large number of samples in order to obtain consistent outcomes. Thousands or ten of thousands of samples may be needed in this regard. It quickly becomes impractical when each sample in the simulation is a nonlinear dynamic analysis of a complex structural model. This thesis proposes an alternative approach for deriving a simulation-based fragility by using a statistical technique called a response surface metamodel.

7.1 RESEARCH SUMMARY

This research presents the use of the response surface metamodel in conjunction with Monte Carlo simulation techniques as a tool to derive building seismic fragility. A response surface function is sought to approximate an implicit building seismic response computation using an explicit polynomial function. The response surface methodology applies Design of Experiments (DOE) techniques to identify an efficient set of computer analyses and then use regression analysis to create a polynomial approximation of the analysis results over a specified design space.

Three proposed approaches using response surface metamodels for calculating building fragilities are presented in this research. Approach 1, which is least effective, generates metamodels for buildings subjected to each individual ground motion record in a suite of earthquakes. Seismic uncertainty is included when the earthquake-specific metamodels are randomly selected in the simulation process. Approach 2 adopts the dual response surface concept to generate separate metamodels for the mean and standard deviation of the responses calculated from a suite of ground motions. The final response surface is composed of mean and standard deviation parts and, hence, incorporates seismic uncertainty in the model itself. Approach 3 avoids the shortcoming of having to repeat the process for different earthquake intensity levels by including a parameter defining intensity level in the response surface models. All three approaches yield comparable probability distributions of the response in the case of a simple single-degree-of-freedom system and their outcomes are essentially as good as those obtained from conventional use of Monte Carlo simulation on the complex model.

Two applications of the proposed approaches are presented. The first application is to compute seismic fragilities of a specific building that represents a typical unreinforced masonry firehouse in Mid-America. A firehouse was chosen because they are considered to be essential facilities that must be operational during and after an earthquake for emergency response purposes. Fragility assessment of the firehouse utilizes Approach 3. Simulations of the response surface models with random material properties as well as seismic uncertainties result in the probabilistic description of the responses. This probabilistic response agrees well with the results from a conventional use of the Latin Hypercube Sampling technique ensuring the validity of the proposed approach. The fragility curves of the particular building are obtained from the values of conditional exceedance probabilities for various seismic intensity levels. It is found that there is a high chance that the particular study building, if assumed to be located in Memphis, would satisfy the performance objectives for moderate level earthquakes, but the chance of not fulfilling the objectives increases significantly when strong earthquakes are considered.

In order to investigate the use of these methods for computing fragilities for modified buildings, rehabilitation schemes are proposed for this firehouse in order to improve its performance under earthquakes. Metallic energy dissipation devices are incorporated in the building in order to consume a portion of the input energy from earthquakes and hence reduce the energy dissipation demand in the main structural elements. Two designs of the devices are considered and both of them utilize the flexibility of the floor and roof diaphragms to maximize the energy dissipation in the devices. The response surface approach is applied in calculating fragilities of the

rehabilitated buildings and the resulting fragility curves reveal that the rehabilitated buildings are much more likely than the original building to meet the more stringent "immediate occupancy" performance objectives defined for essential facilities.

The second application of the response surface approach is to rapidly approximate fragilities for a target building portfolio. Seismic loss estimation for a portfolio of buildings generally requires fragility relations for individual buildings in the portfolio in order to assess probable damage due to seismic hazards. While building-specific fragility curves can be determined from brute-force simulations based on complex structural analyses for each building, for portfolio assessment it becomes impractical to produce the needed large number of seismic response analyses. Instead, a response surface metamodel is used to predict the seismic structural response of a specific building characterized by carefully selected macro-level building parameters (e.g., variability in building geometry, age, etc) and micro-level parameters (e.g., material properties) in a simple functional form. The probability densities of the response and the fragility curves specific to a particular building are then generated through Monte Carlo simulation.

A hypothetical portfolio of four buildings is selected as an example. Each of the buildings in the portfolio is unique in terms of its geometric configuration and age. Response prediction models are generated specific to individual buildings. Simulations using random material properties and earthquakes yield a set of fragility curves for each building in the portfolio. The resulting fragility curves are similar to but yet distinctly different from the single generic curve for buildings of similar type. This concept of building-specific fragilities is believed to lead to a more accurate estimate of losses in

comparison to the conventional use of generic curves for all buildings of the same classification.

In summary, the research presents an effective use of the response surface metamodels in prediction of the response and, consequently, the damage due to earthquakes. The closed-form nature of these metamodels makes it practical to employ Monte Carlo methods to carry out probabilistic response computations. Values of the seismic fragility are then obtained directly from the simulation outcomes.

7.2 RESEARCH IMPACT

As stated at the beginning of the thesis, the primary goal of this research is to develop an alternative means for deriving simulation-based seismic fragility curves. The benefits of this computational process can be seen in two applications: (1) a single building, and (2) a building portfolio.

In the case of a single building, the benefits from use of the response surface approaches may not be very prominent. Even though Monte Carlo simulation can be run efficiently using the closed-form response surface functions, ones may argue that the approach may involve in a larger number of structural analyses than that required when the sampling technique is employed. It is admittedly a fair statement in the case of constructing a totally new fragility relation. However, the benefit of the proposed approaches is more obvious for its flexibility when the existing fragility curves need to be adjusted to reflect newly acquired data. For example, better knowledge from field studies or experimental results may result in modification of the probabilistic descriptions of the construction material properties. In this case, the conventional approach (either with the

direct Monte Carlo simulation or with the use of Latin Hypercube sampling) would have to start from the beginning since the entire process is dependent on the types and characteristics of the probability density of the random parameters. On the other hand, when the response surface approach is utilized, it is only necessary to run the simulation using the existing metamodels but with the new probability density of the material parameters (given that no new parameters are added and that the new probability densities do not fall outside the experimental regions). In this case there is no need for any further structural analysis of the building because the existing metamodels are generated without regard to the types of the distribution of the inputs. This is shown to be a major advantage of the proposed approach over the conventional approaches.

The usefulness of the response surface metamodels becomes more apparent in another application to rapidly deriving fragility curves for buildings in a portfolio. While considerable computational cost may be necessary in the process of generating the metamodels, the greatest benefits are their computationally efficiency and versatility in the loss estimation process. After metamodels applicable for building inventory in a geographical region are developed, they can be used for analysis of any portfolio of interest located within the same region. The ability to quickly estimate a fragility relation for an individual building in a target portfolio is a significant step toward more accurate seismic loss estimation.

7.3 RECOMMENDATIONS FOR FUTURE RESEARCH

Many assumptions have been made in the successful use of response surface metamodels in fragility computation. Further research should be carried out in order to

verify or revise these assumptions. The following are specific recommendations for research on the methodology.

- The current study uses Central Composite Design exclusively in formulating the experimental combinations of the input variables. However, some researchers recently suggested that the designs for the non-random deterministic computer experiments (i.e., time-history response analysis) should be space filling. Further investigation is needed on this type of design.
- The response surface model is represented by a second-degree polynomial function in this study. Even though it produces a relatively accurate prediction in a probabilistic sense, a localized response prediction at a particular point may not be as accurate. Other types of metamodels that include a discontinuity in the curvature such as a kriging model or a model with a spline fit should be studied in future research.
- One disadvantage for the response surface model is its lack of accuracy in predicting the responses beyond the range considered in the experimental design. Selection of the experimental ranges must be done with caution. This issue of extrapolation should be addressed in future research.
- Lastly, even though use of the metamodels reduces the computational expense, its tradeoff is with the accuracy of the structural models. The true measure of efficiency is the standard error of the estimates for a given number of structural analyses. This issue should be addressed in future research as well.

Several recommendations can also be made based on the applications of the metamodels.

- In this research, the properties of the metallic energy dissipation devices are assumed deterministic in the fragility computation. In fact, their properties, even with a highly-controlled fabrication process, can also vary to a certain degree. Future research should also take this into account.
- Only two-dimensional seismic response analyses are considered in this study. Three dimensional analyses must eventually be considered in order to incorporate earthquake direction in the metamodels. Earthquake direction is a major source of uncertainty and should also be incorporated in the investigation.
- Spatial correlations of earthquake and potential damage are assumed nonexistent in this research. This assumption is not completely valid since the buildings that are in close proximity may experience similar level of ground shaking and, to a lesser extent, a similar level of damage. A framework to incorporate a measure of correlation is a good topic for future research.
- The hypothetical building portfolio presented in this research is composed of only a single building structural classification. This may be unrealistic because an actual portfolio of interest will likely contain buildings of several structural classifications. Ultimately, regionally derived metamodels for every major building classification must be formulated based on the building inventory data. A similar process to that used in this research for the S1-L

classification can be utilized to generate metamodels for all other building classes.

- Lastly, the thesis presents the use of the metamodels for rapidly computing the fragilities of buildings in a portfolio. However, a more meaningful measure is in terms of monetary loss to a portfolio. A relationship between physical damage and monetary loss and a means to aggregate individual losses are topics for future research.

REFERENCES

Abrams, D. P. (1992), "Strength and Behavior of Unreinforced Masonry Elements," *Proceedings of the Tenth World Conference on Earthquake Engineering*, Madrid, Spain, pp. 3475-3480.

Abrams, D. P., and Shinozuka, M. (1997), "Loss Assessment of Memphis Buildings," Technical Report NCEER-97-0018, National Center for Earthquake Engineering Research, University at Buffalo, State University of New York, Buffalo, NY.

Anagnos, T., Rojahn, C., and Kiremidjian, A. S. (1995), "NCEER-ATC Joint Study on Fragility of Buildings," Technical Report NCEER-95-0003, National Center for Earthquake Engineering Research, University at Buffalo, State University of New York, Buffalo, NY.

Ang, A. H. S., and Tang, W. H. (1975), Probability Concepts in Engineering Planning and Design: Volume 1 – Basic Principles, John Wiley & Sons, Inc., New York.

ATC – Applied Technology Council (1985), "Earthquake Damage Evaluation Data for California," Report ATC-13, Applied Technology Council, Redwood City, CA.

Basöz, N., and Kiremidjian, A. S. (1999), "Development of Empirical Fragility Curves for Bridges," *Proceedings of the 5th U.S. Conference on Lifeline Earthquake Engineering*, Seattle, WA, pp. 693-702.

Box, G. E. P., and Draper, N. R. (1986), *Empirical Model-Building and Response Surfaces*, John Wiley & Sons, Inc., New York, NY.

Box, G. E. P., and Wilson, K. B. (1951), "On the Experimental Attainment of Optimum Conditions," *Journal of the Royal Statistical Society*, Series B, Vol. 13, Issue 1, pp. 1-45.

Bucher, C. G., and Bourgund, U. (1990), "A Fast and Efficient Response Surface Approach for Structural Reliability Problems," *Structural Safety*, Vol. 7, No. 1, pp. 57-66.

Constantinou, M. C., and Sigaher, A. N. (2000), "Energy Dissipation system Configurations for Improved Performance," *Proceedings of the 2000 Structures Congress & Exposition*, Philadelphia, PA.

Cornell, C. A., Jalayer, F., Hamburger, R. O., and Foutch, D. A. (2002), "Probabilistic Basis for 2000 SAC Federal Emergency Management Agency Steel Moment Frame Guidelines," *Journal of Structural Engineering*, Vol. 128, No. 4, pp. 526-533.

Craig, J. I., Goodno, B. J., Towashiraporn, P., and Park, J. (2002), "Response Modification Applications for Essential Facilities," Final Report for Project ST-4, Mid-America Earthquake Center, School of Civil and Environmental Engineering, Georgia Institute of Technology, Atlanta, GA.

DeLaurentis, D., Mavris, D. N., and Schrage, D. P. (1996), "System Synthesis in Preliminary Aircraft Design using Statistical Methods," *Proceedings of the 20th Congress of the International Council of the Aeronautical Sciences*, Sorrento, Italy.

Dimova, S. L., and Elenas, A. (2002), "Seismic Intensity Parameters for Fragility Analysis of Structures with Energy Dissipating Devices," *Structural Safety*, Vol. 24, No. 1, pp. 1-28.

Dumova-Jovanoska, E. (2000), "Fragility Curves for Reinforced Concrete Structures in Skopje (Macedonia) Region," *Soil Dynamics and Earthquake Engineering*, Vol. 19, No. 6, pp. 455-466.

Engelund, W. C., Stanley, D. O., Lepsch, R. A., McMillan, M. M., and Unal, R. (1993), "Aerodynamic Configuration Design using Response Surface Methodology Analysis," *Proceedings of the AIAA Aircraft Design, Systems, and Operations Meeting*, Monterey, CA.

FEMA – Federal Emergency Management Agency (1997), "NEHRP Commentary on the Guidelines for the Seismic Rehabilitation of Buildings," Report No. FEMA-274, Washington, DC.

FEMA – Federal Emergency Management Agency (1998), "Evaluation of Earthquake Damaged Concrete and Masonry Wall Buildings," Report No. FEMA-307, Washington, DC.

FEMA – Federal Emergency Management Agency (2000a), "Prestandard and Commentary for the Seismic Rehabilitation of Buildings," Report No. FEMA-356, Washington, DC.

FEMA – Federal Emergency Management Agency (2000b), "State of the Art Report on Systems Performance of Steel Moment Frames Subject to Earthquake Ground Shaking," Report No. FEMA-355C, Washington, DC.

Fox, E. P. (1994), "The Pratt & Whitney Probabilistic Design System," Proceedings of the 35th AIAA/ASME/ ASCE/ AHS/ASC Structures, Structural Dynamics, and Materials Conference, Hilton Head, SC.

French, S. (2003), "DS-2 Advanced Inventory Technologies," <http://mae.ce.uiuc.edu/Research/Coreslides/ds-2.ppt>, accessed May 2004.

French, S., and Olshansky, R. (2000), "Inventory of Essential Facilities in Mid-America," Project SE-1 Final Report, Mid America Earthquake Center, The University of Illinois, Champaign, IL.

Galambos, T. V., Ellingwood, B., MacGregor, J. G., and Cornell, C. A. (1982), "Probability Based Load Criteria: Assessment of Current Design Practice," *ASCE Journal of Structural Division*, Vol. 108, No. ST5, pp. 959-977.

Goodno, B. J., Craig, J. I., Dogan, T., and Towashiraporn, P. (1998), "Ductile Cladding Connection Systems for Seismic Design," Building and Fire Research Laboratory, NIST, Report GCR 98-758.

Goodno, B. J., Craig, J. I., and Losiriluk, T. (2003), "Performance Objectives for Essential Facilities," Final Report for Project ST-9, Mid-America Earthquake Center, School of Civil and Environmental Engineering, Georgia Institute of Technology, Atlanta, GA.

GTSTRUDL User Guide: Design – Revision 2 (1999), Computer Aided Structural Engineering Center, School of Civil and Environmental Engineering, Georgia Institute of Technology, Atlanta, GA.

Hwang, H. H. M., and Huo, J.-R. (1994a), "Generation of Hazard-Consistent Fragility Curves," *Soil Dynamics and Earthquake Engineering*, Vol. 13, No. 5, pp. 345-354.

Hwang, H. H. M., and Huo, J.-R. (1994b), "Generation of Hazard-Consistent Fragility Curves for Seismic Loss Estimation Studies," Technical Report NCEER-94-0015, National Center for Earthquake Engineering Research, University at Buffalo, State University of New York, Buffalo, NY.

Hwang, H., Liu, J. B., and Chiu, Y.-H. (2000), "Seismic Fragility Analysis of Highway Bridges," Center of Earthquake Research and Information, The University of Memphis, Memphis, TN.

ICC – International Code Council (2000), *2000 International Building Code*, Falls Church, VA.

Jaw, J.-W., and Hwang, H. H. M. (1988), "Seismic Fragility Analysis of Shear Wall Structures," Technical Report NCEER-88-0009, National Center for Earthquake Engineering Research, University at Buffalo, State University of New York, Buffalo, NY.

JCSS – Joint Committee on Structural Safety (2001), "JCSS Probabilistic Model Code," Internet Publication, <http://www.jcss.ethz.ch/JCSSPublications/PMC/PMC.html>

JMP Statistics and Graphics Guide – Version 3 (1995), SAS Institute Inc., Cary, NC.

Kelly, J. M., Skinner, R. I., and Heine, A. J. (1972), "Mechanisms of Energy Absorption in Special Devices for Use in Earthquake Resistant Structures," *Bulletin of New Zealand Society for Earthquake Engineering*, Vol.5, No 3.

Khuri, A. I., and Cornell, J. A. (1987), *Response Surfaces Designs and Analyses*, Marcel Dekker, Inc., New York, NY.

Kim, S.-C., and White, D. W. (2001), "MDOF Response of Low Rise Buildings." Draft Report for Project ST-5, Mid-America Earthquake Center, School of Civil and Environmental Engineering, Georgia Institute of Technology, Atlanta, GA.

Kircher, A. C. (2003), "Earthquake Loss Estimation Methods for Welded Steel Moment-Frame Buildings," *Earthquake Spectra*, Vol. 19, No. 2, pp. 365-384.

Kleijnen, J. P. C. (1974), *Statistical Techniques in Simulation: Part 1*, Marcel Dekker, Inc., New York, NY.

Kramer, S. L. (1996), *Geotechnical Earthquake Engineering*, Prentice Hall, Inc., Upper Saddle River, NJ.

Lin, D. K. J., and Tu, W. (1995), "Dual Response Surface Optimization," *Journal of Quality Technology*, Vol. 21, No. 1, pp. 34-39.

Magenes, G. and Calvi, G. M. (1997), "In-Plane Seismic Response of Brick Masonry Walls," *Earthquake Engineering and Structural Dynamics*, Vol. 26, pp. 1091-1112.

Mann, N. R., Schafer, R. E., and Singpurwalla, N. D. (1974), *Methods for Statistical Analysis of Reliability and Life Data*, John Wiley & Sons, Inc., New York., NY.

Martinez-Romero, E. (1993), "Experiences on the Use of Supplementary Energy Dissipators on Building Structures," *Earthquake Spectra*, Vol. 9, No. 3, pp. 581-625.

Mavris, D. N., and Bandte, O. (1997), "A Probabilistic Approach to Multivariate Constrained Robust Design Simulation," *Proceedings of 1997 World Aviation Conference*, Anaheim, CA.

Mavris, D. N., Bandte, O., and Schrage, D. P. (1996), "Effect of Mission Requirements on the Economic Robustness of an HSCT Concept," *Proceedings of the 18th Annual Conference of the International Society of Parametric Analysts*, Cannes, France.

McCabe, S. L., and Hall, W. J. (1989), "Assessment of Seismic Structural Damage," *Journal of Structural Engineering*, Vol. 115, No. 9, pp. 2166-2183.

McKay, M. D., Beckman, R. J., and Conover, W. J. (1979), "A Comparison of Three Methods for Selecting Vales of Input Variables in the Analysis of Output From a Computer Code," *Technometrics*, Vol. 21, No. 2, pp. 239-245.

McNamara, R. J., Huang, C. D., and Wan, V. (2000). "Viscous-Damper with Motion Amplification Device for High Rise Building Applications," *Proceedings of the 2000 Structures Congress & Exposition*, Philadelphia, PA.

Montgomery, D. C. (1997), *Design and Analysis of Experiments*, John Wiley & Sons, Inc.

Mosalam, K. M., White, R. N., and Gergely, P. (1997), "Computational Strategies for Frames with Infill Walls: Discrete and Smeared Crack Analyses and Seismic Fragility," Technical Report NCEER-97-0021, National Center for Earthquake Engineering Research, University at Buffalo, State University of New York, Buffalo, NY.

NIBS – National Institute of Building Sciences (1999), "HAZUS 99 Earthquake Loss Estimation Methodology," Technical Manual, Washington, DC.

O'Rourke, M. J., and So, P. (1999), "Seismic Behavior of On-Grade Steel Tanks; Fragility Curves," *Proceedings of the 5th U.S. Conference on Lifeline Earthquake Engineering*, Seattle, WA, pp. 849-858.

O'Rourke, M. J., and So, P. (2000), "Seismic Fragility Curves for On-Grade Steel Tanks," *Earthquake Spectra*, Vol. 16, No. 4, pp. 801-815.

Papila, M., and Haftka, R. T. (2000), "Response Surface Approximations: Noise, Error Repair, and Modeling Errors," *AIAA Journal*, Vol. 38, No. 12, pp. 2336-2343.

Park, Y.-J., and Ang, A. H.-S. (1985), "Mechanistic Seismic Damage Model for Reinforced Concrete," *Journal of Structural Engineering*, Vol. 111, No. 4, pp. 722-739.

Park, J., Craig, J. I., and Goodno, B. J. (2002), "Simple Nonlinear In-Plane Response Models for Assessing Fragility of URM Walls," *Proceedings of the 7th U.S. National Conference on Earthquake Engineering*, Boston, MA.

Peralta, D. F., Bracci, J. M., and Hueste, M. B. D. (2000), "Seismic Performance of Rehabilitated Floor and Roof Diaphragms," Final Report for Project ST-8, Mid-America Earthquake Center, Texas A&M University, College Station, TX.

Perry, C. L., Fierro, E. A., Sedarat, H., and Scholl, R. E. (1993), "Seismic Upgrade in San Francisco Using Energy Dissipation Devices," *Earthquake Spectra*, Vol. 9, No. 3, pp. 559-579.

Pinelli, J.-P. (1992), "Development of Energy Dissipating Cladding Connections for Passive Control of Building Seismic Response," *Ph.D. Thesis*, School of Civil and Environmental Engineering, Georgia Institute of Technology, Atlanta, GA.

Pinelli, J.-P., Craig, J. I., Goodno, B. J., and Hsu, C. C. (1993), "Passive Control of Building Response Using Energy Dissipating Cladding Connections," *Earthquake Spectra*, Vol. 9, No. 3, pp. 529-546.

Pinelli, J. P., Moor, C., Craig, J. I., and Goodno, B. J. (1996), "Testing of Energy Dissipating Cladding Connections," *Earthquake Engineering and Structural Dynamics*, Vol. 25, pp. 129-147.

Prakash, V., Powell, G. H., and Campbell, S. (1993), "DRAIN-2dx Base Program Description and User Guide," Version 1.10, Dept. of Civil Engineering, University of California, Berkeley, CA.

Rajashekhar, M. R., Adidam, S. S. R., and Ellingwood, B. R. (1996), "Structural Reliability Analysis Through Response Surfaces," *Journal of Structural Engineering*, Structural Engineering Research Centre, Madras, India, Vol. 22, No. 4, pp. 179-192.

Rajashekhar, M. R., and Ellingwood, B. R. (1993), "A New Look at the Response Surface Approach for Reliability Analysis," *Structural Safety*, Vol. 12, No. 3, pp. 205-220.

Rix, G. J. (2003), "Earthquake Ground Motion Simulation," Internet Publication, <http://www.ce.gatech.edu/research/mae_ground_motion/>, accessed May 2004.

Rodriguez, M. E., and Aristizabal, J. C. (1999), "Evaluation of a Seismic Damage Parameter," *Earthquake Engineering and Structural Dynamics*, Vol. 28, pp. 463-477.

SBCC – Southern Building Code Congress (1969), *Southern Standard Building Code, 1969 Edition*, Birmingham, AL.

SBCCI – Southern Building Code Congress International (1991), *1991 Standard Building Code*, Birmingham, AL.

Scholl, R. E. (1988), "Added Damping and Stiffness Elements for Earthquake Damage and Loss Control," Proceedings of Conference XLI: A Review of Earthquake Research Applications in the National Earthquake Hazards Reduction Program: 1877-1987, USGS Open File, Report No. 88-13-A, San Diego, CA.

Schueremans, L., and Gemert, D. V. (1999), "Evaluating the Reliability of Structural Masonry Elements Using the Response Surface Technique," *Proceeding of the 8th International Conference on Durability of Building Materials and Components*, Vancouver, Canada.

Seya, H., Talbott, M. E., and Hwang, H. H. M. (1993), "Probabilistic Seismic Analysis of a Steel Frame Structure," *Engineering Mechanics*, Vol. 8, No. 2, pp. 127-136.

Skinner, R. I., Kelly, J. M., and Heine, A. J. (1973). "Energy Absorption Devices for Earthquake Resistant Structures," *Proceeding of the 5th World Conference on Earthquake Engineering*, Rome, Italy, pp. 2924-2933.

Skinner, R. I., Kelly, J. M., and Heine, A. J. (1975). "Hysteretic Dampers for Earthquake-Resistant Structures," *Earthquake Engineering and Structural Dynamics*, Vol.3, pp. 287-296.

Shinozuka, M., Feng, M. Q., Kim, H.-K., Kim, S.-H. (2000a), "Nonlinear Static Procedure for Fragility Curve Development," *Journal of Engineering Mechanics*, Vol. 126, No. 12, pp. 1287-1295.

Shinozuka, M., Feng, M. Q., Lee, J., and Naganuma, T. (2000b), "Statistical Analysis of Fragility Curves," *Journal of Engineering Mechanics*, Vol. 126, No. 12, pp. 1224-1231.

Simpson, T. W., Peplinski, J. D., Koch, P. N., and Allen, J. K. (2001), "Metamodels for Computer-Based Engineering Design: Survey and Recommendations," *Engineering with Computers*, Vol. 17, No. 2, pp.129-150.

Simsir, C. C., Aschheim, M. A., and Abrams, D. P. (2002), "Response of Unreinforced Masonry Bearing Walls Situated Normal to the Direction of Seismic Input Motions," *Proceedings of the 7th U.S. National Conference on Earthquake Engineering*, Boston, MA.

Song, J., and Ellingwood, B. R. (1999), "Seismic Reliability of Special Moment Steel Frames with Welded Connections: II," *Journal of Structural Engineering*, Vol. 125, No. 4, pp. 372-384.

Soong, T. T., and Dargush, G. F. (1997), *Passive Energy Dissipation Systems in Structural Engineering*, John Wiley & Sons Ltd., West Sussex, England.

Tyler, R.G. (1978), "Tapered Steel Energy Dissipators for Earthquake Resistant Structures," *Bulletin of the New Zealand Society for Earthquake Engineering*, Vol.11, No. 4, pp 282-294.

Venter, G., Haftka, R. T., and Chirehdast, M. (1997), "Response Surface Approximations for Fatigue Life Prediction," Proceedings of the 38th AIAA/ASME/ASCE/AHS/ASC Structures, Structural Dynamics, and Material Conference and AIAA/ASM/AHS Adaptive Structures Forum, Kissimmee, FL.

Welch, W. J., Yu, T.-K., Kang, S. M., and Sacks, J. (1990), "Computer Experiments for Quality Control by Parameter Design," *Journal of Quality Technology*, Vol. 22, No. 1, pp. 15-22.

Wen, Y. K., and Wu, C. L. (2001), "Uniform Hazard Ground Motions for Mid-America Cities," *Earthquake Spectra*, Vol. 17, No. 2, pp. 359-384.

Whittaker, A. S., Bertero, V. V., Thompson, C. L., and Alonso, L. J. (1991), "Seismic Testing of Steel Plate Energy Dissipation Devices," *Earthquake Spectra*, Vol. 7, No. 4, pp. 563-604.

Williams, R. A., Stephenson, W. J., Odum, J. K., and Worley, D. M. (2003), "Seismic Velocities from High-Resolution Surface-Seismic Imaging at Six ANSS Sites Near Memphis, Tennessee," Open-File Report 03-218, U.S. Department of the Interior, U.S. Geological Survey, Golden, CO.

Wong, K. K. F., and Wang, Y. (2001), "Energy-Based Damage Assessment on Structures during Earthquakes," *The Structural Design of Tall Buildings*, Vol. 10, pp. 135-154.

Wyss, G. D., and Jorgensen, K. H. (1998). "A User's Guide to LHS: Sandia's Latin Hypercube Sampling Software," Technical Report SAND98-0210, Sandia National Laboratories, Albuquerque, NM.

Yamazaki, F., Hamada, T., Motoyama, H., and Yamauchi, H. (1999), "Earthquake Damage Assessment of Expressway Bridges in Japan," *Proceedings of the 5th U.S. Conference on Lifeline Earthquake Engineering*, Seattle, WA, pp. 361-370.

Yao, T. H.-J., and Wen Y.-K. (1996), "Response Surface Method for Time-Variant Reliability Analysis," *Journal of Structural Engineering*, Vol. 122, No. 2, pp. 193-201.

Yi, T. (2004), "Experimental Investigation and Numerical Simulation of an Unreinforced Masonry Structure with Flexible Diaphragms," *Ph.D. Thesis*, School of Civil and Environmental Engineering, Georgia Institute of Technology, Atlanta, GA.

Yi, T., Moon, F., Leon, R., and Kahn, L. (2002), "Performance Characteristics of Unreinforced Masonry Low-Rise Structure Before and After Rehabilitation," *Proceedings of the 7th U.S. National Conference on Earthquake Engineering*, Boston, MA.

VITA

Peeranan Towashiraporn was born on May 15, 1974 in Bangkok, Thailand. He graduated with a Bachelor of Sciences in Civil Engineering in 1996 from Chulalongkorn University. He then entered the Georgia Institute of Technology in the Fall of 1996 to pursue graduate study in the School of Civil and Environmental Engineering. After receiving his Master of Science in Civil Engineering, he started working on his Ph.D. research with Dr. Barry Goodno and Dr. James Craig in the Fall of 1998.